NONLINEAR VIBRATION ANALYSIS OF CRACKED STRUCTURES — APPLICATION TO TURBOMACHINERY ROTORS WITH CRACKED BLADES

by

Akira Saito

A dissertation submitted in partial fulfillment
of the requirements for the degree of
Doctor of Philosophy
(Mechanical Engineering)
in The University of Michigan
2009

Doctoral Committee:

Professor Christophe Pierre, Co-Chair
Associate Research Scientist Matthew P. Castanier, Co-Chair
Professor J. Wayne Jones
Associate Professor Bogdan I. Epureanu

To my family and friends

ACKNOWLEDGEMENTS

I would like to express my sincere gratitude to my advisors and co-chairs of my doctoral committee, Professor Christophe Pierre and Dr. Matt Castanier for their generous support and guidance, and for giving me the opportunity to pursue my doctoral degree. I am also grateful to the remaining members of my doctoral committee, Professor Epureanu and Professor Jones for their valuable comments and suggestions.

I would also like to thank former and current members of Structural Dynamics Laboratory and Vibrations and Acoustics Laboratory, including Geng Zhang, Eric Baik, Soo-Yeol Lee, Sang Heon Song, Jia Li, Zhijiang He, Olivier Poudou, Keychun Park, Andrew Madden, Darren Holland, Sung-Kwon Hong, Chulwoo Jung, Joosup Lim, and Kiran D'Souza, for their insights and suggestions.

Finally I would like to extend my gratitude to my parents, sister, and our cats for their patience and encouragements.

TABLE OF CONTENTS

LIST OF FIGURES

Figure

LIST OF TABLES

Table

CHAPTER I

Introduction

1.1 Dissertation Objectives

Cracking of metallic components in complex structural systems is an important structural health consideration for ground vehicles, ships, and aircraft. Detecting cracks, and predicting fatigue life of structures has motivated many fundamental investigations into crack initiation, fracture propagation, and nonlinear dynamics. This research concerns the dynamics of cracked structures, where the focus is placed on the development of the *computational* analysis framework for understanding their nonlinear vibration responses. This work has important applications to structural health monitoring, and damage detection of complex structures, with special attention to turbomachinery rotors with cracked blades.

Vibration analysis of cracked structures is an emerging area of research due to its practical importance and numerous issues that arise in the context of linear and nonlinear dynamics theories. From a practical viewpoint, due to the growing demands for reliable damage detection techniques, vibration-based methods have been developed for various types of mechanical and aerospace structures, such as microelectromechanical systems (MEMS) to large jet engines, and airframes.

From a theoretical viewpoint, vibration problems of cracked structures possess *nonlinearity* due to the intermittent contact of the crack surfaces, which is called the "closing

crack" or "breathing crack" effect. This nonlinearity obstructs the application of the conventional linear vibration analysis tools, such as modal analysis and harmonic response analysis. The most widely used method for tackling nonlinear vibration problems is the application of conventional time integration methods, which is computationally very expensive even with today's powerful computers. Therefore the development of accurate, efficient, and stable vibration analysis framework for such structures is both challenging and greatly needed.

Another computational issue arises for the analysis of nonlinear vibration of turbomachinery rotors with cracked blades, which is caused by the *symmetry-breaking* due to cracking. For the nominal design of a bladed disk in a turbine engine rotor, the vibration analysis of bladed disks can be greatly simplified by introducing the concept of *cyclic symmetry* where all the sectors are assumed to be identical. However, the cyclic symmetry of bladed disks is destroyed if there are small differences in material properties or geometric characteristics between individual blades, which is called *mistuning*. Although mistuning is typically small in terms of individual blade properties, it can cause a drastic effect on the system response. In particular, mistuning can also cause localization of the vibration about a few blades, and the attendant concentration of vibration energy can lead to sharp increases in maximum blade amplitude and stress levels. Therefore, it is important to consider the effects of the nonlinearity caused by the cracking, as well as the complication caused by the other mistuning effects, in order to understand the basic dynamics of such structures.

Moreover, as the crack changes its geometrical properties, such as location, width, and length, it has been observed that the vibration modes of cracked structures show an intricate behavior, represented as *eigenvalue loci veerings*. Here, "veerings" refers to regions in an eigenvalue plot where the loci approach each other and almost cross as the parameter

is changed, but instead of crossing they appear to veer away from each other, with each locus then following the previous path of the other. In these regions, it is known that there are interactions between vibration modes, which may lead to *localization* of vibration modes. And hence it may accelerate the growth of the damage due to the concentration of vibration energy to the damaged location. Furthermore with regard to the veering phenomena for nonlinear structural systems such as the cracked structures investigated in this research, very little is known as to how the nonlinearities influence the response near such regions.

Furthermore, when considering very realistic computational models that have a large number of degrees of freedom (DOF), one has to apply *reduced order modeling* techniques in order to capture the essential dynamics with a smaller number of DOF. This greatly improves the computational efficiency of the analysis, but for the vibration problems of the kind dealt in this research, the computational time as well as the accuracy of the results are greatly dependent on the complexity and the preciseness of the modeled nonlinearity. Namely, the choice and the number of DOF involved in the contacting region at the crack faces are the key factors for controlling the accuracy and computational time of the analysis. Therefore, in conjunction with the conventional reduced order modeling techniques, it is necessary to construct an efficient way to control the complexity of the nonlinearity.

Motivated by these issues, the objectives of this research are to gain better understanding of intrinsic nonlinear vibration phenomena in cracked structures, and to develop new analysis techniques, with special attention to turbomachinery rotors with cracked blades. In particular, they are summarized as follows:

- To develop an efficient nonlinear vibration analysis framework for a rotating cracked blade

- To extend the analysis framework developed for the analysis of a cracked blade to

the analysis of a turbomachinery rotor with a cracked blade

- To gain a basic understanding of a cracked structure near the natural frequency veerings and to develop an efficient and accurate method to approximate the nonlinear resonant frequencies

- To develop an efficient reduced order modeling framework for the analysis of a cracked structure with a large number of nonlinear DOF

1.2 Background

1.2.1 Crack-closing effect

Early investigations on vibration of cracked structures generally used an assumption that the cracks are always open, and thus contact between the crack surfaces does not occur. For example, Shen and Pierre developed the cracked beam theory for beams with a single edge crack [1] and with symmetric cracks [2], such that the effects of location and depth of the cracks on the dynamics of the beams can be investigated. It is convenient to assume that the crack is always open because the system remains linear. However, this assumption is not accurate in some cases. For instance, for structures with fatigue-induced cracks, the gaps between the crack surfaces are very small and the closing of the crack surfaces occurs in reality. In particular, Gudmundson [3] reported that experimentally measured natural frequencies of a beam with a fatigue crack differ from those obtained analytically without considering the crack closing effect.

If one considers the repetitive opening and closing of the crack surfaces, a case that is referred to as a closing or breathing crack, then the system is nonlinear. The significance of the effect of crack closing on the structural dynamics is reflected by the growing number of research activities. For instance, Shen and Chu [4] have investigated the effects of crack closing by employing the bi-linear oscillator representation, and they have shown that the

dynamics in the time history and in the frequency response possess an apparent nonlinearity. Chondros *et al.* [5] formulated an analytical model of a cracked beam including the effect of crack closing. They succeeded in validating their theory by comparing the analytically calculated lowest natural frequencies of the cracked beam with experimentally measured values. Pugno *et al.* [6] investigated the nonlinear dynamic response of beams with multiple closing cracks. Bovsunovsky and Surace [7] reported the superharmonic vibrations of a beam with a breathing crack. However, the systems treated in those studies were limited to simple structures such as beams and plates.

In addition to cracks, in order to accurately capture the dynamics of a rotating structure such as a bladed disk in a turbine engine rotor, considering the effects of rotation on the structural response is important. An extensive literature survey regarding research activities on rotating beams was provided by Bazoune [8]. It should be noted that the change in the rotating equilibrium configuration due to the inertial loading is of particular interest for the vibration analysis of cracked structures. The initial gap between the crack surfaces can change significantly with increasing rotation speed.

1.2.2 Symmetry-breaking

For the nominal design of a bladed disk in a turbine engine rotor, the vibration analysis of bladed disks can be greatly simplified by introducing the concept of cyclic symmetry where all the sectors are assumed to be identical. However, the cyclic symmetry of bladed disks is destroyed if there are small differences in material properties or geometric characteristics between individual blades, which is called mistuning. Although mistuning is typically small in terms of individual blade properties (e.g., blade-alone natural frequency variations on the order of 1%), it can have a drastic effect on the system response. In particular, mistuning can cause localization of the vibration about a few blades, and the

attendant concentration of vibration energy can lead to sharp increases in maximum blade amplitude and stress levels. Therefore, a large amount of research activities have been conducted for analyzing the vibration of mistuned bladed disks [9–11].

In contrast, there have been relatively few papers published to date concerning localization and other effects on the forced vibration response of bladed disks due to cracking of blades. The studies by Kuang and Huang [12, 13] considered free and forced response analysis of rotating, shrouded bladed disks by modeling each blade as an Euler-Bernoulli beam where the crack effect was treated as local disorder of the system. They showed that the existence of the crack may change the vibration response of a bladed disk significantly, and cause mode localization. In their recent work [14], they analyzed the stability of a rotating bladed disk using Euler-Bernoulli beam models in conjunction with Galerkin's method for formulating the equations of motion, which they solved with perturbation techniques. Fang *et al.* [15] investigated vibration localization of bladed disks due to cracks for various parameters—including internal coupling factor, crack severity, engine order of excitation, and number of blades—using a model with blades being treated as Euler-Bernoulli beams, and the crack being modeled as a local stiffness loss based on a fracture mechanics-based model. It was shown that even a small crack can cause vibration mode and forced response localization. Hou [16] investigated crack-induced mistuning in an analytical study based on a lumped-mass beam model, in which the local stiffness loss due to cracking was expressed with a flexibility matrix method. However, all of these previous studies used simplified models for cracked blades. Most importantly, their models were *linear*, in the sense that *the nonlinearity caused by the crack closing effect was not taken into account*.

1.2.3 Nonlinear vibration analysis methods

Since the vibration problems investigated in this research are not linear by nature, application of conventional vibration techniques such as frequency response analysis and modal analysis can lead to inaccurate results.

Namely for the linear systems, frequency response can be accurately obtained by applying harmonic forcing to the systems, and examining the amplitude and phase of the resulting displacements field. This typically involves the assumption that if the forcing is expressed as a harmonic function, then the response is also expressed as a harmonic function with the same frequency as the forcing. This assumption is no longer valid for the nonlinear systems. Instead, the steady-state response of such systems should be considered as a general periodic function. There are analytical and computational techniques for obtaining the steady-state solutions of such systems, such as the Lindstedt-Poincaré method, method of multiple scales, the Krylov-Bogoliubov-Mitropolsky method, and the harmonic balance method [17]. In particular, it is known that the harmonic balance method can be applied to *strongly* nonlinear systems, and it produces accurate results with reasonable and controllable computational costs. Therefore in this research, the Harmonic Balance method is employed to calculate the steady-state response of the cracked structures. The method uses an assumption that the steady-state solution of a nonlinear system can be expressed as a sum of harmonic functions with frequencies that are integer multiples or fractional parts of the forcing frequency. Harmonic Balance techniques have been widely used to analyze various types of systems with geometric nonlinearities such as dry-friction systems [18], blades with shroud constraints [19], bladed disks with dry-friction dampers [20], and bladed disks with contact interfaces [21, 22]. Pioneering contributions for using this type of technique include the alternating frequency/time-domain (AFT) method introduced by Cameron and Griffin [23] and the Fast Galerkin method proposed by Ling and Wu [24].

For both of these methods, the nonlinear forces are evaluated in the time domain and are transformed back to the frequency domain by applying the Fast Fourier Transform (FFT). A method named hybrid frequency/time domain (HFT) method was proposed by Guillen and Pierre [25] as the application of the AFT concept to dry-friction damped systems by evaluating the nonlinear friction force in the time domain. By the application of modified Broyden's method for solving the resulting nonlinear algebraic solution achieved efficient analysis of large-scale complicated friction damped structures. The method was further extended by Poudou and Pierre [20], such that the linear DOF of the system can be condensed out and the final nonlinear equations contain only the nonlinear DOF. This order-reduction technique in the solution level, in conjunction with the Craig-Bampton method of component mode synthesis [26] in the preprocessing level, attained a compact yet accurate reduced set of nonlinear equations. Utilizing the Hybrid Powell method [27] for solving the nonlinear equations also contributed to the enhancement of the efficiency of the method. Furthermore, the method was applied to vibration analysis of systems with intermittent contact [28] as well as cracked beams [29] based on the successive application of the penalty method [30].

On the other hand, the modal analysis for a linear system is a method to understand the intrinsic vibration frequencies and shapes of the system, by simply calculating the eigenvalues and eigenvectors. This cannot be applied to the nonlinear systems, because the assumption that the system has to be linear when calculating eigenvalues and eigenvectors is not valid anymore. In particular, the cracked systems have *discontinuities* that open and close during a vibration cycle, and hence the most linearization techniques fail to predict the intrinsic system vibration frequencies and shapes. This class of nonlinear dynamical systems is called a *piecewise-linear system*, because the system consists of multiple linear systems separated by discontinuities. In this research, as a way to approximate the non-

linear counterpart of the eigenvalues for such systems, an approximation method called *bilinear frequency approximation* is generalized and used to approximate the nonlinear resonant frequencies of cracked structures. The bilinear frequency was introduced as an exact solution for a single-DOF piecewise-linear oscillator (e.g., [31]). It was based on the fact that the eigenvalue of each linear system of the piecewise-linear oscillator can be calculated by a standard way, and the actual vibration frequency of the piecewise linear system can be obtained as an explicit function of the frequencies of the linear systems. It was then applied to various systems such as a multi-DOF system with a clearance [32], and simple cracked beams [4, 5, 33, 34] as an *approximation* method to predict the nonlinear resonant frequencies of cracked beams.

1.3 Dissertation Outline

The remaining chapters of this dissertation are compiled from a collection of three manuscripts submitted to scientific journals (either in review or in print) and one manuscript prepared for journal submission. Therefore some of the background materials as well as mathematical developments are repeated in various chapters.

Chapter II is devoted for the development of the nonlinear forced response analysis framework for a rotating cracked blade. In particular, the solution of the forced vibration response of a cracked turbine engine blade is investigated. Starting with a finite element model of the cracked system, the Craig-Bampton method of component mode synthesis is used to generate a reduced-order model that retains the nodes of the crack surfaces as physical degrees of freedom. The nonlinearity due to the intermittent contact of the crack surfaces, which is caused by the opening and closing of the crack during each vibration cycle, is modeled with a piecewise linear term in the equations of motion. Then, the efficient solution procedure for solving the resulting nonlinear equations of motion is presented.

The approach employed in this study is a multi-harmonic, hybrid frequency/time-domain (HFT) technique, which is an extension of the traditional harmonic balance method. First, a simple beam model is used to perform a numerical validation by comparing the results of the new method to those from transient finite element analysis (FEA) with contact elements. It is found that the new method retains good accuracy relative to FEA while reducing the computational costs by several orders of magnitude. Second, a representative blade model is used to examine the effects of crack length and rotation speed on the resonant frequency response. Several issues related to the rotation are investigated, including geometry changes of the crack, shifts in resonant frequencies, and the existence of multiple solutions. For the cases considered, it is found that the nonlinear vibration response exhibits the jump phenomenon only when rotation is included in the model.

Chapter III extends the analysis framework developed in Chapter II to the vibration analysis of turbomachinery rotor with a cracked blade. The influence of small, random blade-to-blade differences (mistuning) and rotation on the forced response are also considered. Starting with a finite element model, a hybrid-interface method of component mode synthesis (CMS) is employed to generate a reduced-order model (ROM). The crack surfaces are retained as physical degrees of freedom in the ROM so that the forces due to contact in three-dimensional space can be properly calculated. The resulting nonlinear equations of steady-state motion are solved by applying an alternating frequency/time-domain method, which is much more computationally efficient than traditional time integration. Using this reduced-order modeling and analysis framework, the effects of the cracked blade on the system response of an example rotor are investigated for various mistuning levels and rotation speeds. First, the advantages of the selected hybrid-interface CMS method are discussed and demonstrated. Then, the resonant frequency shift associated with the stiffness loss due to the crack and the vibration localization about the cracked

blade are thoroughly investigated. In addition, the results of the nonlinear ROMs are compared to those obtained with linear ROMs as well as blade-alone ROMs. It is shown that several key system vibration characteristics are not captured by the simpler models, but that some insight into the system response can be gained from the blade-alone response predictions. Furthermore, it is demonstrated that while the effects of the crack often appear similar to those of mistuning, the effects of mistuning and damage can be distinguished by observing and comparing the response across multiple families of system modes.

Chapter IV examines the veering phenomenon due to the change in the crack parameters, which is motivated by the observation of two, closely-spaced resonant peaks in the frequency response of a turbomachinery rotor with a cracked blade in Chapter III. Of particular interest is the vibration response in parameter regions where the natural frequency loci show veerings. For a representative finite element model, it is shown that the veerings due to crack length variation involve the switching of mode shapes and modal interactions. The nonlinearity caused by the crack closing effect is then introduced, and its effect on the vibration response near the veerings is discussed. The nonlinear forced response analysis is carried out using a hybrid frequency/time domain method, which is based on the method of harmonic balance. The nonlinear vibration response near loci veerings and crossings due to the variation of crack length is investigated in detail. Finally, a novel method for estimating the nonlinear resonant frequency is introduced by generalizing the concept of bilinear frequency approximation, and the method is validated with the results of nonlinear forced response analysis for several veering regions.

Chapter V proposes a novel reduced order modeling framework for nonlinear vibration problems of elastic structures involving intermittent contact. Of particular interest is a vibration problem of plate-like elastic structures with a crack with a large number of degrees of freedom involved on the crack surfaces. Due to the localized nature of such

nonlinearity, the number of degrees of freedom on the surfaces greatly affects the computational time of the analysis. Therefore, reducing the number of degrees of freedom on the crack surfaces without significantly sacrificing the accuracy of the results is a critical issue for conducting vibration analysis of such structures in a reasonable amount of time. The focus is placed on the development of an efficient algorithm to select a set of nodes on the crack surfaces, where nonlinear boundary conditions are imposed. The method is developed based on a master degrees of freedom selection procedure for Guyan reduction, and its accuracy, efficiency, and optimality are discussed in detail and compared with those aspects of previous methods. The advantages of the new method are demonstrated in terms of the accuracy of the frequency response and the corresponding time trajectories.

Finally in Chapter VI, conclusions are drawn and the contributions of this dissertation are summarized, and ideas for future work are also discussed.

CHAPTER II

Efficient Nonlinear Vibration Analysis of the Forced Response of Rotating Cracked Blades

2.1 Introduction

The vibration of cracked structures has attracted considerable interest from many researchers [35] due to its practical importance and the numerous issues that arise in the context of linear and nonlinear dynamics theories. From a practical viewpoint, due to the growing demands for reliable damage detection techniques, vibration-based methods have been developed for various types of structures such as turbine blades [36] and MEMS structures [37].

In the early stages of this area of study, most investigations used an assumption that the cracks of the structures are always open, and thus contact between the crack surfaces does not occur. For example, Shen and Pierre developed the cracked beam theory for beams with a single edge crack [1] and with symmetric cracks [2], such that the effects of location and depth of the cracks on the dynamics of the beams can be investigated. It is convenient to assume that the crack is always open because the system remains linear. However, this assumption is not accurate in many cases. For example, for structures with fatigue-induced cracks, the gaps between the crack surfaces are very small and the closing of the crack surfaces occurs in reality. In particular, Gudmundson [3] reported that experimentally

measured natural frequencies of a beam with a fatigue crack differed from those obtained analytically without considering the crack closing effect.

If one considers the repetitive opening and closing of the crack surfaces, a case that is referred to as a closing or breathing crack, then the system is nonlinear. The significance of the effect of closing of the cracks is reflected by the growing number of research activities. For instance, Shen and Chu [4] have investigated the effects of crack closing by employing the bi-linear oscillator representation, and they have shown that the dynamics in the time history and in the frequency response possess an apparent nonlinearity. Chondros *et al.* [5] formulated an analytical model of a cracked beam including the effect of crack closing. They succeeded in validating their theory by comparing the analytically calculated lowest natural frequencies of the cracked beam with experimentally measured values. Pugno *et al.* [6] investigated the nonlinear dynamic response of beams with multiple closing cracks. Bovsunovsky and Surace [7] reported the superharmonic vibrations of a beam with a breathing crack. However, the systems treated in those studies were limited to simple structures such as beams and plates.

Furthermore, if the cracked structure is a rotating machinery component, such as a bladed disk in a turbine engine rotor, then considering the effects of rotation on the nonlinear vibration response is important. An extensive literature survey regarding research activities on rotating beams was provided by Bazoune [8]. It should be noted that the change in the rotating equilibrium configuration due to the inertial loading is of particular interest for the vibration analysis of cracked structures. The initial gap between the crack surfaces can change significantly with increasing rotation speed.

In this chapter, an efficient method to analyze the nonlinear vibration of a rotating structure with a crack is proposed. In particular, the solution of the forced vibration of a cracked turbine engine blade is investigated. The closing effect of the crack and the effects

of rotation, including the change in the equilibrium configuration of the crack surfaces due to quasi-static deformation of the rotating blade, are considered in this study.

For the steady-state response analysis, an asymptotic technique based on the Harmonic Balance Method [17] is used in this study. Harmonic Balance techniques have been widely used to analyze various types of systems with geometric nonlinearities such as dry-friction systems [18], blades with shroud constraints [19], bladed disks with dry-friction dampers [20], and bladed disks with contact interfaces [21, 22]. Pioneering contributions for using this type of technique include the Fast Galerkin method proposed by Ling and Wu [24], and the alternating frequency/time-domain (AFT) method introduced by Cameron and Griffin [23]. For both of these methods, the nonlinear forces are evaluated in the time domain and are transformed back to the frequency domain by applying the Fast Fourier Transform (FFT). The hybrid frequency/time-domain (HFT) method was proposed by Guillen and Pierre [25, 38] as the application of the AFT concept to dry-friction damped systems by evaluating the nonlinear friction force in the time domain. They also used the modified Broyden's method for solving the resulting nonlinear algebraic solution and achieved efficient analysis of large-scale complicated friction-damped structures. The HFT method was further extended by Poudou and Pierre [20], such that the linear degrees of freedom of the system were condensed out. This order-reduction technique in the solution level, in conjunction with the Craig-Bampton method of component mode synthesis [26] in the preprocessing level, attained a compact yet accurate set of nonlinear equations. Poudou and Pierre used the Hybrid Powell method [27] for solving the nonlinear equations, and showed that this further enhanced the efficiency of the HFT method. Furthermore, the method was applied to vibration analysis of systems with intermittent contact [28] as well as cracked beams [29] based on the successive application of the penalty method.

In this chapter, this analysis framework is further developed by introducing a method for modeling the intermittent contact of the crack surfaces under changes in quasi-static equilibrium configurations due to rotation. This enables the analysis of the important effects of both rotation and crack closing for various crack lengths and operating conditions. For some cases, it is found that the nonlinear vibration response exhibits the jump phenomenon only when rotation is included in the model.

This chapter is organized as follows. In section 2.2, the background theory is reviewed and the proposed modeling and analysis method for rotating cracked structures is derived. In section 2.3, the method is applied to the forced response analysis of a finite element (FE) model of a cracked beam to perform numerical validation. The forced response results are compared to those from transient finite element analysis (FEA) with contact elements. In section 2.4, the method is applied to the finite element (FE) model of a cracked blade with a simple yet representative geometry. The effects of crack closing on the forced response under both static and rotating conditions are examined and compared. As a potential application to damage detection, the shifts in blade resonant frequencies due to cracks are investigated. Conclusions from this chapter are summarized in section 2.5.

2.2 Mathematical Modeling

2.2.1 Equations of motion for rotating structures

For a structure that is rotating about a fixed axis with constant angular velocity Ω, the position vector of a point on the structure can be expressed as $\mathbf{r} = \boldsymbol{\rho} + \mathbf{u}$ where $\boldsymbol{\rho}$ is the undeformed position vector and $\mathbf{u}$ is the displacement vector measured from the undeformed position. Both vectors are defined in the body-fixed, rotating reference frame. The formulation of the equations of motion can be separated into two parts as follows. First, by decomposing the displacement vector into its quasi-static and dynamic components,

$\mathbf{u} = \mathbf{u}_s + \mathbf{u}_d$, the quasi-static displacement due to the centripetal acceleration is obtained by solving the following quasi-static equilibrium equation,

$$(\mathbf{K} - \Omega^2 \mathbf{K}^g)\mathbf{u}_s = \Omega^2 \mathbf{K}^g \boldsymbol{\rho} \tag{2.1}$$

where $\mathbf{K}^g$ is the spin-softening matrix derived from the centripetal acceleration. The stress state of the whole structure and the geometry of the crack surfaces at the equilibrium are determined from Eq. (2.1). The stress state at the equilibrium affects the stiffness of the structure, and hence results in the change of the equations of motion and the associated reduced-order model, as will be discussed later. Furthermore, the rotation can lead to a gap between the crack surfaces in the equilibrium configuration, which results in a qualitative change in the nonlinear vibration response. Next, the dynamic components of the equations of motion of the structure can be expressed as,

$$\mathbf{M}\ddot{\mathbf{u}}_d + (\mathbf{C} - \Omega \mathbf{C}^g)\dot{\mathbf{u}}_d + (\mathbf{K} + \mathbf{K}^s - \Omega^2 \mathbf{K}^g)\mathbf{u}_d = \mathbf{b} \tag{2.2}$$

where $\mathbf{M}$, $\mathbf{C}$, and $\mathbf{K}$ are the mass, damping, and stiffness matrices of the structure under a non-rotating condition; $\mathbf{b}$ is the external force applied to the structure; $\Omega \mathbf{C}^g$ is the gyroscopic damping matrix; and $\mathbf{K}^s$ is the geometric stiffness matrix that is a first-order approximation to the stiffness change due to the nonlinear stiffening effect of the rotation. In this study, the gyroscopic damping matrix $\Omega \mathbf{C}^g$ is neglected because the Coriolis effects are not significant for a blade or a beam with a small thickness-to-width ratio [39]. However, the matrices $\Omega^2 \mathbf{K}^g$ and $\mathbf{K}^s$ are included, and they are generated using the commercial finite element code ANSYS [40]. It is noted that, for the types of structures considered in this study, the combined effect from both geometric stiffness and the spin softening matrices tends to increase the natural frequencies as the rotational speed increases.

2.2.2 Reduced-order modeling

Typically, finite element models of complex structures such as bladed disk assemblies have a large number of degrees of freedom (DOF). Therefore, before attempting to solve the nonlinear vibration problem for a cracked structure, it is advantageous to use some form of modal analysis to condense DOF that are not subject to the nonlinear contact forces and thus reduce the model size. For this purpose, the Craig-Bampton method [26] of component mode synthesis (CMS) is employed in this study. The system DOF are first partitioned into a set of active DOF and a set of omitted DOF. The physical DOF of the nodes on the crack surfaces are chosen as active DOF in the reduced-order model so that the motion of the nodes in the physical three-dimensional space can be tracked. Other DOF that need to be tracked in physical coordinates, such as key response points, can also be included in the active set. For each active DOF, a constraint mode is defined as the static shape induced in the structure by a unit displacement at that DOF, while all the other active DOF are held fixed. In addition to the constraint modes, a set of normal modes associated with the omitted DOF is calculated by holding all the active DOF fixed. These normal modes can then be truncated for a frequency range of interest to reduce the model size.

Defining the Craig-Bampton transformation matrix $\mathbf{\Psi}_{\mathrm{CB}}$, which contains the constraint modes and the truncated set of normal modes, the equations of motion of the undamped system can be reduced to the following equation

$$\mathbf{M}_{\mathrm{CB}}\ddot{\mathbf{q}} + \mathbf{K}_{\mathrm{CB}}\mathbf{q} = \mathbf{b}_{\mathrm{CB}}, \quad \mathbf{q}, \mathbf{b}_{\mathrm{CB}} \in \mathbb{R}^{n_{nm}+n_a} \tag{2.3}$$

where $\mathbf{M}_{\mathrm{CB}} = \mathbf{\Psi}_{\mathrm{CB}}^{\mathrm{T}}\mathbf{M}\mathbf{\Psi}_{\mathrm{CB}}$, $\mathbf{K}_{\mathrm{CB}} = \mathbf{\Psi}_{\mathrm{CB}}^{\mathrm{T}}\mathbf{K}\mathbf{\Psi}_{\mathrm{CB}}$, $\mathbf{u} = \mathbf{\Psi}_{\mathrm{CB}}\mathbf{q}$, $\mathbf{b}_{\mathrm{CB}} = \mathbf{\Psi}_{\mathrm{CB}}^{\mathrm{T}}\mathbf{b}$, n_{nm} is the number of retained normal modes, and n_a is the number of active DOF. The generalized coordinates $\mathbf{q}$ now contain both the active DOF and the truncated set of modal coordinates,

i.e., $\mathbf{q} = [\mathbf{u}_a^{\mathrm{T}}, \mathbf{u}_n^{\mathrm{T}}]^{\mathrm{T}}$ where $\mathbf{u}_a$ is the vector of displacements corresponding to the active DOF, and $\mathbf{u}_n$ is the vector of modal coordinates. In general, the size of the reduced-order model is much smaller than the size of the original finite element model, i.e., $n_{nm} + n_a \ll n_{\mathrm{FEM}}$.

It is noted that the Craig-Bampton method is usually used to reduce multiple components and then assemble them into a global model of a larger structure. However, here it is used because it provides a convenient modeling framework for systems with contact nonlinearity [41], such as the cracked blade discussed in this chapter, especially when the number of DOF contributing to the nonlinearity is much smaller than the number of the other (linear) DOF. In the proposed modeling method for the cracked structures, the DOF associated with the nodes describing the crack surfaces are retained as active DOF in the reduced-order-model, and hence they are directly accessible in the equations of motions to calculate the contact forces. Furthermore, the modal properties of interest of the original FE model, which are mostly the contributions from the large number of linear DOF in the original system, can still be preserved with smaller number of linear DOF in the reduced-order-model.

2.2.3 Equations of motion for cracked structures

Given a reduced-order model of a rotating structure with cracks, the equations of motion of the structure can be written as

$$\mathbf{M}\ddot{\mathbf{q}} + \mathbf{C}\dot{\mathbf{q}} + \mathbf{K}\mathbf{q} = \mathbf{b} + \mathbf{f}(\mathbf{q}) \tag{2.4}$$

where $\mathbf{b}$ is the external forcing vector, and $\mathbf{f}(\mathbf{q})$ is the vector of nonlinear forces due to the intermittent contact at the cracks. Recall that all the finite element DOF on the crack surfaces are retained as active DOF in the reduced-order model. The nonlinear forces and the associated coordinate transformations at the crack surfaces are discussed in detail in

the following subsection.

2.2.4 Crack surface modeling

In considering the nonlinear interaction at the crack surfaces, the relative motion of the surfaces plays an important role. Namely, since the structure is discretized into an FE model and the DOF associated with the nodes on the crack surfaces are retained in the reduced-order model, the relative motion of the nodes determines the behavior of the nonlinear force. In the analysis of contacting bodies using FE models, determination of contact points and calculation of contact forces are not usually trivial because a node on one surface does not necessarily coincide with a node on the other surface at the moment of contact. Therefore, a *contact pair* is defined as two nodes that are considered to be in contact with each other when certain conditions are satisfied. Each contact pair is labeled, and a set of numbers of contact pairs is defined as $\mathcal{C}_{cp}$. In addition, a set of node numbers that form the contact pairs is defined as $\mathcal{C}_c$. The contact conditions and the resulting linear transformation are summarized as follows.

In this analysis, only the normal displacement of the nodes on the crack surfaces is considered. In the following formulation, the subscript 1 of the normal vectors denotes this direction. In addition, the normal direction is chosen such that the origin of the normal vector is on the surface that belongs to the *stiffer* side of the structure. In this chapter, this surface is referred to as surface A. For each contact pair, the node on the surface A is called node A and the other node is called node B, which is on the surface B.

The normal vector at the node A of the ith contact pair is not uniquely determined if the node belongs to multiple elements, which is the general case. Hence, in the proposed method, the normal vector at the node A of the ith contact pair is taken to be the mean

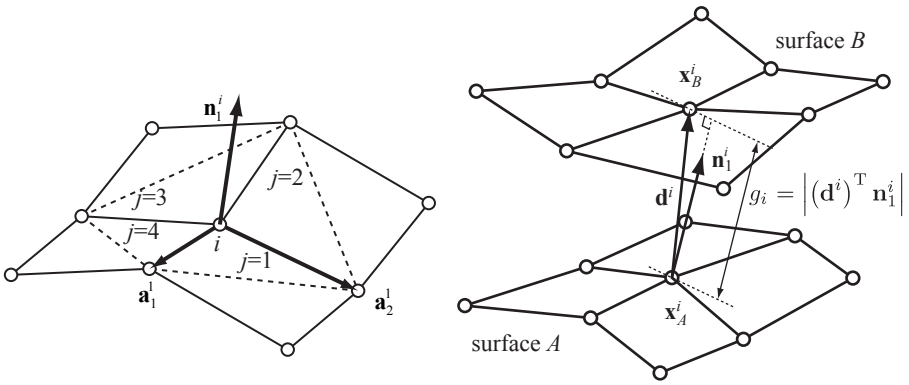

(a) (b)

Figure 2.1: (a) Normal vector at ith node with $N_e^i = 4$, (b) Definition of gap for the ith contact pair

norm, which is defined as

$$\mathbf{n}_1^i = \frac{\sum_j^{N_e^i} \mathbf{c}_j^i}{||\sum_j^{N_e^i} \mathbf{c}_j^i||}, \quad \text{where} \quad \mathbf{c}_j^i = \frac{\mathbf{a}_1^j \times \mathbf{a}_2^j}{||\mathbf{a}_1^j \times \mathbf{a}_2^j||}, \quad i \in \mathcal{C}_{cp} \tag{2.5}$$

where $\mathbf{a}_1^j$ and $\mathbf{a}_2^j$ are the vectors that connect the node A and its adjacent nodes in the jth element, and N_e^i is the number of surface elements which contain the node as one of their vertices. N_e^i depends on the number of elements where the node belongs. For example, $N_e^i = 4$ if the node forms vertices of four elements such as shown in Fig. 2.1a. Care must be taken in the choice of $\mathbf{a}_1^j$ and $\mathbf{a}_2^j$ such that their cross product points outward from the surface.

For the case of a rotating structure, in general there is an initial gap between the crack surfaces. The amount of the gap at the equilibrium must be calculated so that the contact between nodes can be detected properly. The two nodes of the ith contact pair are assumed to be aligned along the normal direction $\mathbf{n}_1^i$ at the equilibrium, and the contact occurs when the relative distance between the nodes becomes zero. Let $\mathbf{d}^i$ be the vector of relative

distance between the node A and node B, i.e.,

$$\mathbf{d}^i = (\mathbf{x}_B^i - \mathbf{x}_A^i), \quad i \in \mathcal{C}_{cp} \tag{2.6}$$

where $\mathbf{x}_A^i$ and $\mathbf{x}_B^i$ denote the equilibrium positions of the node A and node B of the ith contact pair. The *gap* of the ith contact pair, g_i, is then defined as the projection of $\mathbf{d}^i$ onto the normal direction $\mathbf{n}_1^i$, i.e.,

$$g_i = |(\mathbf{d}^i)^{\mathrm{T}}\mathbf{n}_1^i|, \quad i \in \mathcal{C}_{cp} \tag{2.7}$$

The schematic of the relation between the gap and the contact pairs is shown in Fig. 2.1b.

In order to align one of the coordinates of the nodes along the normal direction, and also to force one of the coordinates to point outward from the surface, a linear transformation is introduced. The three mutually perpendicular directions at the node A are defined as $\mathbf{n}_1^i$, $\mathbf{n}_2^i$, and $\mathbf{n}_3^i$, where $\mathbf{n}_2^i$ is an arbitrarily chosen unit vector that is perpendicular to $\mathbf{n}_1^i$, and $\mathbf{n}_3^i = \mathbf{n}_1^i \times \mathbf{n}_2^i$. The linear transformation can then be defined so that the displacement vector of the node A, $\mathbf{u}_A^i$, and that of the node B, $\mathbf{u}_B^i$, are expressed in the new local coordinate systems, the 1-axis of which is the normal direction defined for the contact pair. Let $\bar{\mathbf{u}}_A^i$ and $\bar{\mathbf{u}}_B^i$ be the displacement vectors in the new coordinate system, then the transformations may be written as

$$\begin{cases} \mathbf{u}_A^i &= \mathbf{P}_A^i \bar{\mathbf{u}}_A^i \quad \text{where} \quad \mathbf{P}_A^i = (\mathbf{n}_1^i, \mathbf{n}_2^i, \mathbf{n}_3^i) \\ \mathbf{u}_B^i &= \mathbf{P}_B^i \bar{\mathbf{u}}_B^i \quad \text{where} \quad \mathbf{P}_B^i = -\mathbf{P}_A^i \end{cases}, \quad i \in \mathcal{C}_{cp} \tag{2.8}$$

Considering all the contact pairs in the set C_{cp}, and defining $\mathbf{q} = [\mathbf{u}_c^{\mathrm{T}}, \mathbf{q}_{nc}^{\mathrm{T}}]^{\mathrm{T}}$, $\overline{\mathbf{q}} = [\overline{\mathbf{u}}_c^{\mathrm{T}}, \mathbf{q}_{nc}^{\mathrm{T}}]^{\mathrm{T}}$, where $\mathbf{u}_c$ contains $\mathbf{u}_A^i$ and $\mathbf{u}_B^i$ for all $i \in \mathcal{C}_{cp}$, $\overline{\mathbf{u}}_c$ contains $\overline{\mathbf{u}}_A^i$ and $\overline{\mathbf{u}}_B^i$ for all $i \in \mathcal{C}_{cp}$, and $\mathbf{q}_{nc}$ contains all the DOF that do not contribute to form contact pairs, the transformation may be assembled into the global matrix form,

$$\begin{bmatrix} \mathbf{u}_c \\ \mathbf{q}_{nc} \end{bmatrix} = \begin{pmatrix} \mathbf{P}_c & \mathbf{0} \\ \mathbf{0} & \mathbf{I} \end{pmatrix} \begin{bmatrix} \overline{\mathbf{u}}_c \\ \mathbf{q}_{nc} \end{bmatrix} \tag{2.9}$$

where $\mathbf{P}_c$ is a block-diagonal matrix with $\mathbf{P}_A^i$ and $\mathbf{P}_B^i$ for all $i \in \mathcal{C}_{cp}$ along its diagonal blocks. This transformation is expressed more compactly as

$$\mathbf{q} = \mathbf{P}\overline{\mathbf{q}} \tag{2.10}$$

Applying this transformation to Eq. (2.4) yields,

$$\overline{\mathbf{M}}\ddot{\overline{\mathbf{q}}} + \overline{\mathbf{C}}\dot{\overline{\mathbf{q}}} + \overline{\mathbf{K}}\overline{\mathbf{q}} = \overline{\mathbf{b}} + \overline{\mathbf{f}}(\overline{\mathbf{q}}) \tag{2.11}$$

where $\overline{\mathbf{M}} = \mathbf{P}^{-1}\mathbf{M}\mathbf{P}$, $\overline{\mathbf{C}} = \mathbf{P}^{-1}\mathbf{C}\mathbf{P}$, $\overline{\mathbf{K}} = \mathbf{P}^{-1}\mathbf{K}\mathbf{P}$, $\overline{\mathbf{b}} = \mathbf{P}^{-1}\mathbf{b}$, and $\overline{\mathbf{f}}(\overline{\mathbf{q}}) = \mathbf{P}^{-1}\mathbf{f}(\mathbf{q})$. From Eq. (2.11), the coordinates can be rearranged so that the *first* coordinates of the nodes of the ith contact pair, which are now alined along the normal direction $\mathbf{n}_1^i$, are featured as follows

$$\overline{\mathbf{M}}^i \begin{bmatrix} \ddot{u}_A^i \\ \ddot{u}_B^i \\ \ddot{\mathbf{u}}_o^i \\ \ddot{\mathbf{q}}_{nc} \end{bmatrix} + \overline{\mathbf{C}}^i \begin{bmatrix} \dot{u}_A^i \\ \dot{u}_B^i \\ \dot{\mathbf{u}}_o^i \\ \dot{\mathbf{q}}_{nc} \end{bmatrix} + \overline{\mathbf{K}}^i \begin{bmatrix} u_A^i \\ u_B^i \\ \mathbf{u}_o^i \\ \mathbf{q}_{nc} \end{bmatrix} = \overline{\mathbf{b}}^i + \begin{bmatrix} f_A^i(u_A^i, u_B^i) \\ f_B^i(u_A^i, u_B^i) \\ \mathbf{f}_o^i \\ \mathbf{0} \end{bmatrix} \tag{2.12}$$

where u_A^i and u_B^i are the first coordinates of nodes A and B of the ith contact pair, $\mathbf{u}_o^i$ and $\mathbf{f}_o^i$ contain the coordinates and nonlinear forces for all other DOF for the nodes in $\mathcal{C}_c$. The nonlinear forces f_A^i and f_B^i are defined as,

$$\begin{cases} f_A^i &= -k^* \langle u_B^i + u_A^i - g_i \rangle \\ f_B^i &= f_A^i \end{cases} \tag{2.13}$$

where k^* is a coefficient that penalizes the relative normal penetration of the nodes, and $\langle \cdot \rangle$ denotes the Macaulay bracket defined as $\langle x \rangle = \frac{1}{2}(x + |x|)$, i.e., $\langle x \rangle = 0$ if $x < 0$, and $\langle x \rangle = x$ if $x \geqslant 0$. In order to exploit the symmetry of Eq. (2.13), the following coordinate transformation is introduced [29]:

$$\begin{bmatrix} u_{nl}^i \\ u_l^i \end{bmatrix} = \frac{1}{\sqrt{2}} \begin{pmatrix} 1 & 1 \\ 1 & -1 \end{pmatrix} \begin{bmatrix} u_A^i \\ u_B^i \end{bmatrix} = \mathbf{R}_c^i \begin{bmatrix} u_A^i \\ u_B^i \end{bmatrix}, \quad i \in \mathcal{C}_{cp} \tag{2.14}$$

Note that $(\mathbf{R}_c^i)^{-1} = (\mathbf{R}_c^i)^{\mathrm{T}} = \mathbf{R}_c^i$. This transformation leads to the separation of the DOF in $i \in \mathcal{C}_{cp}$ into nonlinear DOF, u_{nl}^i, and linear DOF, u_l^i. This nomenclature is based on the result of the transformation of the nonlinear forces:

$$\mathbf{R}_c^i \begin{bmatrix} f_A^i(u_A^i, u_B^i) \\ f_B^i(u_A^i, u_B^i) \end{bmatrix} = \begin{bmatrix} -\sqrt{2}k^* \left\langle u_{nl}^i - g_i/\sqrt{2} \right\rangle \\ 0 \end{bmatrix} \tag{2.15}$$

That is, the nonlinear force acts only upon the nonlinear DOF u_{nl}^i.

Next, $\mathbf{q}$ is re-ordered such that $\mathbf{q} = [\mathbf{u}_A^{\mathrm{T}}, \mathbf{u}_B^{\mathrm{T}}, \mathbf{u}_o^{\mathrm{T}}, \mathbf{q}_{nc}^{\mathrm{T}}]^{\mathrm{T}}$ and a vector $\mathbf{q}'$ is defined as $\mathbf{q}' = [\mathbf{u}_{nl}^{\mathrm{T}}, \mathbf{u}_l^{\mathrm{T}}, \mathbf{u}_o^{\mathrm{T}}, \mathbf{q}_{nc}^{\mathrm{T}}]^{\mathrm{T}}$ where $\mathbf{u}_A$, $\mathbf{u}_B$, $\mathbf{u}_{nl}$, and $\mathbf{u}_l$ contain u_A^i, u_B^i, u_{nl}^i and u_l^i for all $i \in \mathcal{C}_{cp}$ respectively, and $\mathbf{u}_o$ includes the DOF associated to the second and third coordinates of all the nodes in $\mathcal{C}_c$. Assembling $\mathbf{R}_c^i$ into a global matrix form, it may be written as

$$\begin{bmatrix} \mathbf{u}_A \\ \mathbf{u}_B \\ \mathbf{u}_o \\ \mathbf{q}_{nc} \end{bmatrix} = \begin{pmatrix} \mathbf{R}_c^{AA} & \mathbf{R}_c^{AB} & \mathbf{0} & \mathbf{0} \\ \mathbf{R}_c^{BA} & \mathbf{R}_c^{BB} & \mathbf{0} & \mathbf{0} \\ \mathbf{0} & \mathbf{0} & \mathbf{I} & \mathbf{0} \\ \mathbf{0} & \mathbf{0} & \mathbf{0} & \mathbf{I} \end{pmatrix} \begin{bmatrix} \mathbf{u}_{nl} \\ \mathbf{u}_l \\ \mathbf{u}_o \\ \mathbf{q}_{nc} \end{bmatrix} \tag{2.16}$$

or

$$\overline{\mathbf{q}} = \mathbf{R}\mathbf{q}' \tag{2.17}$$

where $\mathbf{R}_c^{AA}$, $\mathbf{R}_c^{AB}$, $\mathbf{R}_c^{BA}$, and $\mathbf{R}_c^{BB}$ contain the components of $\mathbf{R}_c^i$ for all $i \in \mathcal{C}_{cp}$ at appropriate locations. Note again that the transformation matrix $\mathbf{R}$ is orthogonal and symmetric. Defining $\mathbf{q}_{nl} = \mathbf{u}_{nl}$, and $\mathbf{q}_l = [\mathbf{u}_l^{\mathrm{T}}, \mathbf{u}_o^{\mathrm{T}}, \mathbf{q}_{nc}^{\mathrm{T}}]^{\mathrm{T}}$, Eq. (2.11) can then be transformed as follows:

$$\mathbf{M}' \begin{bmatrix} \ddot{\mathbf{q}}_{nl} \\ \ddot{\mathbf{q}}_l \end{bmatrix} + \mathbf{C}' \begin{bmatrix} \dot{\mathbf{q}}_{nl} \\ \dot{\mathbf{q}}_l \end{bmatrix} + \mathbf{K}' \begin{bmatrix} \mathbf{q}_{nl} \\ \mathbf{q}_l \end{bmatrix} = \mathbf{b}' + \begin{bmatrix} \mathbf{f}_{nl}(\mathbf{q}_{nl}) \\ \mathbf{0} \end{bmatrix} \tag{2.18}$$

where $\mathbf{M}' = \mathbf{R}^{-1}\overline{\mathbf{M}}\mathbf{R}$, $\mathbf{C}' = \mathbf{R}^{-1}\overline{\mathbf{C}}\mathbf{R}$, $\mathbf{K}' = \mathbf{R}^{-1}\overline{\mathbf{K}}\mathbf{R}$, $\mathbf{b}' = \mathbf{R}^{-1}\overline{\mathbf{b}}$. The superscript "$\prime$" is omitted for convenience in the subsequent formulation.

2.2.5 Equations of motion in the frequency domain

The solution technique used in this study is an extension of the HFT method [20, 25, 28, 29, 38, 42], which in turn was an extension of the AFT method [23]. Recently, the HFT method has been applied to systems with intermittent contact and cracks by Poudou *et al.* [28, 29, 42]. The basic assumption of this approach is that the steady state response can be expressed as a truncated Fourier series:

$$\mathbf{q} = \begin{bmatrix} \mathbf{q}_{nl} \\ \mathbf{q}_{l} \end{bmatrix} = \Re\left(\sum_{k=0}^{n_h} \left\{ \begin{bmatrix} \mathbf{Q}_k^{nl,c} \\ \mathbf{Q}_k^{l,c} \end{bmatrix} - \mathrm{j} \begin{bmatrix} \mathbf{Q}_k^{nl,s} \\ \mathbf{Q}_k^{l,s} \end{bmatrix} \right\} \mathrm{e}^{\mathrm{j}k\omega t} \right) = \Re\left(\sum_{k=0}^{n_h} (\mathbf{Q}_k^c - \mathrm{j}\mathbf{Q}_k^s) \mathrm{e}^{\mathrm{j}k\omega t} \right) \tag{2.19}$$

where n_h is the number of non-zero harmonics to be used and $\mathrm{j} = \sqrt{-1}$. Note that $\mathbf{Q}_k^c$ and $-\mathbf{Q}_k^s$ are the vectors of real and imaginary parts of kth Fourier coefficients of $\mathbf{q}$, which correspond to the cosine (c) and sine (s) components of the motion. In the same manner, the external force $\mathbf{b}$ and the nonlinear force $\mathbf{f}$ are expressed as

$$\mathbf{b} = \begin{bmatrix} \mathbf{b}_{nl} \\ \mathbf{b}_{l} \end{bmatrix} = \Re\left(\sum_{k=0}^{n_h} \left\{ \begin{bmatrix} \mathbf{B}_k^{nl,c} \\ \mathbf{B}_k^{l,c} \end{bmatrix} - \mathrm{j} \begin{bmatrix} \mathbf{B}_k^{nl,s} \\ \mathbf{B}_k^{l,s} \end{bmatrix} \right\} \mathrm{e}^{\mathrm{j}k\omega t} \right) = \Re\left(\sum_{k=0}^{n_h} (\mathbf{B}_k^c - \mathrm{j}\mathbf{B}_k^s) \, \mathrm{e}^{\mathrm{j}k\omega t} \right) \tag{2.20}$$

$$\mathbf{f} = \begin{bmatrix} \mathbf{f}_{nl} \\ \mathbf{0} \end{bmatrix} = \Re\left(\sum_{k=0}^{n_h} \left\{ \begin{bmatrix} \mathbf{F}_k^{nl,c} \\ \mathbf{0} \end{bmatrix} - \mathrm{j} \begin{bmatrix} \mathbf{F}_k^{nl,s} \\ \mathbf{0} \end{bmatrix} \right\} \mathrm{e}^{\mathrm{j}k\omega t} \right) = \Re\left(\sum_{k=0}^{n_h} (\mathbf{F}_k^c - \mathrm{j}\mathbf{F}_k^s) \, \mathrm{e}^{\mathrm{j}k\omega t} \right) \tag{2.21}$$

Substituting Eqs. (2.19), (2.20), and (2.21) into Eq. (2.18) and applying the method of harmonic balance [17] yields the following equation for the kth harmonic

$$\mathbf{\Lambda}_k \mathbf{Q}_k = \mathbf{B}_k + \mathbf{F}_k \tag{2.22}$$

where $\mathbf{Q}_0 = \mathbf{Q}_0^c$, $\mathbf{B}_0 = \mathbf{B}_0^c$, $\mathbf{F}_0 = \mathbf{F}_0^c$, $\mathbf{\Lambda}_0 = \mathbf{K}$, $\mathbf{Q}_k = [(\mathbf{Q}_k^c)^{\mathrm{T}}, (\mathbf{Q}_k^s)^{\mathrm{T}}]^{\mathrm{T}}$, $\mathbf{B}_k = [(\mathbf{B}_k^c)^{\mathrm{T}}, (\mathbf{B}_k^s)^{\mathrm{T}}]^{\mathrm{T}}$, $\mathbf{F}_k = [(\mathbf{F}_k^c)^{\mathrm{T}}, (\mathbf{F}_k^s)^{\mathrm{T}}]^{\mathrm{T}}$, and

$$\mathbf{\Lambda}_k = \begin{pmatrix} -(k\omega)^2\mathbf{M} + \mathbf{K} & (k\omega)\mathbf{C} \\ -(k\omega)\mathbf{C} & -(k\omega)^2\mathbf{M} + \mathbf{K} \end{pmatrix} \tag{2.23}$$

for $k = 1, \ldots, n_h$. The Eq. (2.22) can be written in partitioned form

$$\begin{pmatrix} \mathbf{\Lambda}_k^{nl,nl} & \mathbf{\Lambda}_k^{nl,l} \\ \mathbf{\Lambda}_k^{l,nl} & \mathbf{\Lambda}_k^{l,l} \end{pmatrix} \begin{bmatrix} \mathbf{Q}_k^{nl} \\ \mathbf{Q}_k^{l} \end{bmatrix} = \begin{bmatrix} \mathbf{B}_k^{nl} \\ \mathbf{B}_k^{l} \end{bmatrix} + \begin{bmatrix} \mathbf{F}_k^{nl} \\ \mathbf{0} \end{bmatrix} \tag{2.24}$$

where, again, each partition has both cosine and sine blocks for $k = 1, \ldots, n_h$ or just a cosine block for $k = 0$. Moreover, the size of the set of nonlinear equations, Eq. (2.24), can be further reduced without any loss of accuracy. That is, the equations can be expressed in terms of the nonlinear variables only [20], and Eq. (2.24) becomes

$$\mathbf{\Lambda}_k^{\mathrm{red}} \mathbf{Q}_k^{nl} = \mathbf{B}_k^{\mathrm{red}} + \mathbf{F}_k^{nl}(\mathbf{Q}^{nl}) \tag{2.25}$$

where

$$\mathbf{\Lambda}_k^{\mathrm{red}} = \mathbf{\Lambda}_k^{nl,nl} - \mathbf{\Lambda}_k^{nl,l}(\mathbf{\Lambda}_k^{l,l})^{-1}\mathbf{\Lambda}_k^{l,nl}$$

$$\mathbf{B}_k^{\mathrm{red}} = \mathbf{B}_k^{nl} - \mathbf{\Lambda}_k^{nl,l}(\mathbf{\Lambda}_k^{l,l})^{-1}\mathbf{B}_k^{l}$$

Assembling this into a global matrix form, the set of nonlinear equations are obtained as

$$\mathbf{\Lambda}^{\mathrm{red}} \mathbf{Q}^{nl} = \mathbf{B}^{\mathrm{red}} + \mathbf{F}^{nl}(\mathbf{Q}^{nl}) \tag{2.26}$$

where $\mathbf{\Lambda}^{\mathrm{red}}$ is a pseudo-block diagonal matrix with $\mathbf{\Lambda}_k^{\mathrm{red}}$ for $k = 0 \ldots n_h$ along its diagonal blocks, $\mathbf{Q}^{nl} = [(\mathbf{Q}_0^{nl})^{\mathrm{T}}, \ldots, (\mathbf{Q}_{n_h}^{nl})^{\mathrm{T}}]^{\mathrm{T}}$, $\mathbf{B}^{\mathrm{red}} = [(\mathbf{B}_0^{\mathrm{red}})^{\mathrm{T}}, \ldots, (\mathbf{B}_{n_h}^{\mathrm{red}})^{\mathrm{T}}]^{\mathrm{T}}$, and $\mathbf{F}^{nl} = [(\mathbf{F}_0^{nl})^{\mathrm{T}}, \ldots, (\mathbf{F}_{n_h}^{nl})^{\mathrm{T}}]^{\mathrm{T}}$. The set of nonlinear equations (2.26) is iteratively solved by the Hybrid Powell Method [27]. One should note that $\mathbf{F}$, which are the Fourier coefficients of the nonlinear force, are obtained at each iteration by applying the Fast Fourier Transform

(FFT) to the time history of the nonlinear force, $\mathbf{f}$, which was obtained by imposing the displacement vector from the previous iteration [28]. This hybrid frequency/time-domain procedure is summarized as:

$$\mathbf{Q}^{nl} \xrightarrow{\mathcal{F}^{-1}} \mathbf{q}(t) \xrightarrow{(2.13)} \mathbf{f}(\mathbf{q}(t)) \xrightarrow{\mathcal{F}} \mathbf{F} \xrightarrow{(2.26)} \mathbf{Q}^{nl} \xrightarrow{\mathcal{F}^{-1}} \cdots \tag{2.27}$$

That is, given a displacement vector from the previous iteration, the forces are solved in the time domain, and then a new displacement vector is solved in the frequency domain. The solution is considered to be converged when the difference between the displacement vectors from consecutive iterations falls below a prescribed tolerance.

2.2.6 Comments on the stability of the steady-state solutions

In time-domain calculations, one may determine the stability of the solution of a nonlinear forced response using Floquet multipliers or Poincaré maps (see Ref. [43], for example). However, these methods cannot be readily applied to the solution process of frequency-domain-based techniques such as the one proposed in this chapter. For such methods, by utilizing the fact that the solution is expanded with a truncated Fourier series, one may use a finite-dimensional approximation of Hill's infinite determinant (see Ref. [43], for example) to determine the stability of the steady-state solutions. Namely, the stability of the solution obtained by such methods can be determined by examining the eigenvalues of a resulting quadratic eigenvalue problem as shown in the Ref. [44], where a non-positive real part of an eigenvalue indicates a stable solution and a negative real part indicates an unstable solution.

2.3 Numerical Validation

For simple, discrete mass-spring-damper systems, it was shown by Poudou *et al.* [28] that the solutions obtained by the HFT method agreed with the results obtained by time

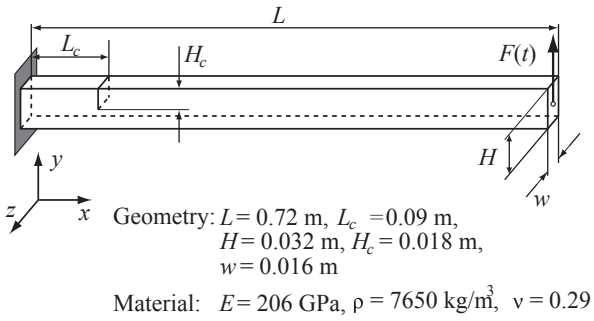

Figure 2.2: Schematic of the cracked beam model used for validation of the HFT method

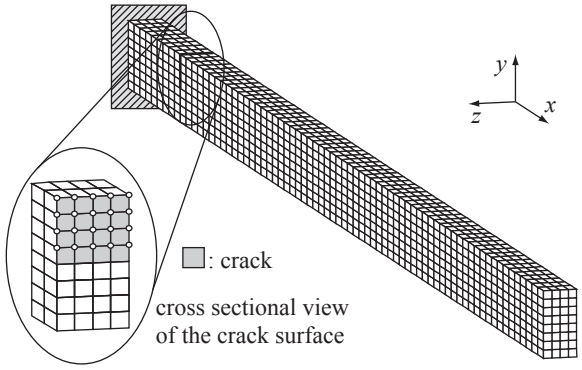

Figure 2.3: Finite element model of the beam

integration methods. However, the validation of the method for a representative FE model of a cracked structure has not yet been provided. In this section, the FE model of a cantilevered cracked beam subject to harmonic excitation is used for validation purposes. The nonlinear, steady state vibration response of the cracked beam is calculated using both the time integration method and the HFT method, and the results are compared.

2.3.1 Cracked beam model

The schematic of the cracked beam model is shown as Fig. 2.2. The crack is located at one-eighth of the length of the beam from the clamped end, and the depth of the crack H_c is 56.3% of the height of the beam H. The forcing is harmonic excitation, $F(t) = A\cos\omega t$, where $A = 1.0$N. The forcing is applied in the y direction at the tip of the beam in order to

excite the first $x-y$-plane bending mode. The damping of the beam is defined as $\mathbf{C} = \beta\mathbf{K}$ where $\beta = 5.0 \times 10^{-4}\ \mathrm{s}^{-1}$.

The finite element model and the cross sectional view of the crack surface are shown in Fig. 2.3. The finite element model has 4608 eight-noded brick elements and 6570 nodes. After applying fixed boundary conditions at one end, the total number of DOF is 9780. There are a total of 40 nodes on the crack surfaces, or 20 contact pairs.

2.3.2 Time integration method

The time integration was performed using the commercial code ANSYS [40]. The Newmark method was used for the time integration, and the augmented Lagrangian method was used as the contact algorithm. The augmented Lagrangian method (see Ref. [45], for example) is an algorithm for enforcing the impenetrability boundary conditions at the contact points by iteratively calculating the Lagrange multipliers using the penalty functions and the Lagrange multipliers of the previous iteration. In general, the method is known to possess better characteristics than of the pure Lagrange multiplier method and the pure penalty method, for static and time transient calculations. The maximum penetration allowed for the contact nodes was set to 0.001 for all contact elements, which is the ratio of the amount of maximum penetration to the element dimension in the normal direction of contact.

2.3.3 Reduced-order model for the HFT method

The Craig-Bampton [26] CMS method was applied to the FE model, and the resulting reduced-order model had 62 DOF, which includes 20 normal modes and 42 active DOF. Of the active DOF, 1 DOF was kept for each of the 40 nodes on the crack surfaces so that the relative motion of the nodes could be tracked along the gap direction during the iteration of the HFT. In addition, 2 active DOF were kept for nodes at the tip of the beam

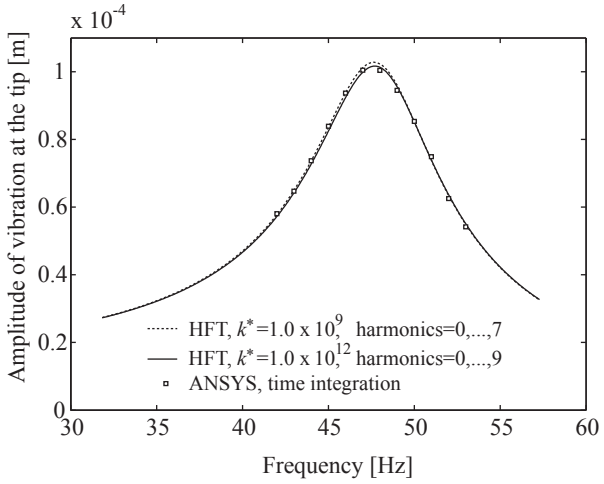

Figure 2.4: Frequency response of the beam

in order to apply external forcing and to track the tip motion.

2.3.4 Results

The frequency response curves obtained by the time integration method and the HFT method are shown in Fig. 2.4. The HFT method was applied with several values of parameters. As can be seen, the results calculated by the HFT method show an excellent agreement with the results by the time integration method. Ideally, the solutions obtained by the HFT method converge as the values of parameters of the HFT go toward infinity. Furthermore, it was previously shown that the value of the penalty coefficient and the number of harmonics are the dominant parameters determining the accuracy of the method [29]. For the calculations considered, increasing the parameters beyond $k^* = 1.0 \times 10^{12}$N/m and harmonics 0 though 9 did not yield a noticeable improvement in the accuracy of the results.

The CPU time required to obtain the solution for a specified frequency using a Sun Blade 1500 workstation (1.0 GHz) is summarized in Table 2.1. The selected values of the

Table 2.1: Average CPU time per frequency

Method	Harmonics	k^* [N/m]	CPU Time [sec]
HFT	0–7	1.0×10^9	9.8×10^{-1}
HFT	0–9	1.0×10^{12}	1.8×10^2
ANSYS Newmark	-	-	1.5×10^4

parameters greatly affect the CPU time of the HFT method. Nevertheless, for both sets of parameters the HFT method is much more efficient than time integration.

With regard to the interpretation of the frequency response of the cracked beam, it should be noted that presence of the crack causes a resonant frequency drop of 7.2%. Furthermore, in this case, the resonant frequency of the cracked beam is independent of the amplitude of vibration because of a characteristic of this type of piecewise linear system. This will be discussed further in section 2.4.

2.4 Effects of Rotation on a Cracked Blade

In this section, the effects of rotation on the forced response of a cracked blade are examined. The effects considered here are: (1) the amplitude dependence of the frequency response, which does not exist for the response of the cracked beams under static condition; and (2) the resonant frequency shift due to the change in the crack length for both static and rotating conditions.

2.4.1 Amplitude dependence of the response

Problem statement

The forced response of the cracked blade is considered under non-rotating and rotating conditions. The finite element model of the blade is shown as Fig. 2.5a, and the deformed configuration of the model rotating at 5000 RPM is shown as Fig. 2.5b. The axis of rotation is parallel to the y-axis at a distance of 0.0833 m from the bottom of the blade. Under the rotating condition, there exists a gap between the crack surfaces due to the inertial force.

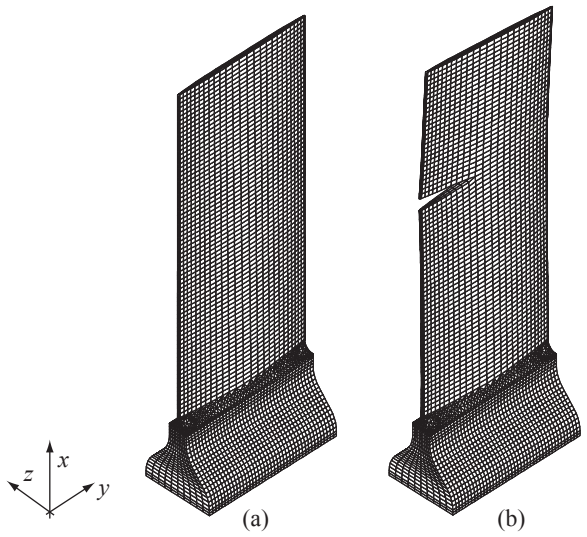

Figure 2.5: (a) FE model of the cracked blade under static condition, (b) deformed equilibrium under rotating condition

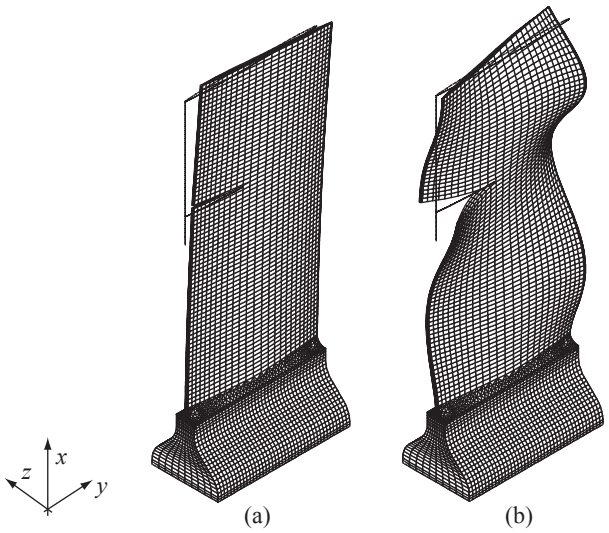

Figure 2.6: Mode shapes of the cracked blade obtained by neglecting the nonlinear boundary condition: (a) sixth mode, (b) tenth mode. Thin lines show undeformed shapes.

The mode of interest is the tenth mode as shown in Fig. 2.6b, and the corresponding natural frequency is 6952.2 Hz. The blade has chord length $H = 0.0508$ m, maximum thickness $t = 0.0015$ m, and span length $L = 0.128$ m, and is made of an aluminum alloy with Young's modulus $E = 72.4$ GPa, density $\rho = 2793.4$ kg/m^3, and Poisson's ratio $\nu = 0.33$. The crack is located at a point 0.0386 m down from the blade tip, which is 30.3% of the span length. The crack length is 0.0160 m, which is 31.6% of the chord length. The finite element model has 28,037 nodes, and there are 104 nodes on the crack surfaces, or 52 contact pairs. The nodes on the blade root are constrained in all three directions, and the resulting finite element model has a total of 77,643 DOF.

After applying the Craig-Bampton method, the reduced-order model had 408 DOF: 312 DOF at the crack surfaces, 36 DOF at the tip of the blade (for convenience of tracking the vibration response of the blade tip in physical coordinates), and 60 modal coordinates. The modal damping factor ζ_r was set to 0.0005, and the damping matrix was defined as $\mathbf{C} = \beta\mathbf{K}$, where $\beta = 2\zeta_r/\omega_r$. Harmonic forcing was applied at the edge of the crack such that the tenth mode was excited. For the HFT method, harmonics 0–9 were kept, and the value of penalty coefficient was set to $k^* = 1.75 \times 10^8$ N/m.

Results

Under the conditions stated above, forced response analysis for both static and rotating conditions was performed for various values of the applied force $\mathbf{b}$. The results are shown in Fig. 2.7. For comparison, the forced response results for both the linear and nonlinear systems are shown in the same graphs. The linear system here means that contact was not enforced, i.e., the nonlinear forces defined in Eq. (2.13) were ignored. As can be seen, the nonlinear systems have higher resonant frequencies than the linear systems for both conditions. This indicates that the compliance of the linear system is greater than that

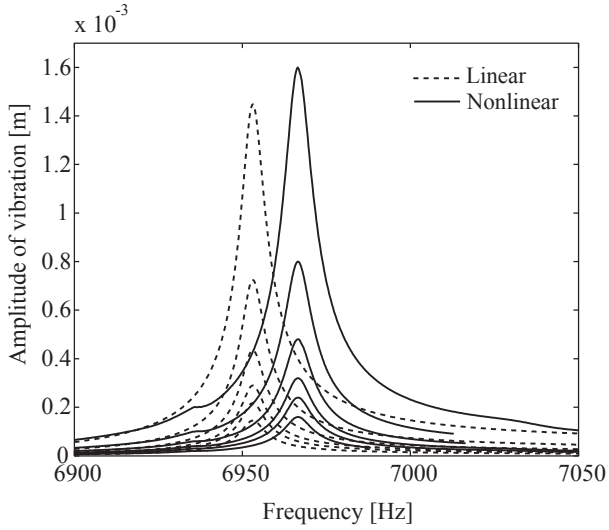

(a)

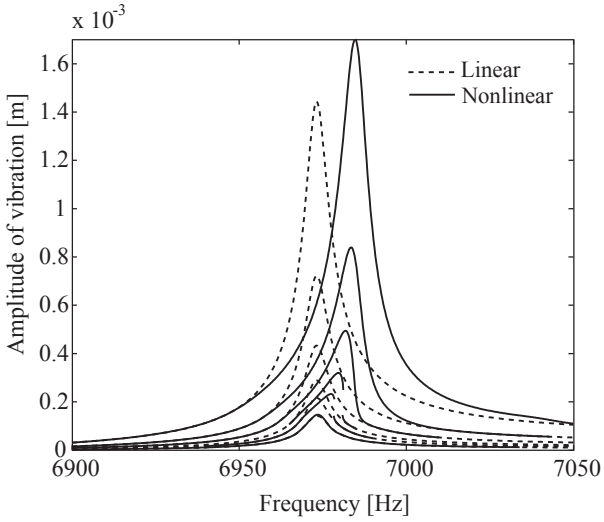

(b)

Figure 2.7: Frequency response under (a) static condition, (b) rotating condition at 5000 RPM for increasing values of $||\mathbf{b}||$=4.44, 6.67, 8.89, 13.3, 22.2, and 44.4 N

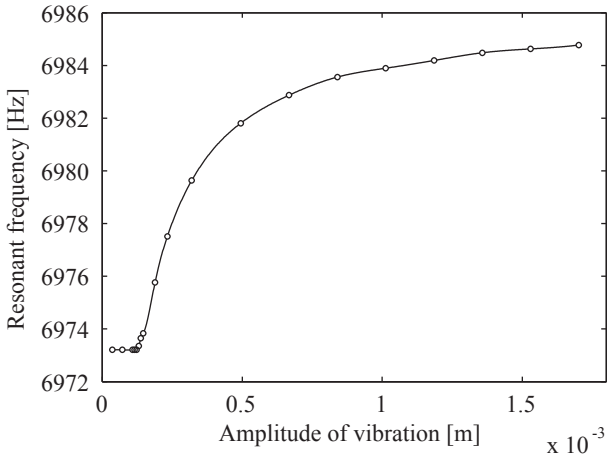

Figure 2.8: Resonant frequency under rotating condition versus amplitude of force

for the nonlinear systems, which makes sense because penetration of the crack surfaces is allowed for the linear case.

A notable distinction between the static and the rotating cases is that the nonlinear response for the static case is independent of the amplitude of the forcing, whereas the frequency response curve for the rotating case becomes bent towards the higher frequency region as the amplitude of the forcing increases. This difference results from the fact that there was a gap between the crack surfaces. The systems considered here can be regarded as piecewise linear systems having 2^N domains with N *switching hyperplanes* (see [46] for example) defined by $u_B^i + u_A^i = g_i$ for $i \in \mathcal{C}_{cp}$, where N denotes the number of contact pairs, or $N = |\mathcal{C}_{cp}|$. The amplitude independence of the forced response is a characteristic of periodically forced piecewise linear oscillators when there are no initial gaps [31]. Namely, as discussed by Zuo and Curnier [47], in the absence of the gap, i.e., if the switching hyperplane passes through the origin, the modal frequencies of the piecewise linear systems are not dependent on the amplitude of vibration due to *positive homogeneity* of the piecewise linear force. This corresponds to the static case for the systems studied here. To be specific, it can be shown that the piecewise linear force defined

in Eq. (2.13) is positively homogeneous of degree 1 if $g_i = 0$, i.e., $f_A^i(\lambda \mathbf{q}) = \lambda f_A^i(\mathbf{q})$, $\forall \lambda > 0$, $\mathbf{q} \in \mathbb{R}^{n_{nm}+n_a}$, $i \in \mathcal{C}_{cp}$. Hence the natural frequencies are independent on the amplitude of vibration, so are the resonant frequencies. For the cases with initial gaps however, as discussed by Chen and Shaw [48], and Jiang *et al.* [46], the piecewise linear forces may not possess positive homogeneity because the switching hyperplane does not pass through the origin. This applies to the rotating cases for the systems studied here.

Furthermore, a significant feature of the rotating response curves is that the bending of the resonance curves vanishes as the force amplitude increases. This is due to the fact that the size of the gap shrinks relative to the response amplitude as the force becomes large, and the results approach those of the limit case in which there is no gap.

In order to better understand the amplitude dependence of the response, the resonant frequencies for rotating cases are plotted versus the amplitude of vibration in Fig. 2.8. As can be seen in Fig. 2.8, the resonant frequency stays constant for small amplitude of vibration, where the system response is still linear. The transition from the linear response to the nonlinear response occurs where the amplitude of vibration is between 1.23×10^{-4} m and 1.30×10^{-4} m. It then rapidly increases and tends to converge to a certain value as the amplitude of forcing increases. This trend in the resonant frequency can also be found in the dependence of response frequency on the amplitude of vibration for a piecewise linear system with initial gaps [46].

Jump phenomenon

For the rotating condition, the existence of multiple solutions has been observed for some values of the forcing $\mathbf{b}$. As an example, the response for $||\mathbf{b}||$=8.89N is shown as Fig. 2.9. This force level resulted in the *jump phenomenon* in the frequency response: as the excitation frequency was swept up through this region, the amplitude of vibration

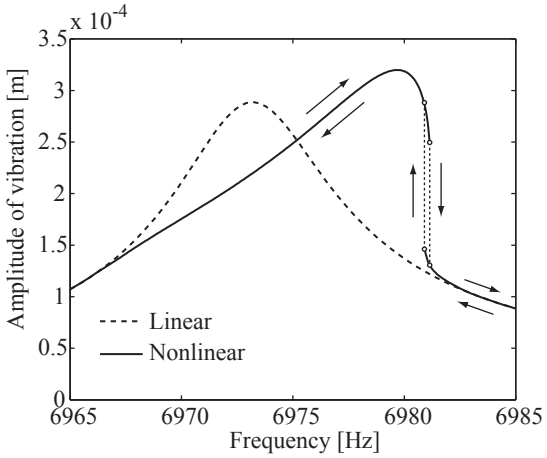

Figure 2.9: Frequency response for $||\mathbf{b}|| = 8.89$N

jumped down to the lower branch of the solutions at a certain frequency; and as the frequency was swept down through this range, the amplitude jumped up to the upper branch of the solutions at a different frequency. It is known that the jump phenomenon occurs in many nonlinear systems (see Ref. [17], for example). For piecewise linear systems with clearances in particular, it has been reported that the phenomenon occurs in many systems such as simple mass-spring discrete systems [49], blades with nonlinear shroud constraints [19], and piecewise linear vibration isolators [50]. For a piecewise linear vibration isolator, the phenomenon was observed experimentally by Narimani *et al.* [51], for example. The numerical results shown in Fig. 2.9 suggest that the jump phenomenon might be observed in tests of rotating cracked blades as well, although the author is not aware of any such experimental findings.

2.4.2 Resonant frequency shift

Problem statement

As discussed in previous sections, the resonant frequencies of cracked blades cannot be predicted precisely from the natural frequency of the linear system. Moreover, if a gap between the crack surfaces exists, the resonant frequency may be dependent on the

forcing level. Thus, the nonlinear effects due to the crack surfaces as well as the rotation effects can both play a key role in determining the resonant frequencies of the rotating cracked blades. For example, suppose the resonant frequencies are used to identify the information of the cracks (e.g., the length of the cracks), the natural frequency may not predict it correctly. In other words, the crack length deduced from the natural frequencies may be smaller than the one predicted from the actual resonant frequencies.

In this section, the effects of rotation on the crack-induced frequency shift for various lengths of cracks are investigated. The same blade model as in the previous section is used. The modes of interest are the tenth mode, which was discussed earlier, and the sixth mode, which is the first edgewise bending mode shown in Fig. 2.6a The frequency shift *FS* is defined as

$$FS = \frac{f_r - f_0}{f_0} \tag{2.28}$$

where f_r is the resonant frequency of the cracked blade, and f_0 is the natural frequency of the non-cracked blade. The parameters for the HFT methods, such as the number of harmonics and the value of penalty coefficient, are the same as those used in the previous section. For both static and rotating cases, the value of the amplitude of the force is chosen to be $||\mathbf{b}|| = 6.67$ N.

Results

The resonant frequency versus the crack length ratio for the tenth mode and the sixth mode are shown in Figs. 2.10a and 2.11a. The frequency shift FS versus the crack length ratio is plotted in Figs. 2.10b and 2.11b.

First, there is a clear distinction between the static and the rotating cases for both modes as shown in both Fig. 2.10a and 2.11a. Specifically, the natural frequencies for the rotating cases are greater than those of the static cases for a given crack length ratio. This

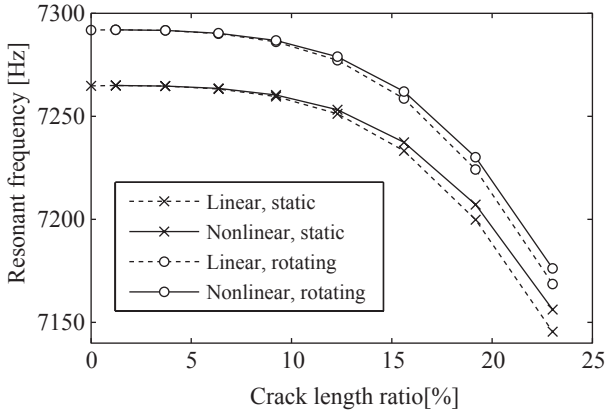

(a)

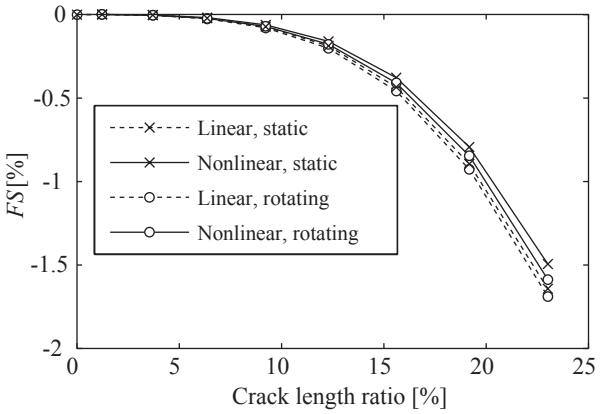

(b)

Figure 2.10: Frequency shift for the tenth mode: (a) resonant frequency versus crack length, (b) resonant frequency shift versus crack length

is due to the change in the stiffness matrix of the FE model by the centrifugal loading, which appears in Eq. (2.2). (Although only the stiffness matrix of the original FE model is changed by the inertial effect, both mass and stiffness matrices of the reduced-order model are changed.)

Second, the effect of nonlinearity becomes more significant as the crack length grows, i.e., the difference between the resonant frequencies of the nonlinear cases and the linear cases for both static and rotating cases becomes more apparent. However, the effect of rotation on the degree of nonlinearity (i.e., the qualitative change in the frequency re-

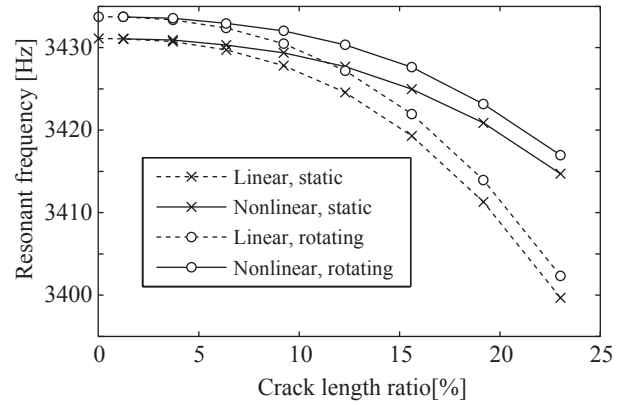

(a)

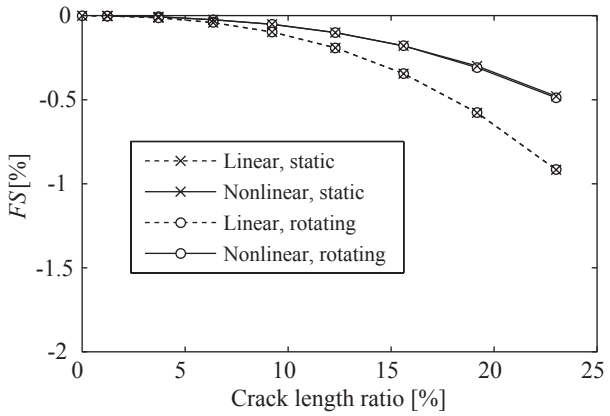

(b)

Figure 2.11: Frequency shift for the sixth mode: (a) resonant frequency versus crack length, (b) resonant frequency shift versus crack length

sponse due to the existence of the gap between the crack surfaces discussed in the previous section) is not evident in the resonant frequencies themselves.

On the other hand, if the frequency shift FS is considered, the distinction due to the inertial effects nearly vanishes. Therefore, one can almost isolate the effects of nonlinearity from the resonant frequencies. For the tenth mode, there is not a significant difference between linear and nonlinear cases for both static and rotating conditions. This is because the motion of the crack surfaces is almost perpendicular to the normal directions of these surfaces at the moment of contact, as can be seen in Fig. 2.6b.

For the sixth mode however, we can see a large difference between the linear and nonlinear cases. This is because the motion of the crack surfaces is mostly along the normal directions of these surfaces at the moment of contact. In this case, the contact forces on the crack surfaces have a significant stiffening effect on the resonant vibration frequency.

2.5 Conclusions

An efficient method was presented for reduced-order modeling and nonlinear vibration analysis of rotating cracked structures. This method accounts for the change in the equilibrium configuration of the crack surfaces due to rotation and the attendant influence on the forced vibration response due to the intermittent contact of the crack surfaces.

The individual and combined effects of rotation and intermittent contact on the forced response were examined in detail for an example of a cracked blade. First, a validation study was conducted by comparing the results obtained by the proposed method with those obtained by time integration for a cracked beam. The proposed method produced results that agree very well with those calculated by time integration while reducing computational costs by as much as five orders of magnitude. Second, the amplitude dependence of the forced response of a cracked blade was investigated. It was found that the frequency response is dependent on the forcing level only if the blade is rotating. This is due to the existence of an initial gap between the crack surfaces for the rotating equilibrium position, which causes a qualitative change in the frequency response. For some forcing levels, the jump phenomenon was observed. Third, the crack-induced shifts in resonant frequencies of the blade were investigated for various crack lengths. It was shown that the effect of rotation on the resonant frequencies is significant in terms of: (1) the stiffening effect due to the change in the system matrices, and (2) the qualitative change in the nonlinear sys-

tem due to the initial gap. The influence of nonlinearity on the resonant frequency did not appear to exceed that of the stiffening effect. On the other hand, the effect of nonlinearity on the frequency *shift* is more significant than the effect from rotation.

Although fairly simple beam and blade finite element models were used in this chapter, the proposed method can be applied to more realistic, large-scale finite element models of complex structures. In particular, the capability of efficiently predicting crack-induced frequency shifts suggests that the proposed method may be applicable to structural health monitoring of rotating structures, such as bladed disks in turbine engines.

CHAPTER III

Effects of a Cracked Blade on Mistuned Turbine Engine Rotor Vibration

3.1 Introduction

In the typical design of each stage (bladed disk) of a turbine engine rotor, all blades are intended to be identical. Thus, for the nominal design, the vibration analysis can be greatly simplified by using cyclic symmetry solvers. However, the cyclic symmetry of a bladed disk is destroyed if there are small differences in material properties or geometric characteristics among the blades, which is called mistuning. Although mistuning is typically small in terms of individual blade properties (e.g., blade-alone natural frequency variations on the order of 1%), it can have a drastic effect on the system response. In particular, mistuning can cause localization of the vibration about a few blades, and the attendant concentration of vibration energy can lead to sharp increases in maximum blade amplitude and stress levels. Therefore, a large amount of research has been conducted for analyzing the vibration of mistuned bladed disks, which has been summarized in several survey papers [9–11].

In contrast, there have been relatively few papers published to date concerning localization and other effects on the forced vibration response of bladed disks due to cracking of blades. The studies by Kuang and Huang [12, 13] considered free and forced response

analysis of rotating, shrouded bladed disks by modeling each blade as an Euler-Bernoulli beam where the crack effect was treated as local disorder of the system. They showed that the existence of the crack may change the vibration response of a bladed disk significantly, and cause mode localization. In their recent work [14], they analyzed the stability of a rotating bladed disk using Euler-Bernoulli beam models in conjunction with Galerkin's method for formulating the equations of motion, which they solved with perturbation techniques. Fang *et al.* [15] investigated the vibration localization of bladed disks due to cracks for various parameters—including internal coupling factor, crack severity, engine order of excitation, and number of blades—using a model with blades being treated as Euler-Bernoulli beams, and the crack being treated as a local stiffness loss based on a fracture mechanics model. It was shown that even a small crack can cause vibration mode and forced response localization. Hou [16] investigated crack-induced mistuning in an analytical study based on a lumped-mass beam model, in which the local stiffness loss due to cracking was expressed with a flexibility matrix method. McAdams *et al.* [52] examined the effects of crack and manufacturing variations on the vibrational response of turbine engine blades using finite difference and lumped parameter models of Euler Bernoulli beams with the crack being modeled as a local decrease in Young's modulus.

However, these previous studies used simplified models for cracked blades. Most importantly, their models were *linear*. That is, *the nonlinearity caused by the crack closing effect was not taken into account*, which may change the dynamic response of the cracked blades significantly (see [3] for example). The crack closing effect is the displacement-dependent nonlinearity caused by the repetitive opening and closing of crack surfaces during each vibration cycle, which occurs especially when a fatigue-induced crack is considered. Therefore, the forced response analysis of beams or blades with closing cracks is fundamentally nonlinear, and typically difficult to solve.

In this chapter, an efficient nonlinear vibration analysis method for predicting the forced response of a rotor with a cracked blade is presented and used to carry out numerical investigations. The analysis technique is summarized as follows. Starting with a finite element (FE) model of a representative bladed disk with one cracked blade, a hybrid-interface method of component mode synthesis (CMS) is used to retain the FE degrees of freedom (DOF) on the crack surfaces as active (physical) DOF for evaluation of nonlinear boundary conditions while condensing the other DOF with modal analysis. This yields an accurate and compact reduced-order model (ROM) that can be used for the nonlinear forced response analysis. Then, the nonlinear steady-state response analysis is performed using a Hybrid Frequency/Time (HFT) domain method, which is based on the application of Harmonic Balance Method [17] in conjunction with the Fast Fourier Transform (FFT) for the evaluation of nonlinear forces. Pioneering contributions for using this type of technique include the Fast Galerkin method of Ling and Wu [24] and the Alternating Frequency/Time domain method of Cameron and Griffin [23]. Since then, this approach has been applied to analyze various types of forced vibration problems of nonlinear systems, such as the recent studies on simplified cracked rotating shafts [53], torsional systems with clearance nonlinearity [54], and friction dampers for bladed disks [55]. Poudou and Pierre [29] applied the HFT method to the nonlinear forced response analysis of cracked beams with closing cracks, which was followed by the extension of the method to the analysis of rotating cracked blades [56].

There are three main contributions of this chapter. The first is to extend the analysis framework previously developed by the authors for a single cracked blade [29, 56] to a full blade assembly with a cracked blade, including accounting for both mistuning and nonlinear crack closing effects. The second is to provide a better understanding of the fundamental vibration response characteristics of such systems and to examine the impli-

cations of various levels of approximation with respect to modeling the cracked blade. The third is to consider potential applications of the proposed method and the new findings to damage detection and structural health monitoring of turbomachinery rotors.

This chapter is organized as follows. In section 3.2, the mathematical formulations of the reduced-order modeling approach and the HFT method are briefly reviewed. In section 3.3, a numerical validation of the proposed reduced-order modeling approach is performed by applying the hybrid CMS method to the nonlinear forced response problem of a single-piece bladed disk (blisk) with a cracked blade. The results are then compared with the results obtained with the ROM generated from the classical Craig-Bampton CMS method [26]. In section 3.4, results of nonlinear forced response analyses for rotors with a cracked blade are shown. In particular, the relationship between the analysis of a blade alone and the full blisk, the effects of mistuning, and the effects of rotation are discussed in detail. The conclusions from this chapter are stated in section 3.5.

3.2 Mathematical Formulation

3.2.1 Equations of Motion

Assuming a rotor with a cracked blade is modeled as a linear elastic structure and the associated governing equation is spatially discretized by the finite element method, the semi-discrete form of the governing equation is written as

$$\mathbf{M}\ddot{\mathbf{u}}(t) + \mathbf{C}\dot{\mathbf{u}}(t) + \mathbf{K}\mathbf{u}(t) = \mathbf{b}(t) + \mathbf{f}(\mathbf{u}) \tag{3.1}$$

where $\mathbf{u}, \mathbf{b}, \mathbf{f} \in \mathbb{R}^n$, $\mathbf{M}, \mathbf{C}, \mathbf{K} \in \mathbb{R}^{n \times n}$, n is the number of DOF, $\mathbf{u}$ is a vector of nodal displacements of all nodes, $\mathbf{M}$, $\mathbf{C}$, and $\mathbf{K}$ are mass, damping, and stiffness matrices, $\mathbf{b}$ is the external force vector, and $\mathbf{f}(\mathbf{u})$ is the nonlinear force vector caused by the intermittent contact at the crack. The external force acting on each blade is assumed to be a traveling wave excitation whose frequency is related to the rotational speed of the rotor, which is

called engine order excitation. The force on each blade is expressed here as:

$$\mathbf{b}_i(t) = \boldsymbol{\beta} \cos\left(\omega t - \phi_i\right), i = 1, \ldots, N \tag{3.2}$$

where i is the blade number, N is the total number of blades, $\boldsymbol{\beta}$ is the forcing amplitude vector, and ω is the angular frequency of excitation. The term ϕ_i is the interblade phase angle, defined as $\phi_i = (i-1)2\pi C/N$, where C is the (integer) engine order of excitation.

3.2.2 Reduced-Order Modeling

Finite element models of rotors typically have a large number of DOF and hence the computational cost of vibration analyses can be expensive. In chapter II, the Craig-Bampton method [26] of CMS was used to reduce the model size before performing nonlinear forced response analysis of a rotating cracked blade. In particular, the motion was represented by a linear combination of static constraint modes and a truncated set of fixed-interface normal modes, and the associated ROM was obtained. The Craig-Bampton method is a stable reduced-order modeling technique that enables one to retain the crack surface DOF as physical coordinates while condensing the remaining DOF with modal analysis. However, for studies of cracked structures, it suffers from slow modal convergence because of the discrepancy between the boundary condition to calculate the fixed-interface normal modes and that of the actual vibration problem of the cracked structures. Namely, the actual response shape of the cracked structure is dissimilar to the fixed-interface normal modes, which are the modes of the structure with the crack surface DOF held fixed.

In order to enhance the modal convergence characteristics of the ROM, a free-interface or hybrid CMS technique can be employed. In this study, a hybrid CMS method is used. The Ritz vectors used in the method are constraint modes $\boldsymbol{\Psi}_c$, inertia relief attachment modes $\boldsymbol{\Psi}_a$ (if rigid body motion exists), and a truncated set of free-interface normal modes

$\mathbf{\Phi}_k$. The use of free-interface normal modes instead of fixed-interface normal modes assures faster modal convergence of the ROM, as discussed in section 3.3. Let the displacement vector $\mathbf{u}$ be partitioned into boundary DOF, $\mathbf{u}_b$, and interior DOF $\mathbf{u}_i$. By denoting the inertia relief attachment coordinates, and a truncated set of free-interface modal coordinates as $\mathbf{p}_a$ and $\mathbf{p}_k$, the linear projection is represented as [57],

$$\mathbf{u} = \mathbf{\Psi}_H \mathbf{q}, \text{ or } \begin{bmatrix} \mathbf{u}_b \\ \mathbf{u}_i \end{bmatrix} = \begin{pmatrix} \mathbf{I} & \mathbf{0} & \mathbf{0} \\ \mathbf{\Psi}_{ic} & \hat{\mathbf{\Psi}}_a & \hat{\mathbf{\Psi}}_k \end{pmatrix} \begin{bmatrix} \mathbf{u}_b \\ \mathbf{p}_a \\ \mathbf{p}_k \end{bmatrix} \tag{3.3}$$

where $\hat{\mathbf{\Psi}}_a = \mathbf{\Psi}_{ia} - \mathbf{\Psi}_{ic}\mathbf{\Psi}_{ba}$, $\hat{\mathbf{\Psi}}_k = \mathbf{\Phi}_{ik} - \mathbf{\Psi}_{ic}\mathbf{\Phi}_{bk}$, $\mathbf{I}$ is the identity matrix, $\mathbf{\Psi}_{ic}$ is the boundary partition of $\mathbf{\Psi}_c$, $\mathbf{\Psi}_{ia}$ and $\mathbf{\Psi}_{ba}$ denote the interior and the boundary partitions of $\mathbf{\Psi}_a$, and $\mathbf{\Phi}_{ik}$ and $\mathbf{\Phi}_{bk}$ denote the interior and the boundary partitions of $\mathbf{\Phi}_k$. It should be noted that the size of $\mathbf{q}$, defined here as n_r, is typically much smaller than n, and thereby the application of Eq. (3.3) to Eq. (3.1) yields a much smaller number of equations:

$$\mathbf{M}_H \ddot{\mathbf{q}} + \mathbf{C}_H \dot{\mathbf{q}} + \mathbf{K}_H \mathbf{q} = \overline{\mathbf{b}} + \overline{\mathbf{f}}(\mathbf{q}) \tag{3.4}$$

where $\mathbf{M}_H = \mathbf{\Psi}_H^{\mathrm{T}} \mathbf{M} \mathbf{\Psi}_H$, $\mathbf{C}_H = \mathbf{\Psi}_H^{\mathrm{T}} \mathbf{C} \mathbf{\Psi}_H$, $\mathbf{K}_H = \mathbf{\Psi}_H^{\mathrm{T}} \mathbf{K} \mathbf{\Psi}_H$, $\overline{\mathbf{b}} = \mathbf{\Psi}_H^{\mathrm{T}} \mathbf{b}$, and $\overline{\mathbf{f}} = \mathbf{\Psi}_H^T \mathbf{f}$. In the following subsections, the subscript H as well as the bars are omitted for convenience.

3.2.3 Intermittent Contact Problem for a Cracked Structure

Here the treatment of nonlinear boundary conditions at the crack surfaces is briefly reviewed. The nonlinear force acting on a pair of nodes on both surfaces are calculated by a method developed by Poudou *et al.* [28, 42]. Namely, suppose there is a pair of possibly contacting nodes during the vibration, denoted by c, with initial gap g_c along their normal, and the relative displacement of those nodes along the normal direction of the surfaces is

expressed as $q_c(t)$. Assuming frictionless contact, the contact force acting upon the contact pair along the normal, f_c, at a discrete time instant t_i, is then expressed as the following relationship [28]

$$f_c(q_c(t_i)) = k^*(q_c^*(t_i) - q_c(t_i)) \tag{3.5}$$

where $0 \leqslant t_i \leqslant 2\pi/\omega$, $i = 1, \ldots, n_t$, n_t is the number of sampling points for taking the FFT, k^* is a given penalty parameter, $q_c(t_i)$ is the displacement of contacting DOF, and $q_c^*(t_i)$ is the *reference* displacement defined as $q_c^*(t_i) = q_c(t_i)$ if $q_c(t_i) \leqslant g_c$, and $q_c^*(t_i) = g_c$ if $q_c(t_i) \geqslant g_c$, which satisfies the boundary condition exactly and converges toward $q_c(t)$ in the limit of $k^* \to \infty$.

3.2.4 Hybrid Frequency/Time Domain Method

For steady-state response, it is assumed that $\mathbf{q}(t)$ can be approximated with a truncated Fourier series:

$$\mathbf{q}(t) = \sum_{k=0}^{n_h} (\mathbf{Q}_k^c \cos(k\omega t) + \mathbf{Q}_k^s \sin(k\omega t)) \tag{3.6}$$

where superscripts *c* and *s* denote cosine and sine components, and n_h denotes the number of non-zero harmonics. It is noted that only the super-harmonic components are considered in this formulation, as the nonlinearity caused by the crack is assumed to be weak enough in the sense that period-doubling bifurcation as well as the subsequent transition to chaotic behavior do not occur, which entails sub-harmonic components in the response even if the external forcing is single-harmonic excitation [58, 59]. Furthermore, a preliminary study by the authors showed that the sub-harmonic components were not significant for the nonlinear forced response of similar structures.

Assuming that $\mathbf{b}(t)$ and $\mathbf{f}(\mathbf{q})$ can also be expressed as truncated Fourier series that are similar to Eq. (3.6), application of the method of Harmonic Balance [17] then yields a set

of nonlinear algebraic equations:

$$\mathbf{\Lambda Q} = \mathbf{B} + \mathbf{F}(\mathbf{Q}) \tag{3.7}$$

where $\mathbf{Q}$, $\mathbf{B}$, and $\mathbf{F}$ contain Fourier coefficients of $\mathbf{q}$, $\mathbf{b}$, and $\mathbf{f}$, i.e.,

$$\mathbf{Q} = [(\mathbf{Q}_0^c)^{\mathrm{T}}, (\mathbf{Q}_1^c)^{\mathrm{T}}, (\mathbf{Q}_1^s)^{\mathrm{T}}, \ldots, (\mathbf{Q}_{n_h}^c)^{\mathrm{T}}, (\mathbf{Q}_{n_h}^s)^{\mathrm{T}}]^{\mathrm{T}} \tag{3.8}$$

$$\mathbf{B} = [(\mathbf{B}_0^c)^{\mathrm{T}}, (\mathbf{B}_1^c)^{\mathrm{T}}, (\mathbf{B}_1^s)^{\mathrm{T}}, \ldots, (\mathbf{B}_{n_h}^c)^{\mathrm{T}}, (\mathbf{B}_{n_h}^s)^{\mathrm{T}}]^{\mathrm{T}} \tag{3.9}$$

$$\mathbf{F} = [(\mathbf{F}_0^c)^{\mathrm{T}}, (\mathbf{F}_1^c)^{\mathrm{T}}, (\mathbf{F}_1^s)^{\mathrm{T}}, \ldots, (\mathbf{F}_{n_h}^c)^{\mathrm{T}}, (\mathbf{F}_{n_h}^s)^{\mathrm{T}}]^{\mathrm{T}} \tag{3.10}$$

and $\mathbf{\Lambda}$ is a matrix with $\mathbf{\Lambda}_k$ on its diagonal blocks defined as

$$\mathbf{\Lambda}_k = \begin{cases} \mathbf{K} & \text{for } k = 0 \\ \begin{pmatrix} -(k\omega)^2\mathbf{M} + \mathbf{K} & (k\omega)\mathbf{C} \\ -(k\omega)\mathbf{C} & -(k\omega)^2\mathbf{M} + \mathbf{K} \end{pmatrix} & \text{for } 1 \leqslant k \leqslant n_h \end{cases} \tag{3.11}$$

It is noted that the size of Eq. (3.7) is $n_r(2n_h + 1)$ if all harmonics from $k = 1$ through n_h are used. The Fourier coefficients of the nonlinear force, $\mathbf{F}(\mathbf{Q})$, are evaluated by applying the FFT to the time history of the nonlinear force, which is calculated by Eq. (3.5), for all pairs of contacting DOF.

The size of the nonlinear algebraic equations is further reduced by applying a condensation technique to the linear DOF [20, 29] of Eq. (3.7) as follows. The equations for the kth harmonic number of Eq. (3.7) can be written in the following partitioned form:

$$\begin{pmatrix} \mathbf{\Lambda}_k^{nl,nl} & \mathbf{\Lambda}_k^{nl,l} \\ \mathbf{\Lambda}_k^{l,nl} & \mathbf{\Lambda}_k^{l,l} \end{pmatrix} \begin{bmatrix} \mathbf{Q}_k^{nl} \\ \mathbf{Q}_k^{l} \end{bmatrix} = \begin{bmatrix} \mathbf{B}_k^{nl} \\ \mathbf{B}_k^{l} \end{bmatrix} + \begin{bmatrix} \mathbf{F}_k^{nl} \\ \mathbf{0} \end{bmatrix} \tag{3.12}$$

where superscripts nl and l denote the partitions for nonlinear and linear DOF, respectively. Namely, the nonlinear DOF are defined as the DOF where the contact force Eq. (3.5) is applied, whereas all the other DOF are defined as the linear DOF. By solving the lower

partition of the Eq. (3.12) for $\mathbf{Q}_k^l$, and substituting it to the upper partition of the equation, the equation can now be written with $\mathbf{Q}_k^{nl}$ only:

$$\mathbf{\Lambda}_k^{\mathrm{red}}\mathbf{Q}_k^{nl} = \mathbf{B}_k^{\mathrm{red}} + \mathbf{F}_k^{nl}(\mathbf{Q}^{nl}) \tag{3.13}$$

where $\mathbf{\Lambda}_k^{\mathrm{red}} = \mathbf{\Lambda}_k^{nl,nl} - \mathbf{\Lambda}_k^{nl,l}(\mathbf{\Lambda}_k^{l,l})^{-1}\mathbf{\Lambda}_k^{l,nl}$ and $\mathbf{B}_k^{\mathrm{red}} = \mathbf{B}_k^{nl} - \mathbf{\Lambda}_k^{nl,l}(\mathbf{\Lambda}_k^{l,l})^{-1}\mathbf{B}_k^{l}$. Assembling Eq. (3.13) for all k results in $n_{cp}(2n_h + 1)$ nonlinear equations to be solved, where n_{cp} denotes the number of contact pairs:

$$\mathbf{\Lambda}^{\mathrm{red}}\mathbf{Q}^{nl} = \mathbf{B}^{\mathrm{red}} + \mathbf{F}^{nl}(\mathbf{Q}^{nl}) \tag{3.14}$$

where $\mathbf{\Lambda}^{\mathrm{red}}$ is a pseudo-block diagonal matrix with $\mathbf{\Lambda}_k^{\mathrm{red}}$ for all k along the diagonal, $\mathbf{Q}^{nl} = [(\mathbf{Q}_0^{nl})^{\mathrm{T}}, \ldots, (\mathbf{Q}_{n_h}^{nl})^{\mathrm{T}}]^{\mathrm{T}}$, $\mathbf{B}^{nl} = [(\mathbf{B}_0^{nl})^{\mathrm{T}}, \ldots, (\mathbf{B}_{n_h}^{nl})^{\mathrm{T}}]^{\mathrm{T}}$, and $\mathbf{F}^{nl} = [(\mathbf{F}_0^{nl})^{\mathrm{T}}, \ldots, (\mathbf{F}_{n_h}^{nl})^{\mathrm{T}}]^{\mathrm{T}}$. The nonlinear equations are then solved by the hybrid Powell method [27] in conjunction with an iterative method that successively solves the equations with increasing penalty parameter k^* [28]. It is noted that at each iteration step, the nonlinear force Eq. (3.5) is evaluated for a given trajectory of q_c in the *time* domain, and an FFT is taken to convert it to the *frequency* domain. The nonlinear equations are then solved, and the obtained Fourier coefficients of $\mathbf{Q}$ are transformed back to the *time* domain again, in order to be used to evaluate the nonlinear force Eq. (3.5). This process is repeated until the solution converges.

3.3 Numerical Validation of Hybrid CMS Method

In this section, a numerical validation of the hybrid CMS method is carried out. Both Craig-Bampton and hybrid CMS methods are applied to the FE model of a blisk with one cracked blade, and the associated nonlinear forced response analyses are performed. It is noted that the Craig-Bampton method used with HFT method was numerically validated with time integration method [56], and therefore the results with the Craig-Bampton

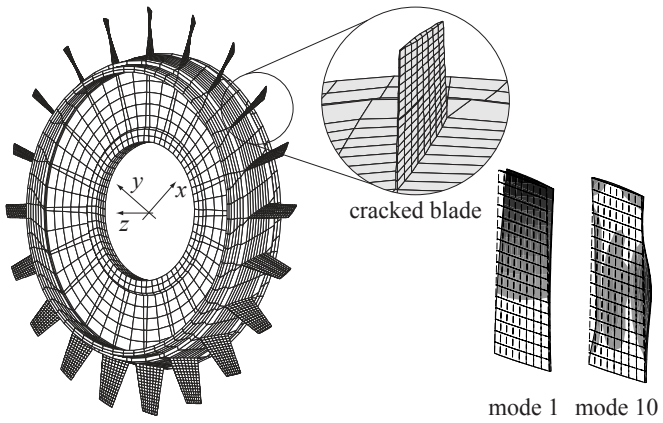

Figure 3.1: Finite element model of the blisk with a 37.5% cracked blade, and healthy blade modes of interest

method are used here as reference results.

The FE model used in this study was a representative academic blisk model with 20 blades, consisting of 19 identical, healthy blades and one cracked blade, as shown in Fig. 3.1. The material was modeled as a Titanium alloy with Young's modulus $E = 114\text{GPa}$, density $\rho = 4420\text{kg}/\text{m}^3$, and Poisson's ratio $\nu = 0.31$. This model is used throughout this chapter.

The modes of interest in this study are the blade-dominated modes—that is, modes for which most of the vibration energy is concentrated in the blades. Such modes are typically much more sensitive to the cracking of blades than the ones that are disk-dominated. For some blade-dominated modes, both the system mode shapes and the natural frequencies are greatly affected by the cracking. Therefore, modeling, simulating, and understanding the effects of cracks on blade-dominated modes are investigated in this work, with the underlying goal of providing the foundation for developing new crack detection methods for turbine engine rotors.

The initial frequency region of interest corresponds to the first blade-dominated mode family, whose natural frequencies lie in the range 382.3–388.9 Hz. The blade motion in

this family of modes is characterized by the first flexural bending mode of a blade (mode 1 in Fig. 3.1).

The system was excited by applying harmonic forcing at the tip of each blade with engine order 2 excitation. The nodes on the rims of the disk were constrained only along the axial (z) direction, such that the disk could slide in the $x - y$ plane. The resulting number of DOF was 33,498. The damping model was Rayleigh damping without mass matrix contribution, i.e., $\mathbf{C} = \beta\mathbf{K}$ where $\beta = 2\zeta_r/\omega_r$, and the modal damping ratio ζ_r was assumed to be 0.001.

For the generation of the ROM, 20 nodes located at the blade tips (one node per blade) and 12 nodes on the crack surfaces (6 contact pairs) were kept as active DOF. The number of normal modes kept for each method was 100. This resulted in an ROM size of 196 DOF for each method. For the generation of the ROMs by both methods, the commercial FE software ANSYS [40] was used.

With these ROMs, the nonlinear forced response was calculated with the HFT method with $n_h = 9$, and with 6 contact pairs this yielded 114 unknown variables in Eq. (3.7). The results are shown in Fig. 3.2 where only the envelope of displacement norms at the tips of all blades are shown. As can be seen, the response calculated with the hybrid ROM agrees very well with that calculated with Craig-Bampton ROM. It should be noted at this point that there are two peaks in the response: the peak at higher frequency contributed from the responses of healthy (non-cracked) blades, and the other one solely from the cracked blade. A detailed discussion about this is given in later sections.

In order to examine the mode participation from each normal mode, the averaged mode participation factor over the frequency range was defined as

$$\overline{\mathbf{Q}} \triangleq (1/n_f) \sum_{k=1}^{n_f} \mathbf{Q}(\omega_k)/||\mathbf{Q}(\omega_k)||_2 \tag{3.15}$$

where n_f is the number of sampling points over the frequency range and ω_k is the frequency at the kth sampling point. As plotted in Fig. 3.3a, there are approximately 100 contributing modes from a wide range of frequencies when the system was modeled with the CB method. This indicates that a large number of normal modes must be retained in the ROM to achieve high accuracy, which could become a major problem as the number of DOF or the number of blades increases. On the other hand, as can be seen in Fig. 3.3b, there are only 23 significantly responding modes for the model employing the hybrid CMS method, which are in the frequency range of the first blade-dominated mode family. This indicates that, for the calculation of nonlinear forced response of the blisk with a cracked blade, only a relatively small number of modes need to be retained to form the ROM if the hybrid method used. As such, a new ROM was generated with these 23 modes, and the same nonlinear forced response calculation was performed. These results are also shown in Fig. 3.2, and it is seen that the ROM with 23 modes produced an accurate solution with relative error of less than 0.051% over the frequency range of interest. Thus, the hybrid-interface CMS method has an advantage over the fixed-interface Craig-Bampton CMS method for producing a compact yet accurate ROM that can be used for the nonlinear forced response analysis of a rotor with a cracked blade.

3.4 Analysis of the Blisk with a Cracked Blade

In this section, the forced response analysis of a blisk with a cracked blade is investigated with the proposed analysis framework. In addition, the applicability of this analysis framework to structural health monitoring is discussed.

3.4.1 Linear Cracked Blade Model Versus Nonlinear Cracked Blade Model

If one creates an FE model with a crack and performs forced response analysis or modal analysis without considering the crack-closing effect, then the response is linear.

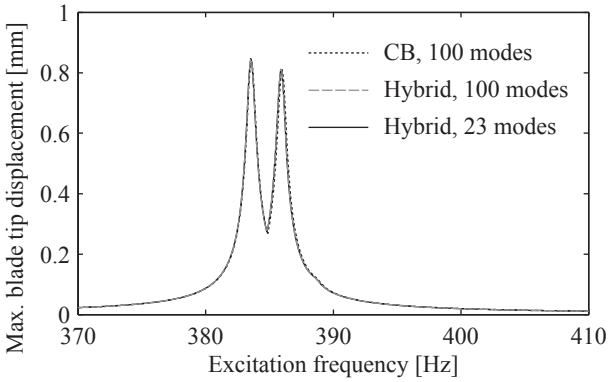

Figure 3.2: Nonlinear frequency response of the blisk with a cracked blade subjected to engine order 2 excitation

This modeling approach does not preserve cyclic symmetry in the geometry of the tuned system, but it does yield a linear system. This approach is referred to as linear cracked blade model in this chapter. The nonlinear cracked blade model is the cracked blade model where the intermittent contact of the crack surfaces during the vibration is fully considered.

In Fig. 3.4a and c, the forced response in the frequency ranges of the first and tenth blade-dominated mode families are shown for the blisk with the nonlinear cracked blade model.

The harmonics used for the results in Figs. 3.4a and 3.4c were 0–9, and the value of the penalty coefficient was $k^* = 1.0 \times 10^6$N/mm. These values are used for the subsequent analyses in this chapter. It is noted that a convergence study showed that the resonant frequencies of cracked-blade-dominated modes shown in Fig. 3.4a and c have at most 0.01% relative error with respect to the results calculated with two orders of magnitude greater penalty coefficient. As can be seen, the frequency response function predicted by the linear cracked blade does not match that predicted by the nonlinear cracked blade model. The most notable distinction between the results from the linear model and the nonlinear model

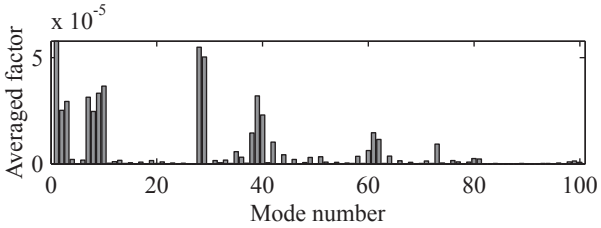

(a) Fixed-interface normal modes (Craig-Bampton method)

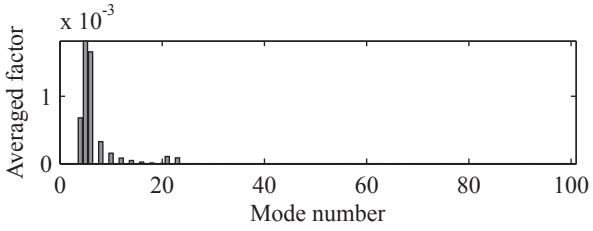

(b) Free-interface normal modes (hybrid method)

Figure 3.3: Averaged mode participation factor versus mode number

is that the resonant frequencies of the cracked-blade-dominated response shift significantly toward higher frequencies for the nonlinear case. This effect is due to the intermittent contact at crack surfaces, the so-called closing or breathing crack effect. Namely, the stiffness of the cracked blade is underestimated by the linear model that neglect contact, and so are the resonant frequencies. In summary, the behavior of the nonlinear model cannot be precisely captured by a linear model in terms of predicting vibration amplitudes and resonant frequency shifts. However, the shifts in resonant frequencies can be estimated from the analysis of a single cracked blade [56].

3.4.2 Relevance of the Analysis of a Blade Alone

As briefly mentioned in the previous subsection, the cracked-blade-localized modes are isolated from the other modes in the mode family for the cases shown in Fig. 3.4a and c. Furthermore, it appears that the effect of crack-induced nonlinearity on the other modes in the family is much smaller than the influence on the resonances of the cracked blade

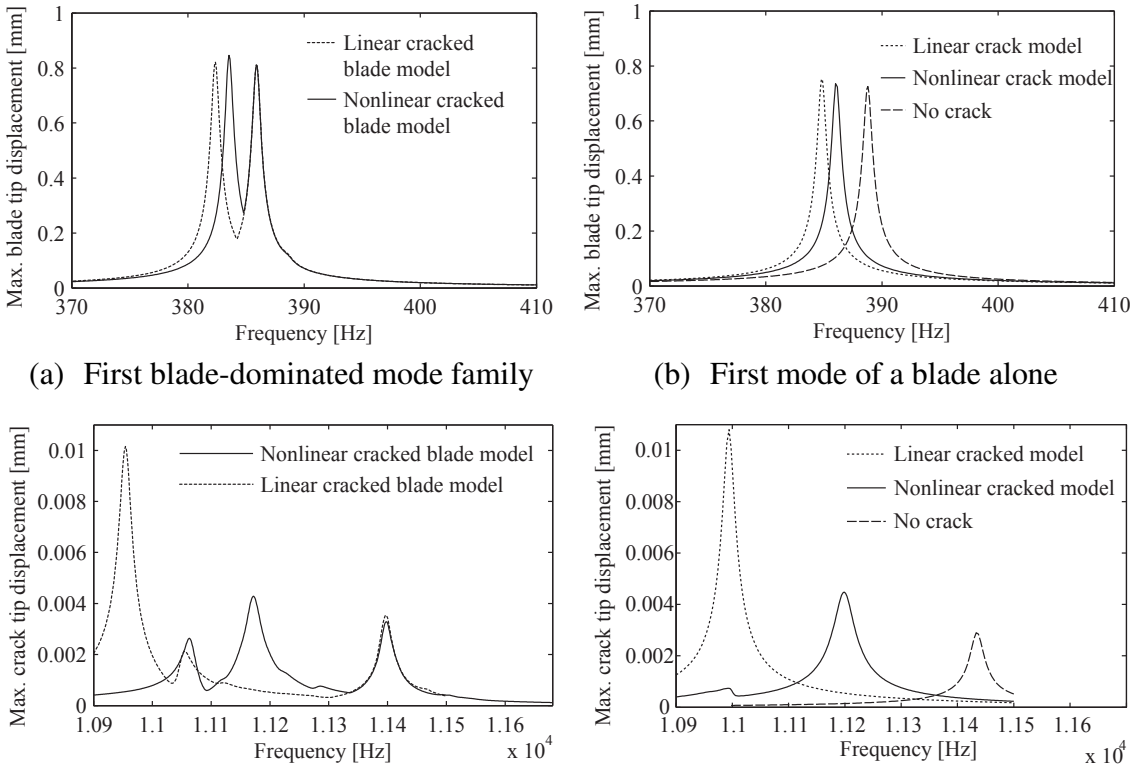

(a) First blade-dominated mode family

(b) First mode of a blade alone

(c) Tenth blade-dominated mode family

(d) Tenth mode of a blade alone

Figure 3.4: Frequency response of the bladed disk model with a cracked blade, and the blade-alone models

itself. With this observation, the corresponding cracked blade is analyzed in isolation, with a cantilevered boundary condition at the disk-blade interface, and its relationship to the blisk with a cracked blade is discussed.

The blade-alone modes of interest are the first and tenth modes (see Fig. 3.1), which correspond to the dominant blade motion in the families of blisk modes analyzed in the previous section. The corresponding FE model of the cracked blade was the same component of the original FE model of the blisk. The reduced-order model consisted of 39 active DOF and 100 modal coordinates. The harmonics used in the HFT method were 0–9 for the calculation of the first and tenth mode. Following the same analysis framework as before, the forced response calculations of the cantilevered blade were performed. The results for the frequency ranges of the first and tenth blade modes are shown in Figs. 3.4b and 3.4d. Clearly, these results show that the response of the blade alone qualitatively agrees with the response of a corresponding blisk with a cracked blade shown in Figs. 3.4a and 3.4c. That is, the resonances for linear cracked, nonlinear cracked, and uncracked models of the cantilevered blade are in agreement with their blisk counterparts. This indicates that for these particular modes with this crack length, the vibration behavior of a blisk could be qualitatively captured by the blade-alone analysis. Indeed, although the absolute values of the resonant frequencies do not coincide, if one compares the ratio of frequency *shifts* for both the blisk with a cracked blade and blade-alone cases, they are in good agreement with approximately 0.1% absolute error as shown in Table 3.1.

From a structural health monitoring perspective, this may indicate that the results of a blade-alone analysis could be used in combination with frequency response data measured for the full rotor to detect a crack in a blade and estimate its severity. Note, however, that the effects of blade mistuning have not been taken into account yet. The combined effects of a crack and mistuning are investigated in the next subsection.

Table 3.1: Comparison of Frequency Shifts (FS)

Mode	FS with blade alone [%]	FS with blisk [%]
First	-0.7167	-0.6085
Tenth	-2.050	-1.980

3.4.3 Effects of Mistuning

For the analyses in the previous sections, the blisks were assumed to be tuned except for the existence of a crack. However, for real systems, small mistuning effects exist due to various factors such as manufacturing tolerances and in-service wear. Thus, it is desirable to consider the small mistuning effects in the analysis to simulate the realistic conditions. In this chapter, the small mistuning effect is assumed to have a negligible effect on the blade-alone mode shapes and only alter the blade-alone natural frequencies or modal stiffnesses. In particular, it is introduced simply by altering the Young's modulus of the ith blade by the following relationship

$$E_i = (1 + \delta_i)E_0 \tag{3.16}$$

where E_0 is the nominal Young's modulus, and δ_i is a mistuning value that is sampled from a uniform distribution with mean value 0 and standard deviation σ.

First, in order to observe the significance of the effects of small mistuning combined with the effects of a cracked blade on the vibration response, the blisk model with a linear cracked blade model as well as with the stiffness mistuning defined by Eq. (3.16) was examined. Modal analysis for the first mode family and the tenth mode family was performed and the results for the first mode family are shown in Fig. 3.5 where Fig. 3.5a shows a mode localized about the cracked and Fig. 3.5b shows a mode localized about a healthy blade. The results for the tenth blade-dominated mode family are shown in Fig. 3.6, where Figs. 3.6a and 3.6b show modes localized about the cracked blade and Figs. 3.6c and 3.6d show modes localized about two different healthy blades. These re-

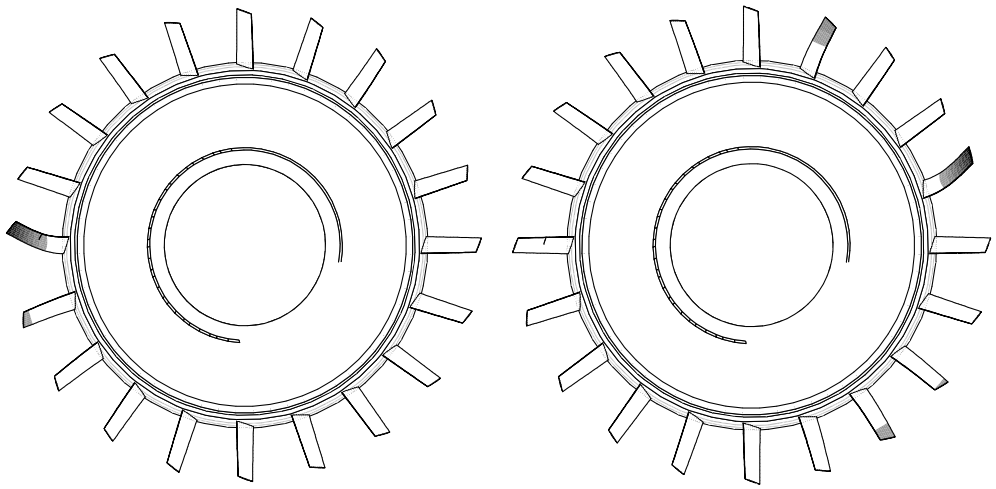

(a) Cracked-blade localized, 383.1 Hz (b) Healthy-blade localized, 387.7 Hz

Figure 3.5: Strongly localized modes in the first blade-dominated mode family, σ=0.01

sults illustrate that the cracking leads to at least one mode that is localized about the same cracked blade for different mode families. Moreover, they show that the mistuning can also lead to strong localization, but the localization may occur about different blades for different mode families. Next, the nonlinear forced response analyses are considered. The analysis framework is the same as before, i.e., after the application of Eq. (3.16) to the Young's moduli of blades, the ROM is calculated using the hybrid CMS method. The HFT method is then applied. The calculation results for the first and tenth modes with σ =0.01 and 0.04 are shown in Figs. 3.7 and 3.8. The envelope of the responses from all the blades as well as the response of the cracked blade for each linear and nonlinear cracked blade model are shown in each plot. For the first blade-dominated mode family, the effect of the crack appears almost only on the resonant peak associated with the cracked-blade-localized mode shown in Fig. 3.7a. However, the peak is not isolated from the cluster of the other resonant peaks. This is because the frequency shift induced by the crack lies in the range of the frequency shifts caused by the small mistuning, even for σ=0.01. This result indicates that, for this crack length and mode, the effect of nonlinearity due to the

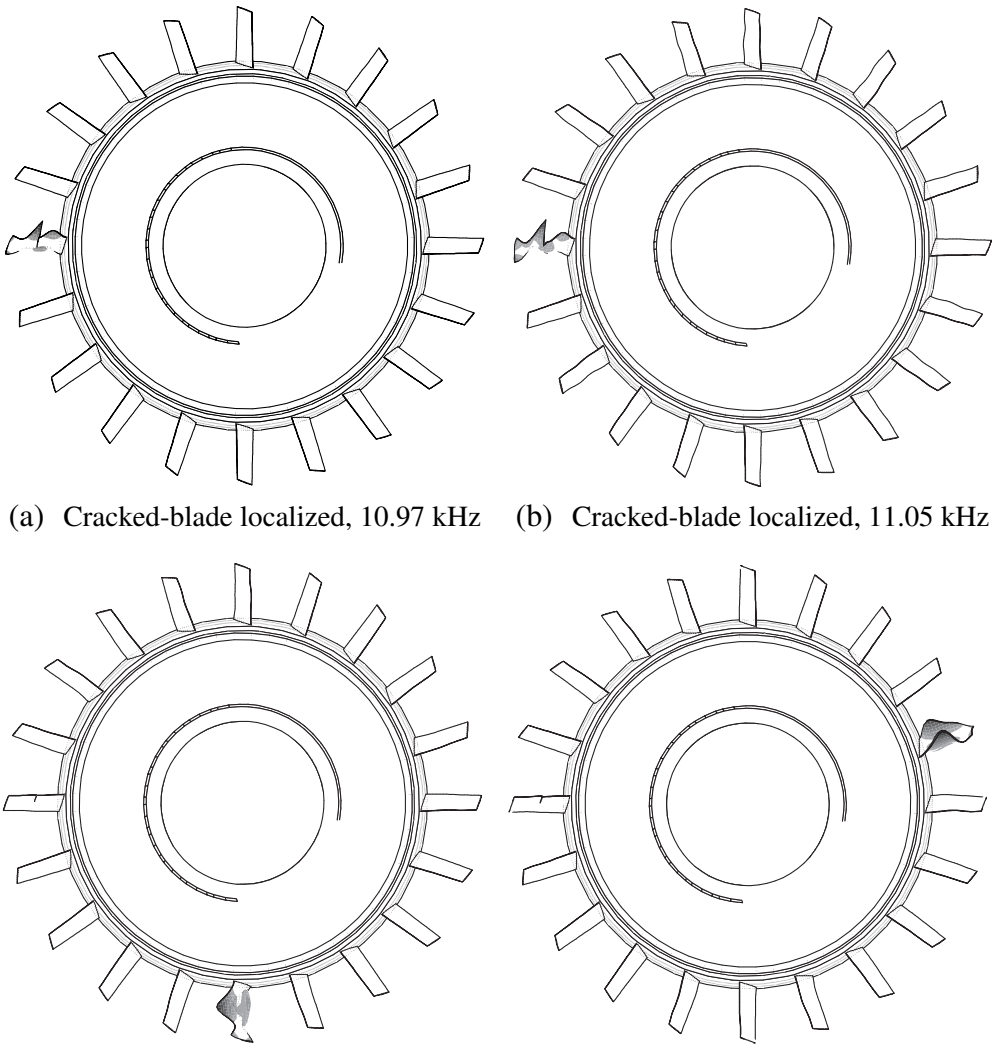

(a) Cracked-blade localized, 10.97 kHz (b) Cracked-blade localized, 11.05 kHz

(c) Healthy-blade localized, 11.40 kHz (d) Healthy-blade localized, 11.44 kHz

Figure 3.6: Strongly localized modes in the tenth blade-dominated mode family, σ=0.01

crack on the frequency response is very localized to the cracked blade. Hence, it might be predicted by the blade-alone analysis, as was discussed in section 3.4.2. However, the effect may not be distinct from the effects of small, random mistuning. That is, the effect of cracking may not be observable in the frequency response data.

In contrast, as can be seen in Fig. 3.8, the resonant peaks associated with the cracked blade are still isolated from the other modes in the family for the tenth blade-dominated mode family even for σ=0.04, in terms of both the amplitude of vibration and the peak

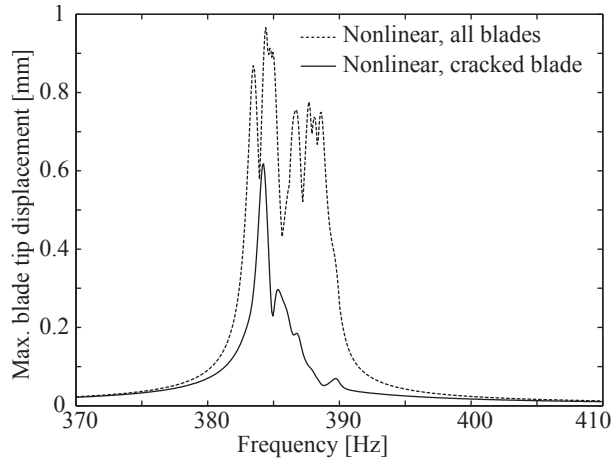

(a) σ=0.01

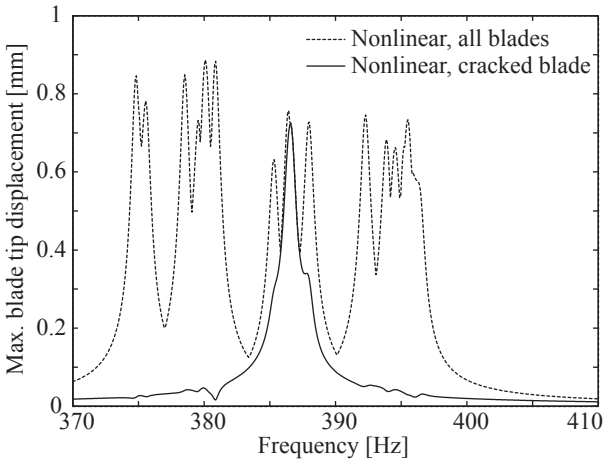

(b) σ=0.04

Figure 3.7: Forced response for the first blade-dominated mode family

frequency. This suggests that the resonant peak associated with the cracked blade is distinguishable from the other scattered peaks due to mistuning. That is, for this mode family, the effect of cracking is strong enough that it may be observable in the frequency response data even for a relatively large mistuning level.

It is noted that the localization patterns for the forced response shapes with a nonlinear cracked blade were observed to be similar to the linear forced response counterparts. Hence, the mode shapes shown in Figs. 3.5 and 3.6 are representative of the localization seen in the nonlinear forced response results.

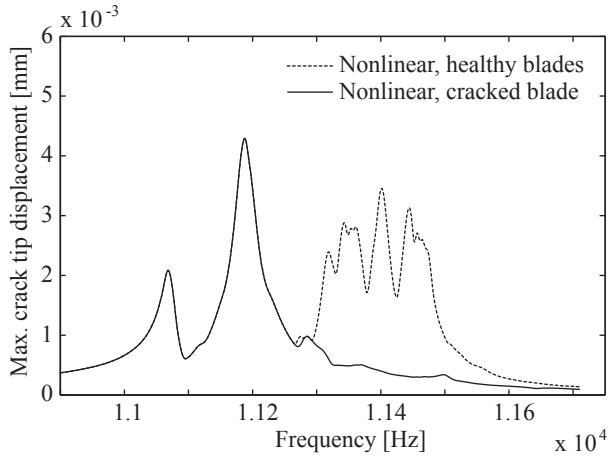

(a) σ=0.01

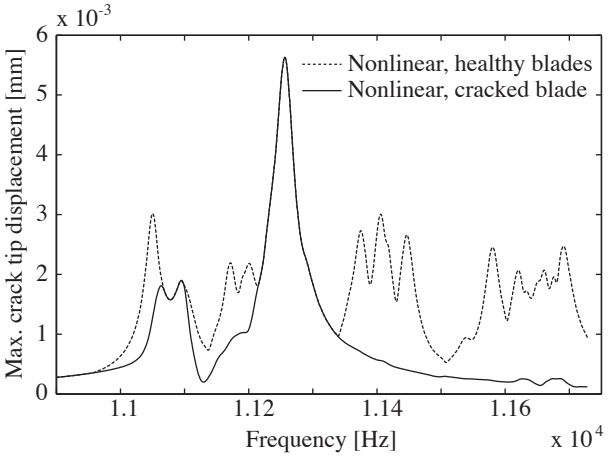

(b) σ=0.04

Figure 3.8: Forced response for the tenth blade-dominated mode family

3.4.4 Effects of Rotation

In previous sections, the effects of rotation on the vibration response were not considered. In this section, the geometric change in the quasi-static equilibrium position under rotation, and the change in the system matrices of the ROM due to the geometric change, are included in the analysis.

First, the geometric change in the equilibrium position leads to an initial gap between the crack surfaces, such as illustrated in Fig. 3.9. This effect should not be ignored, be-

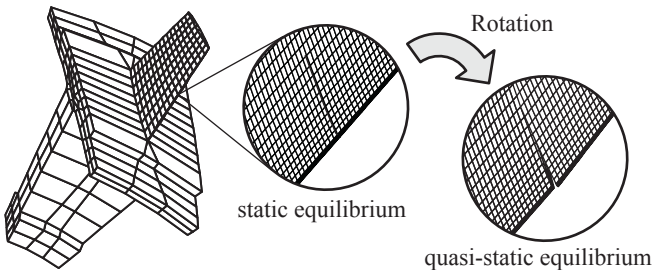

Figure 3.9: Crack opening due to rotation

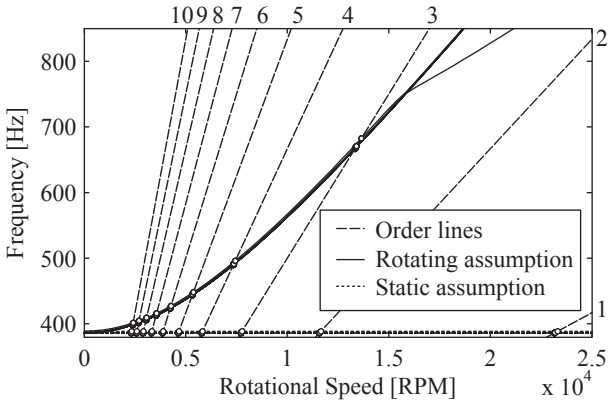

Figure 3.10: Campbell diagram plot for the first blade-dominated mode family

cause it is known that the existence of initial gap can strongly influence the characteristics of resulting *piecewise linear* systems. In particular, it can lead to amplitude-dependent response. In the proposed method, the initial gap at the crack is calculated separately by solving the quasi-static problem due to the rotation.

Second, the effect on the system matrices appears as the rotational-speed-dependent natural frequencies, which is typically seen as a stiffening effect. In Fig. 3.10, the natural frequencies of the blisk with rotating and static assumptions are shown. As can be seen, the natural frequencies increase as rotational speed increases under the rotating assumption, whereas they do not with the static assumption. This means that the ROM should also depend on the rotational speed. However, in the proposed approach, the ROM is calculated at a single rotational speed, and the matrices are assumed to be constant within the frequency

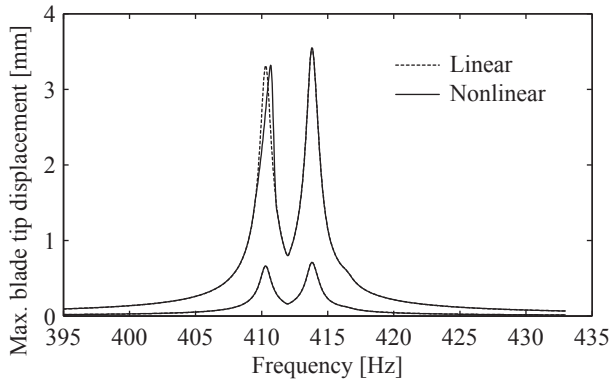

(a) Engine order 7

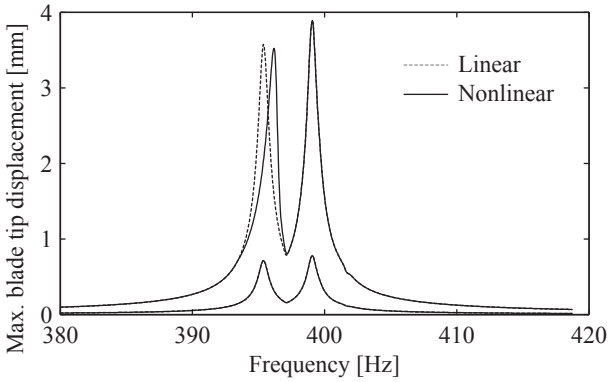

(b) Engine order 10

Figure 3.11: Frequency response of the rotating, tuned blisk with a cracked blade for forcing amplitudes of 0.1 N and 0.5 N

range of interest during the frequency response analysis. The rotational speed where the ROM is calculated is estimated by obtaining the intersections of the natural frequencies and the *order line* of the engine order of interest in the *Campbell diagram*, as shown in Fig. 3.10. The order lines can be drawn by using the fact that the excitation frequency of forcing f is expressed as $f = C\Omega/60$, where C is the engine order of excitation and Ω is the rotational speed in revolutions per minute.

With these assumptions, forced response simulations were performed for the frequency range of the first blade-dominated mode family, using various values of the forcing amplitude. The results shown in Fig. 3.11 are shown for the tuned blisk subject to engine order

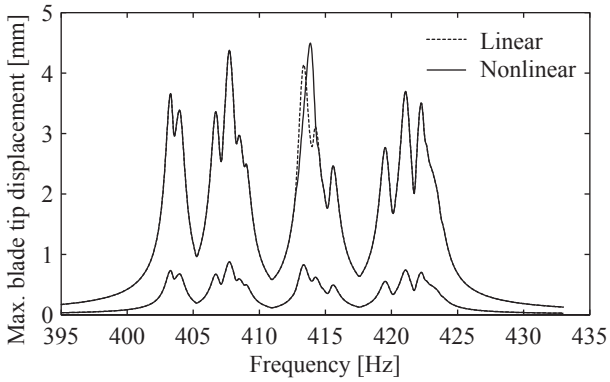

(a) Engine order 7

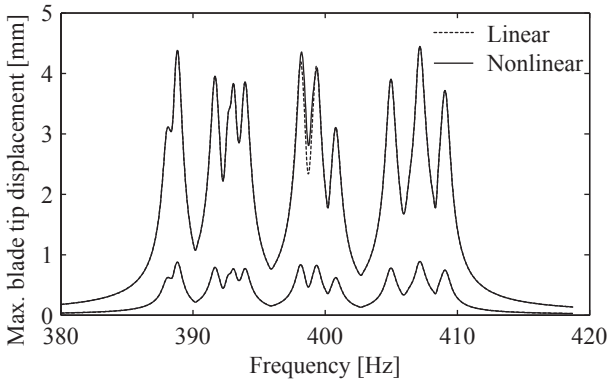

(b) Engine order 10

Figure 3.12: Frequency response of the rotating, mistuned (σ=0.04) blisk with a cracked blade for forcing amplitudes of 0.1 N and 0.5 N

7 and 10 excitations. It can clearly be seen that for small forcing levels, the nonlinear response is identical to the linear responses. However, for increasing values of forcing level, it is seen that the peak corresponding to the cracked blade bends toward a higher frequency. The forcing level at which the nonlinear response starts to differ from the linear response is dependent on the rotational speed, because the amount of initial gap is dependent on the rotational speed. Also, the amount of bending in the frequency response curve is dependent on the engine order of excitation, because it determines the rotational speed at which the ROM and the initial gap are calculated. As before, the influence of the nonlinearity appears mostly in the peak associated with the cracked blade only.

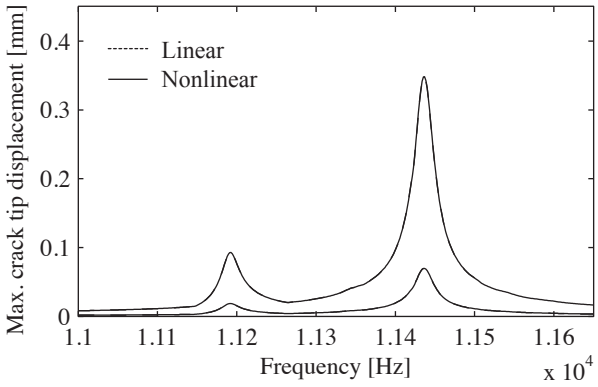

(a) Tuned blisk with a cracked blade

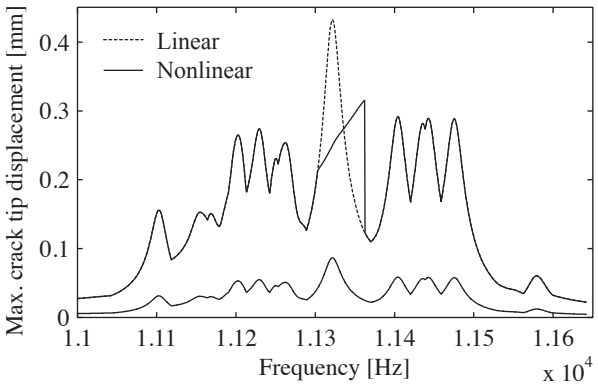

(b) Mistuned blisk with a cracked blade

Figure 3.13: Frequency response of the rotating, mistuned (σ=0.04) blisk with a cracked blade for forcing amplitudes of 2.0 N and 10.0 N with engine order 64

Forced response simulations with mistuning of standard deviation σ=0.04 were also performed, and the results are shown in Fig. 3.12. As predicted with the static assumption in section 3.4.3, the nonlinear effect is very localized to the response of the cracked blade for both engine order 7 and 10 excitation cases. However, the effects may not be distinguishable from the other scattered modes due to mistuning.

Moreover, the forced response calculations were performed for the frequency range of the tenth blade-dominated mode family for various values of the forcing amplitude, and representative results are shown in Fig. 3.13, where the blisk is subject to engine order 64

excitation. The results shown in Fig. 3.13a are for the tuned blisk with a cracked blade, and those shown in Fig. 3.13b are for the blisk with a cracked blade and mistuning of standard deviation $\sigma = 0.04$. As can be seen in Fig. 3.13a, the response shows a localized peak that corresponds to the cracked-blade-dominated mode for each forcing level. However the linear and nonlinear response are identical for these forcing levels, as the amplitude of vibration of the nodes on the crack surfaces does not exceed the size of initial gap at the crack due to the quasi-static deformation. On the other hand, for the case with mistuning, a strongly localized and nonlinear response can be seen in Fig. 3.13b. Namely, due to the mistuning effect, the cracked-blade-dominated peak is not isolated from the other peaks anymore. However as the forcing level increases, the nonlinearity emerges as the bending of the frequency response curve, only on the peak corresponding to the cracked-blade-dominated mode. Furthermore, the nonlinearity leads to the *jump phenomenon* that implies the existence of multiple solutions, which is one of the characteristics of the frequency response of cracked structures with gaps [56]. Again, this phenomenon is localized to the cracked blade and occurs around the resonant frequency corresponding to the cracked-blade-dominated mode.

It was noted that in chapter II, even though the absolute values of the resonant frequencies differ for the static and rotating cases, the corresponding frequency *shifts* predicted for the cracked blade may be in good agreement [56]. Combining this with the discussion in section 3.4.2, this indicates that it may be possible to use static analysis to predict the frequency shifts for rotating conditions, considering that the nonlinearity appears almost only in the response of the cracked blade.

3.5 Conclusions

In this chapter, a modeling and analysis framework for the nonlinear forced response of a rotor with a cracked blade was presented. The basic approach was to employ a combination of a hybrid-interface CMS modeling method, a contact detection algorithm, and the HFT nonlinear vibration analysis method. In section 3.3, the advantage of the hybrid CMS method over the Craig-Bampton method was discussed, and the ROM generated by the hybrid method was validated numerically. In section 3.4, the vibration of a bladed disk with a cracked blade was investigated. In section 3.4.2, it was shown that the results of the blade-alone analysis may be used to predict the frequency shifts of the full bladed disk with one cracked blade. In section 3.4.3, the behavior of the system with small mistuning was studied. The forced response results revealed that, for certain mode families, the resonance associated with a cracked-blade-dominated mode could be distinguished from the many other resonant peaks due to small mistuning. In section 3.4.4, the effects of rotation on the response were examined. It was shown that the nonlinearity depends on the rotational speed as well as the forcing level. Moreover, the nonlinear effect is localized to the response of the cracked blade only, even with mistuning.

Although the FE model presented in this chapter is a simple and relatively small academic model, the proposed analysis framework can be readily applied to the analysis of other bladed disk models and cracks with different geometries. The extension of the method to the case of multiple cracks can also be handled by the method. More comprehensive parametric studies considering additional crack lengths, crack locations, numbers of cracks, mistuning levels, modes of interest, etc., have not yet been carried out.

However, based on this initial investigation, some key observations with respect to damage detection are summarized as follows:

1. Both mistuning and cracks can lead to strong localization of the forced response
2. Mistuning can lead to localization about different blades for different mode families
3. A crack tends to lead to localization about the same (cracked) blade for all mode families
4. For certain mode families, the effect of the crack will be relatively strong compared to that of mistuning, such that the cracked-blade-dominated response may appear at a significantly lower frequency and may also include unique characteristics such as a double resonance peak
5. The relative strength of the effects of a crack on the system response for different mode families, and thus the observability of the cracked-blade-dominated resonance, can be estimated to some extent with a nonlinear vibration analysis of a single blade

It should be noted that a detailed sensitivity analysis in terms of crack length and depth, as well as an experimental study, will eventually be needed for validating the applicability of the technique to practical damage identification of turbomachinery rotors. However, these topics are beyond the scope of this chapter.

Finally, it is noted that the analysis results and findings shown in this chapter are well suited for use in interpreting data acquired with existing vibration measurement techniques for rotor blades, such as tip timing (e.g., [60]). Tip timing uses a non-contacting method with optical probes, and it is widely used for turbomachinery applications. The advantage of the tip timing technique is that the vibration displacement of every blade can be measured without interference, and thus the resonant frequencies associated with forced response patterns featuring strong localization about individual blades can be identified.

Therefore, the authors believe that the analysis results and findings reported in this chapter could be used for designing algorithms for onboard damage detection and health monitoring systems for turbine engine rotors.

CHAPTER IV

Estimation and Veering Analysis of Nonlinear Resonant Frequencies of Cracked Plates

4.1 Introduction

It is well known that the natural frequencies of cracked elastic structures differ from their healthy counterparts. A comprehensive literature survey of research activities regarding the vibration problems of various structures with cracks is found in the work by Dimarogonas [35]. In this chapter, linear and nonlinear vibration of a cantilevered rectangular plate with a crack is investigated. The primary focus of this study is the vibration response near the *eigenvalue loci veerings* and *crossings* that occur as the crack length or location is varied. This work was motivated by an observation of closely-spaced nonlinear resonant frequencies with similar mode shapes, in the nonlinear frequency response of a turbine engine rotor with a cracked blade [61].

Eigenvalue loci veerings, also known as avoided crossings, or eigenvalue avoidance, are observed in plots of eigenvalues versus a system parameter. In particular, a veering refers to a region in which two eigenvalue loci approach each other and almost cross as the system parameter is changed, but instead of crossing they appear to veer away from each other, with each locus then following the previous path of the other [62]. Although this phenomenon was initially regarded as an "aberration" caused by approximation methods

applied to the original infinite-dimensional eigenvalue problems [63], it was shown by Perkins and Mote [64] that the phenomenon can be observed for continuous systems. Since then, several researchers have noted and investigated the relation between veerings and mode localization phenomena [65–67]. In conjunction with the localization, it is known that the veerings are associated with coupling between the modes, which is typically seen as the mixed mode shapes near the veering regions. There can also be a mixing between modes in different physical domains, such as electrical and mechanical domains [68]. These phenomena have also been investigated for the damaged structures, such as two-span weakened column [69], and cables with damage [70].

For vibration problems of cracked rectangular plates, variations in natural frequencies and mode shapes due to crack length variations have been known for a long time. The initial contribution to the study of vibration problems of cracked rectangular plates was made by Lynn and Kumbasar [71], who calculated the vibration frequency drop of plates due to cracking by numerically solving the Fredholm integral equation of the first kind. Petyt [72] also investigated the variation of frequency of fundamental mode due to crack length by experiments and a finite element method. Those contributions were followed by a number of investigations based on plate vibration theory, including those by Stahl and Keer [73], Hirano and Okazaki [74], Solecki [75], and Yuan and Dickinson [76]. Although the trajectories of frequencies versus crack length appear in these articles, the veering regions and associated dynamics of the cracked plates near those regions were not highlighted. Liew *et al.* [77] applied a domain decomposition method to obtain the out-of-plane vibration frequencies of cracked plates, and they not only confirmed the results found by Stahl and Keer [73] and Hirano and Okazaki [74] but also considered a wider range of crack length ratio. It is noted that they examined a plate with a centrally-located internal crack and reported *frequency crossings* instead of veerings. In other words, for this

case they observed that two approaching eigenvalue loci would intersect as crack length increased, which is also known as *crossover*. More recently, Ma and Huang [78] also reported variations in natural frequencies and associated mode shapes due to changes in crack length for a square plate with an edge crack, based on experiments and finite element analysis. As was mentioned by many others, Ma and Huang stated that the nonlinearity due to the *crack closing effect* has to be considered for the in-plane bending case, but crack closing was neglected in their study because their work focused on the out-of-plane bending vibration.

In the studies of cracked rectangular plate vibrations reviewed above, the in-plane bending vibration was not considered and thus the crack closing effect was not examined. In contrast, the issue of crack closing effect naturally arose in the studies of vibration problems of cracked beams, for which in-plane bending vibration is typically of primary research interest. For the study of cracked Bernoulli-Euler beams, a pioneering contribution was made by Christides and Barr in their application of the Hu-Washizu-Barr variational principle to the cracked beam problem [79]. Further extension was made by Shen and Pierre for Bernoulli-Euler beams with symmetric cracks [1] and single-edge cracks [2]. A generalization to the theory was made by Chondros *et al.* [80]. However, in these studies, the nonlinear effect was not considered. Gudmundson [3] pointed out that measured natural frequencies of a beam with a fatigue crack differ from those calculated without considering the crack closing effect. He also addressed the significance of the crack closing effect for accurately predicting the frequency shifts due to cracking. The crack closing effect is also known to cause phenomena that appear only in nonlinear response cases, such as superharmonic and subharmonic resonances [6, 7] and period doubling bifurcations [34, 58].

One of the methods to estimate the (primary) resonant frequencies of the cracked

beams is the application of the *bilinear frequency* approximation. This was initially introduced for calculating the effective resonant frequencies of piecewise linear oscillators (e.g., Shaw and Holmes [31]), and it has been used for approximating the effective vibration frequency of multi-DOF piecewise linear systems (e.g., Butcher [32]). It has also been used for estimating the natural frequency of cracked beams [4,5,34]. Chati *et al.* [33] extended the concept of the bilinear frequency to study the vibration of a cracked beam using a multi-DOF oscillator model. They assumed that if the crack is sufficiently shallow, the actual and bilinear mode shapes are close to each other, and thus the frequency can be approximated by the bilinear frequency. Most of the methods reviewed above assume that the crack has only two states—closed or open. This assumption is accurate when the relative motion of the crack surfaces is simple, such as the in-plane bending vibration of cantilevered beams. However, in general, the motion of crack surfaces is more complicated, and there may be more than two states. For example, crack closing may proceed gradually and/or occur at different regions on the crack surfaces at different times.

The closing crack was also modeled by equivalent linear model by Kisa and Brandon [81], with the assumption that the stiffness change due to a crack can be expressed as a linear combination of the stiffness matrix of uncracked beam and that due to cracking and contact. An emerging approach for dealing with this issue is the application of Nonlinear Normal Modes [46–48]. However, the applicability of this approach is still limited to simple structures or simplified vibration problems, due mostly to its computational costs for constructing the nonlinear normal modes.

With regard to the veering phenomena for nonlinear structural systems, very little is known about how the nonlinearities influence the response near the veering regions. Lacarbonara *et al.* [82] investigated nonlinear modal interactions of an imperfect beam near veering regions, the nonlinearities of which are quadratic and cubic nonlinearities due to

large-amplitude vibration, through perturbation and bifurcation analyses. They observed distinguishing features in the response, such as mode localization due to nonlinear coupling and frequency-island generation, which illustrates the richness of the dynamics in veering regions for nonlinear structural systems.

In this chapter, the vibration of cracked cantilevered plates in frequency veering regions is investigated. As reviewed above, veering phenomena have not been studied thoroughly for cracked structures, in either the linear or nonlinear dynamics regime. Regarding the vibration of cantilevered cracked plates, the research reviewed above focused only on the out-of-plane vibration, and crack closing effects were intentionally neglected. On the other hand, studies of cracked beams have focused on in-plane bending in most cases. Thus, the crack closing effect on the vibration response has been investigated in many studies of cracked beams. However, veering and modal interaction phenomena between in-plane and out-of-plane vibration modes have not been studied in this context. Moreover, in general, the veering phenomena in nonlinear structural systems have not been studied well. Therefore, in this chapter, first the eigenvalue loci veering due to cracking is examined using a cracked cantilevered plate example without considering the crack closing effect. The crack closing effect is then included and associated nonlinear resonant frequencies are identified. A novel method for accurately estimating the nonlinear resonant frequencies is then introduced, by generalizing the concept of bilinear frequency approximation that utilizes the results of linear eigenvalue analyses of the system. The method is validated by comparing the results with those calculated by the nonlinear forced response analysis. Furthermore, the applicability of the method near the veering regions is discussed, and the effects of the crack closing on the resonant frequencies are discussed in detail for some specific veering regions.

This chapter is organized as follows. In section 4.2, the cracked plate vibration prob-

lem and the finite element model are introduced. In section 4.3, the linear free response of a cracked plate is considered using a finite element model of a three-dimensional cantilevered plate with a planar surface-breaking crack that runs parallel to the cantilevered edge, and the associated frequency veering and crossing phenomena are shown. In section 4.4, a solution technique for the nonlinear forced response analysis, called the hybrid frequency/time (HFT) method, is briefly reviewed. The nonlinear forced response calculation is then carried out and the effects of nonlinearity to the response in the neighborhood of representative veering regions are discussed in detail. In section 4.5, the method for estimating the nonlinear resonant frequency is introduced as a generalization to the bilinear frequency approximation. Finally, conclusions are summarized in section 4.6.

4.2 Cracked Plate Model

In this chapter, the vibration of a cantilevered rectangular plate comprised of linear isotropic elastic material is considered. The plate is discretized with a standard finite element method (FEM), and the deformation is assumed to be infinitesimally small. In this study, nonlinearities other than the one due to intermittent contact at the crack surfaces are not considered. Namely, the governing equation of the cracked plate is

$$\mathbf{M}\ddot{\mathbf{u}}(t) + \mathbf{C}\dot{\mathbf{u}}(t) + \mathbf{K}\mathbf{u}(t) = \mathbf{b}(t) + \mathbf{f}(\mathbf{u}); \quad \mathbf{M}, \mathbf{C}, \mathbf{K} \in \mathbb{R}^{n\times n}, \mathbf{u}, \mathbf{b}, \mathbf{f} \in \mathbb{R}^n \tag{4.1}$$

where $\mathbf{u}$ is the displacement vector, $\mathbf{M}$, $\mathbf{C}$ and $\mathbf{K}$ denote the mass, damping, and stiffness matrices, $\mathbf{b}(t)$ denotes the time-dependent external force, and $\mathbf{f}(\mathbf{u})$ denotes the nonlinear force caused by the intermittent contact at the crack.

A finite element (FE) model of a cantilevered plate with a transverse crack is shown in Fig. 4.1, where $h = 1.5 \times 10^{-1}$m, $l = 6.0 \times 10^{-2}$m, $t = 3.0 \times 10^{-3}$m. The material model is steel with Young's modulus $E = 200$GPa, density $\rho = 7800$kg/m^3, and Poisson's ratio $\nu = 0.3$. The FE model is composed of 6,750 brick linear elements and has approximately

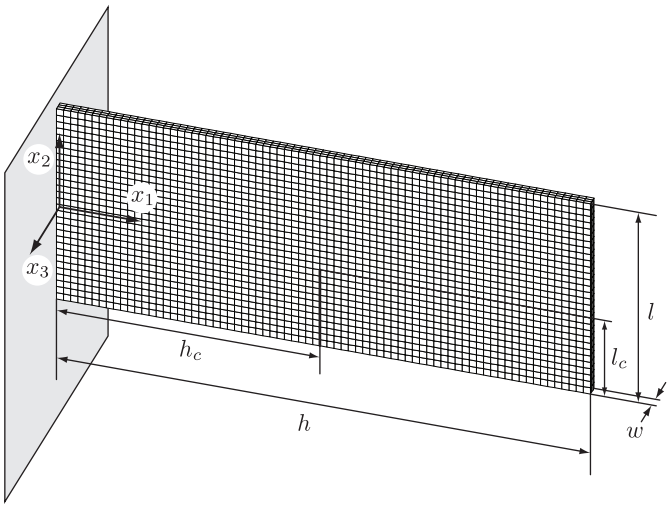

Figure 4.1: Finite element model of the cracked plate

28,000 DOF. This FE model is used for all the numerical results in this chapter, and the generation of the FE model as well as component mode synthesis were performed with the commercial code ANSYS [40].

4.3 Linear Free Response Analysis

4.3.1 Natural frequency variation due to variations in crack location and length

For the FE model shown in Fig. 4.1, eigenvalue analysis was performed for various values of l_c/l and h_c/h, and the results for the first 15 natural frequencies for two representative cases are shown in Fig. 4.2. First, Fig. 4.2(a) shows the results where the crack length was fixed at $l_c/l = 40\%$, and the crack location was varied as $1.33 \leqslant h_c/h \leqslant 97.3\%$. As can be seen, the changes in the natural frequencies due to the variation in h_c/h are quite complicated, and multiple loci veerings and crossings are observed. For example in Fig. 4.2(a), starting around $h_c/h = 15\%$, modes 10 and 11 approach each other, but rather than crossing they veer away near $h_c/h = 19\%$ with high curvature. Second, the crack location was fixed at $h_c/h = 50\%$, and the crack length was varied, the results of

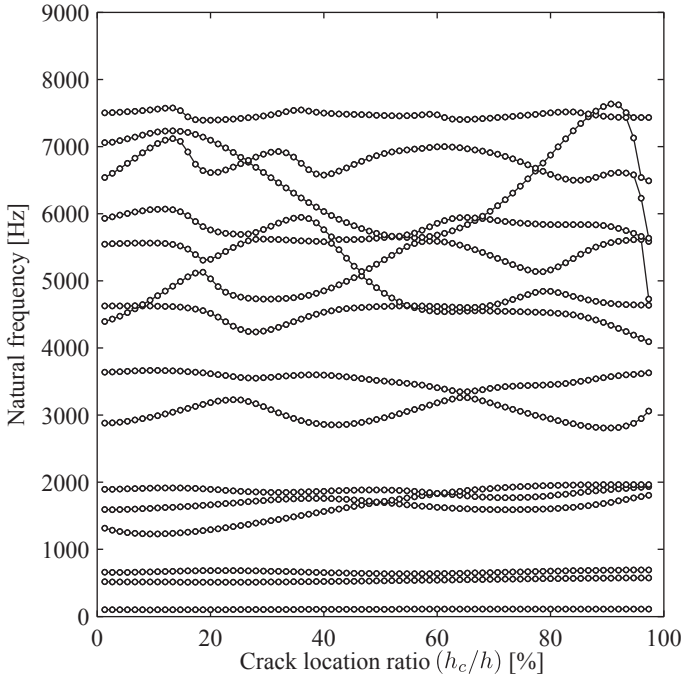

(a)

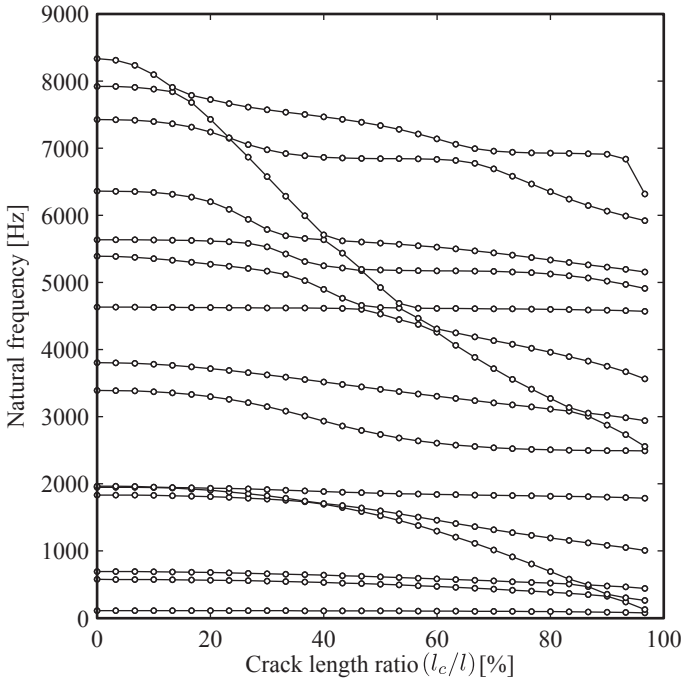

(b)

Figure 4.2: First 15 natural frequencies versus (a) crack location ratio h_c/h for $l_c/l = 0.40$, (b) crack length ratio l_c/l for $h_c/h = 0.50$

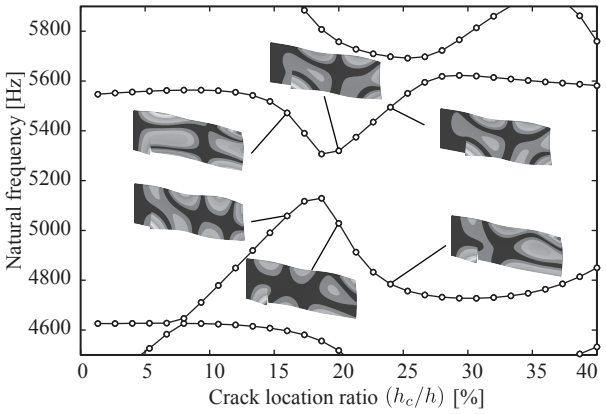

(a)

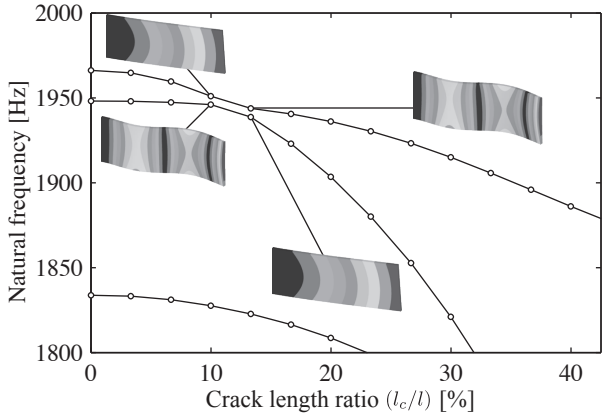

(b)

Figure 4.3: Magnified veeering/crossing regions and associated mode shapes: (a) 10th and 11th modes for $l_c/l = 0.40$; (b) fifth and sixth modes for $h_c/h = 0.50$.

which are shown in Fig. 4.2(b). The most notable distinction from the case in Fig. 4.2(a) is that the natural frequency variation due to crack length change is monotonic, i.e., as l_c/l increases, all natural frequencies tend to decrease. Although the amount of frequency drop is dependent on the mode of interest, this is due to the fact that the stiffness of the plate decreases monotonically for all modes as the crack length increases.

4.3.2 Mode shape variation due to variations in crack location and length

In order to see the veering regions more closely, and to see the variations in the mode shapes, representative cases are shown in Figs. 4.3 and 4.4. Figure 4.3(a) shows the veer-

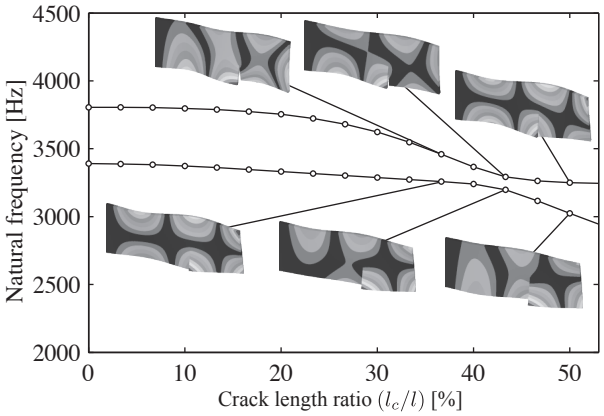

Figure 4.4: Magnified veering between modes seven and eight for $h_c/h = 0.63$

ing between the modes 10 and 11 for $l_c/l = 40\%$, where $1.33 \leqslant h_c/h \leqslant 40\%$. An important characteristic of the loci veering is the mode shapes associated with the natural frequencies on each locus before veering are interchanged during the veering in a continuous manner [64]. This is illustrated in Fig. 4.3(a), which shows that mode shapes 10 and 11 become mixed and then appear to begin switching as the crack location ratio is increased through the veering region. On the other hand in Fig. 4.3(b), the region for the mode shape switching between modes five and six is narrow, and it appears to be a loci crossing. This can be explained by considering that mode five (before switching) corresponds to the second out-of-plane bending mode whereas mode six (before switching) corresponds to the first in-plane bending mode, and there is little or no coupling between these modes due to their geometric dissimilarity. Fig. 4.4 shows another veering region due to crack length variation, for modes seven and eight with crack location $h_c/h = 0.63$. For this case, both mode mixing and switching can be observed in a more continuous manner than the cases observed in Fig. 4.3.

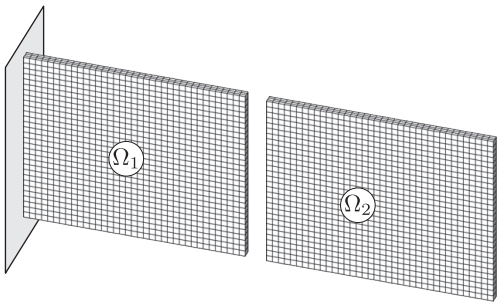

Figure 4.5: Plate divided into two substructures

4.4 Nonlinear Forced Response Analysis

In the previous section, the interchanging of modes as well as mode coupling were observed in frequency veering and crossing regions. However, only natural frequencies of the linear system were considered. The nonlinearity due to contact of the crack surfaces was neglected. In this section, a method to calculate the nonlinear resonant frequencies of the cracked plate is described. The method is then applied to the calculation of nonlinear resonant frequencies in veering/crossing regions, and their characteristics are discussed.

4.4.1 Component Mode Synthesis

In order to generate a reduced-order model, the plate is separated into two components (substructures) Ω_1 and Ω_2 along the crack path, as shown in Fig. 4.5, and a hybrid-interface method of component mode synthesis (CMS) [57, 83] is employed. The CMS methods have been widely used for the vibration analysis of systems such as friction-damped systems [22, 42, 84], build-up structures [85], and cracked structures [56, 81]. This process is advantageous over the direct application of FE analysis because it provides improved computational efficiency while maintaining direct access to the dynamics of the crack-surface DOF. Furthermore, it has good accuracy relative to the original FE model over the frequency range of interest. The accessibility to the nodes on the crack surfaces is essential

to the proper calculation of the boundary condition at the crack surfaces, which is modeled as contact/impact forces in the formulation described in 4.4.2. Namely, the dynamics of the FE degrees of freedom are projected onto constraint modes $\mathbf{\Psi}_c$, inertia relief attachment modes $\mathbf{\Psi}_a$ (if rigid-body motion exists), and a truncated set of free-interface normal modes $\mathbf{\Phi}_k$. Interested readers may consult, e.g., Craig [86], for the detailed formulation of each mode set.

Let the displacement vector $\mathbf{u}$ be partitioned into boundary DOF, $\mathbf{u}_b$, and interior DOF $\mathbf{u}_i$. By denoting the inertia relief attachment coordinates and a truncated set of free-interface modal coordinates as $\mathbf{q}_a$ and $\mathbf{q}_k$, the linear projection is expressed as,

$$\begin{bmatrix} \mathbf{u}_b \\ \mathbf{u}_i \end{bmatrix} = \begin{pmatrix} \mathbf{I} & \mathbf{0} & \mathbf{0} \\ \mathbf{\Psi}_{ic} & \hat{\mathbf{\Psi}}_a & \hat{\mathbf{\Psi}}_k \end{pmatrix} \begin{bmatrix} \mathbf{u}_b \\ \mathbf{q}_a \\ \mathbf{q}_k \end{bmatrix} \tag{4.2}$$

where $\hat{\mathbf{\Psi}}_a = \mathbf{\Psi}_{ia} - \mathbf{\Psi}_{ic}\mathbf{\Psi}_{ba}$, $\hat{\mathbf{\Psi}}_k = \mathbf{\Phi}_{ik} - \mathbf{\Psi}_{ic}\mathbf{\Phi}_{bk}$, $\mathbf{I}$ is the identity matrix, $\mathbf{\Psi}_{ic}$ is the boundary partition of $\mathbf{\Psi}_c$, $\mathbf{\Psi}_{ia}$ and $\mathbf{\Psi}_{ba}$ denote the interior and the boundary partitions of $\mathbf{\Psi}_a$, and $\mathbf{\Phi}_{ik}$ and $\mathbf{\Phi}_{bk}$ denote the interior and the boundary partitions of $\mathbf{\Phi}_k$. Denoting Eq. (4.2) with a compact notation, $\mathbf{u} = \mathbf{\Psi}\mathbf{q}$, the application of Eq. (4.2) to Eq. (4.1) yields a smaller number of equations, i.e.,

$$\mathbf{M}'\ddot{\mathbf{q}} + \mathbf{C}'\dot{\mathbf{q}} + \mathbf{K}'\mathbf{q} = \mathbf{b}' + \mathbf{f}'(\mathbf{q}) \tag{4.3}$$

where $\mathbf{M}' = \mathbf{\Psi}^{\mathrm{T}}\mathbf{M}\mathbf{\Psi}$, $\mathbf{C}' = \mathbf{\Psi}^{\mathrm{T}}\mathbf{C}\mathbf{\Psi}$, $\mathbf{K}' = \mathbf{\Psi}^{\mathrm{T}}\mathbf{K}\mathbf{\Psi}$, $\mathbf{b}' = \mathbf{\Psi}^{\mathrm{T}}\mathbf{b}$, and $\mathbf{f}' = \mathbf{\Psi}^{\mathrm{T}}\mathbf{f}$. The superscript "′" is omitted for convenience in the subsequent formulations.

4.4.2 Hybrid frequency/time domain method

For the calculation of steady-state response to harmonic excitation, an extension to the alternating frequency/time-domain method [23], which is based on the concept of the

method of harmonic balance [17], is employed in this study. Because of its computational efficiency and accuracy, this type of method has been developed and applied to forced response problems for various nonlinear systems, such as friction damped systems [18, 22, 84, 87] and cracked shafts [88]. In particular, the hybrid frequency/time-domain method developed by Poudou *et al.* [28, 29, 42] and the authors [56] is applied in this chapter. Namely, the method assumes that the steady-state vibration response of $\mathbf{q}$ in Eq. (4.3), as well as the external force $\mathbf{b}$ and the nonlinear force due to intermittent contact $\mathbf{f}$ are approximated as truncated Fourier series, i.e.,

$$\mathbf{q} = \mathrm{Re}\left(\sum_{k=0}^{n_h}(\mathbf{Q}_k^c - \mathrm{j}\mathbf{Q}_k^s)\mathrm{e}^{\mathrm{j}k\omega t}\right) \tag{4.4}$$

$$\mathbf{b} = \mathrm{Re}\left(\sum_{k=0}^{n_h}(\mathbf{B}_k^c - \mathrm{j}\mathbf{B}_k^s)\,\mathrm{e}^{\mathrm{j}k\omega t}\right) \tag{4.5}$$

$$\mathbf{f} = \mathrm{Re}\left(\sum_{k=0}^{n_h}(\mathbf{F}_k^c - \mathrm{j}\mathbf{F}_k^s)\,\mathrm{e}^{\mathrm{j}k\omega t}\right) \tag{4.6}$$

where $2\pi/\omega$ is the fundamental frequency, n_h is the number of non-zero harmonics and $\mathrm{j} = \sqrt{-1}$. Note that $\mathbf{Q}_k^c$ and $-\mathbf{Q}_k^s$ are the vectors of real and imaginary parts of kth Fourier coefficients of $\mathbf{q}$, where superscripts c and s denote cosine and sine components of the vibration respectively. The same notation is applied to $\mathbf{B}_k^c$, $\mathbf{B}_k^s$, $\mathbf{F}_k^c$, and $\mathbf{F}_k^s$. Substituting Eqs. (4.4) through (4.6) into Eq. (4.3) and considering the orthogonality of harmonic functions, it results in a nonlinear algebraic equation with respect to the Fourier coefficients for kth harmonic number, i.e.,

$$\mathbf{\Lambda}_k\mathbf{Q}_k = \mathbf{B}_k + \mathbf{F}_k(\mathbf{Q}) \tag{4.7}$$

where $\mathbf{Q}_0 = \mathbf{Q}_0^c$, $\mathbf{B}_0 = \mathbf{B}_0^c$, $\mathbf{F}_0 = \mathbf{F}_0^c$, $\mathbf{\Lambda}_0 = \mathbf{K}$, $\mathbf{Q}_k = [(\mathbf{Q}_k^c)^{\mathrm{T}}, (\mathbf{Q}_k^s)^{\mathrm{T}}]^{\mathrm{T}}$, $\mathbf{B}_k = [(\mathbf{B}_k^c)^{\mathrm{T}}, (\mathbf{B}_k^s)^{\mathrm{T}}]^{\mathrm{T}}$, $\mathbf{F}_k = [(\mathbf{F}_k^c)^{\mathrm{T}}, (\mathbf{F}_k^s)^{\mathrm{T}}]^{\mathrm{T}}$, and

$$\mathbf{\Lambda}_k = \begin{pmatrix} -(k\omega)^2\mathbf{M} + \mathbf{K} & (k\omega)\mathbf{C} \\ -(k\omega)\mathbf{C} & -(k\omega)^2\mathbf{M} + \mathbf{K} \end{pmatrix} \tag{4.8}$$

for $k = 1, \ldots, n_h$. Assembling Eq. (4.8) for all $k = 0, 1, \ldots, n_h$,

$$\mathbf{\Lambda Q} = \mathbf{B} + \mathbf{F}(\mathbf{Q}) \tag{4.9}$$

where $\mathbf{\Lambda}$ is a pseudo-block diagonal matrix with Λ_k on its diagonal blocks for $k = 0, \ldots n_h$, $\mathbf{Q} = [\mathbf{Q}_0^{\mathrm{T}}, \ldots, \mathbf{Q}_{n_h}^{\mathrm{T}}]^{\mathrm{T}}$, $\mathbf{B} = [\mathbf{B}_0^{\mathrm{T}}, \ldots, \mathbf{B}_{n_h}^{\mathrm{T}}]^{\mathrm{T}}$, and $\mathbf{F} = [\mathbf{F}_0^{\mathrm{T}}, \ldots, \mathbf{F}_{n_h}^{\mathrm{T}}]^{\mathrm{T}}$. Eq. (4.9) can then be solved with nonlinear algebraic equation solvers. For the numerical examples shown in this chapter, the Hybrid Powell method [27] was employed.

4.4.3 Results of forced response analysis

In this subsection, the result of nonlinear forced response analysis for the cantilevered cracked plate is presented, with the methods described in 4.4.1 and 4.4.2. The damping was chosen to be $\mathbf{C} = \alpha\mathbf{M} + \beta\mathbf{K}$ where $\alpha = 1.22$ and $\beta = 8.16 \times 10^{-9}$, which result in damping that is approximately equivalent to modal (structural) damping ratio $\zeta = 1.00 \times 10^{-4}$ ($\gamma = 2.00 \times 10^{-4}$) within the frequency range of $1900 \leqslant f \leqslant 2000$Hz. Vectors of harmonic forcing, the resultant of which is equal to 1N, is applied to the nodes on the tip face of the plate to excite the modes of interest. The number of harmonics was chosen as $n_h = 9$, which showed convergence in the frequency response. Representative results are shown in Fig. 4.6 where $h_c/h = 0.5$, $l_c/l = 0.167$ for Fig. 4.6(a), and $l_c/l = 0.2$ for Fig. 4.6(b). Fig. 4.6(a) shows the resonant peaks corresponding to modes five and six, which correspond to the third out-of-plane bending and the first in-plane bending modes, respectively, whereas the order of the modes is interchanged in Fig. 4.6(b).

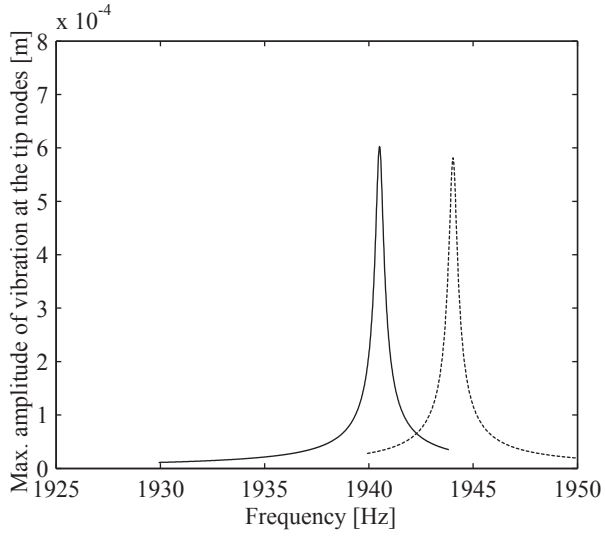

(a)

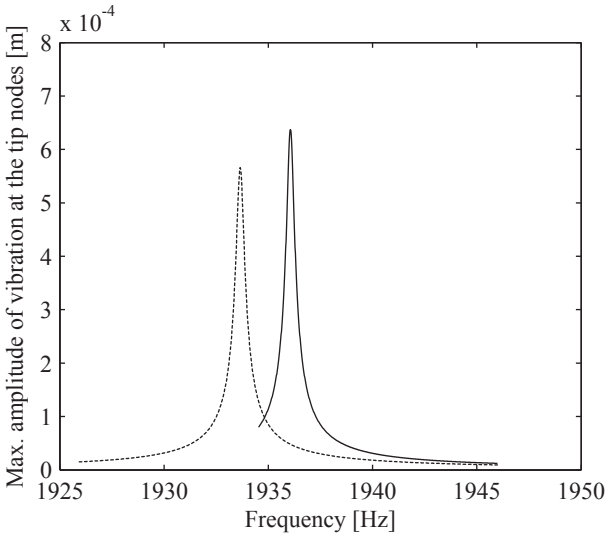

(b)

Figure 4.6: Results of nonlinear harmonic response analysis for $h_c/h = 0.5$: (a) $l_c/l = 0.167$, ——, fifth mode (out-of-plane bending), -----, sixth mode (in-plane bending); (b) $l_c/l = 0.200$, -----, fifth mode (in-plane bending), ——, sixth mode (out-of-plane bending).

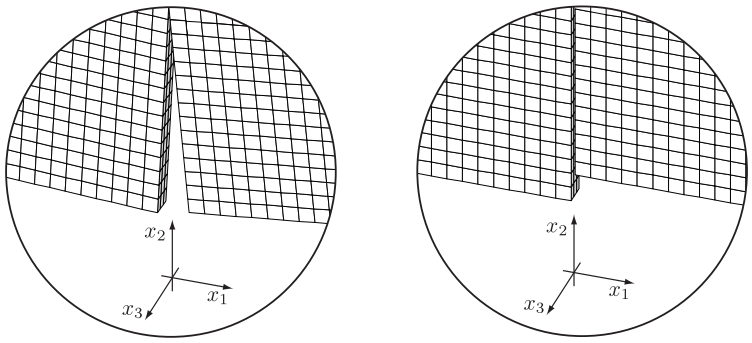

(a) (b)

Figure 4.7: Constraints for bilinear frequency calculation: (a) Open (no constraints); (b) Closed (sliding).

4.5 Bilinear Frequency Approximation

4.5.1 Formulation

As an alternative way of predicting the nonlinear vibration frequencies, the bilinear frequency approximation is generalized for the analysis of three-dimensional cracked structures, and an analysis framework based on reduced-order modeling as well as prediction of mode switching during the veering regions is proposed in this section. The resonant peaks predicted by the forced response to harmonic excitation is then compared with those calculated by the bilinear frequency approximations.

The bilinear frequency was originally introduced as the effective vibration frequency of a piecewise linear, single-DOF system and defined as (e.g., Ref. [31]),

$$\omega_b = \frac{2\omega_1\omega_2}{\omega_1 + \omega_2} \tag{4.10}$$

where ω_b is the bilinear frequency, ω_1 is the natural frequency of one of the linear systems associated with the piecewise linear system, and ω_2 is that of the other linear system of the piecewise linear system. This expression is the exact solution, for the frequency of free oscillation of the piecewise linear single-DOF oscillator with vanishing clearance/gap

at the equilibrium. The application of Eq. (4.10) to a multi-DOF piecewise linear system is rather straightforward if there is only one pair of linear systems. However in the cases of cracked plates formulated with multiple DOF on crack surfaces, it involves multiple piecewise linear systems, or a *conewise* linear systems [47]. Hence an assumption has to be made such that the cracked system has only two linear systems corresponding to two states, i.e., the crack is open or closed. These are designated as states 1 and 2, respectively, in the following formulation. The definition of the states 1 and 2 is a natural extension to that proposed by Chati *et al.* [33], which was applied to the analysis of in-plane bending vibrations of a cracked beam. Namely, with the assumption of the open state, there is no connection between the nodes on one crack surface and the nodes on the other surface (Fig. 4.7(a)), allowing the inter-penetration of the crack surfaces. On the other hand with the closed state, the relative DOF along the direction that is perpendicular to the crack surfaces are fixed to be zero, whereas the other two DOF of each node are allowed to move freely in the plane tangent to the constrained direction (Fig. 4.7(b)). In other words, the crack surfaces are allowed to slide with respect to each other, which is consistent with the assumption employed in the formulation in 4.4.2. Associated mathematical formulation is given as follows.

For a given crack length, eigenvalues of Eq. (4.1) for undamped case with open crack assumption are obtained as

$$\mathbf{K}\boldsymbol{\phi} = \omega_1^2 \mathbf{M}\boldsymbol{\phi} \tag{4.11}$$

where $\boldsymbol{\phi}$ is the eigenvector and ω_1^2 is the associated eigenvalue. On the other hand, the eigenvalues and eigenvectors for the other case, namely the case with allowing sliding of crack surfaces, are obtained by imposing appropriate constraints on Eq. (4.11) as follows. Let A and B denote the crack surfaces facing each other, by assuming that the amplitude of vibration is much smaller than the finite element mesh size on the crack surfaces, it is

possible to identify the finite element nodes that may be in contact during the vibration cycle. Hence such pairs of nodes are numbered and a set $\mathcal{C}_{cp}$ is defined where all numbers that denote the contact pairs are included. Defining g_n as the *gap* between the nodes on the surfaces A and B for the nth contact pair, the constraints to be imposed on the nodes of nth contact pair are expressed as

$$g_n = (u_n)_A - (u_n)_B = 0, \quad n \in \mathcal{C}_{cp} \tag{4.12}$$

where $(u_n)_A$ and $(u_n)_B$ denote the displacements of the nodes on the surface A and B, projected onto the normal direction pointing outward from the surface A or B. It is noted that appropriate coordinate transformation must be applied to the displacement vector based on the normal vector at each node, in order to correctly calculate g_n. It should also be noted that the motion of the nodes in tangential plane that is perpendicular to the normal direction, is not constrained at all by Eq. (4.12), i.e., the nodes are free to slide with each other on the tangential plane. This also indicates that the crack surfaces are assumed to be frictionless, which is widely-employed assumption for the vibration problem of cracked beams and plates. Applying the constraints Eq. (4.12) to the eigenvalue problem Eq. (4.11), a constrained eigenvalue problem is obtained as

$$\begin{bmatrix} \mathbf{K} & \mathbf{N}^{\mathrm{T}} \\ \mathbf{N} & 0 \end{bmatrix} \begin{bmatrix} \boldsymbol{\phi} \\ \boldsymbol{\lambda} \end{bmatrix} = \omega_2^2 \begin{bmatrix} \mathbf{M} & \mathbf{0} \\ \mathbf{0} & \mathbf{0} \end{bmatrix} \begin{bmatrix} \boldsymbol{\phi} \\ \boldsymbol{\lambda} \end{bmatrix} \tag{4.13}$$

where $\mathbf{N}$ is the matrix of coefficients that are associated with Eq. (4.12) and the appropriate transformation matrix, and $\boldsymbol{\lambda}$ is the vector of Lagrange multipliers of size $|\mathcal{C}_{cp}|$. One method to solve this indefinite eigenvalue problem is to use an eigenvalue solver for indefinite systems. Another method is to first eliminate the redundant equations due to the constraint equations Eq. (4.12), and the resulting positive definite eigenvalue problem is then solved by an eigenvalue solver for definite systems. It should be noted that this

methodology can easily be incorporated with the reduced-order modeling framework described in 4.4.1 as the motion of the nodes on the crack surfaces in the three-dimensional space can be captured with the reduced-order model.

With the eigenvalue problems Eqs. (4.12) and (4.13), the ith bilinear resonant frequency ω_{bi} of the cracked plate is approximated based on Eq. (4.10):

$$\omega_{bi} = \frac{2\omega_{1i}\omega_{2i}}{\omega_{1i} + \omega_{2i}} \tag{4.14}$$

where ω_{1i} and ω_{2i} denote the frequencies of the ith mode of the states 1 and 2. It is emphasized that the index i does not denote the index of eigenvalues, but it denotes the index of the eigenvectors of the *non-cracked* plate. Namely, the eigenvectors of the non-cracked plate are indexed based on their natural frequencies, i.e., for non-cracked plate, the eigenvalues are ordered as $\omega_1 \leqslant \omega_2 \leqslant \cdots \leqslant \omega_{N-1} \leqslant \omega_N$ where N is the size of the non-cracked plate model, and corresponding eigenvectors are labeled as $[\boldsymbol{\phi}_1, \boldsymbol{\phi}_2, \ldots, \boldsymbol{\phi}_{N-1}, \boldsymbol{\phi}_N]$. The reason for introducing this ordering will become apparent shortly. The bilinear frequency ω_{bi} for a given crack length is calculated by using the natural frequencies of the corresponding ith mode of the states 1 and 2.

The advantage of this method is that the frequency of the nonlinear response is obtained without calculating the associated response shapes, thus it only involves eigenvalue extraction of two linear systems. However, as mentioned, this method is known to be accurate for systems with a relatively short crack. In addition, a drawback of this method is that the choice of proper pairs of ω_{1i} and ω_{2i} is not apparent with the presence of a veering or crossing, because the mode shapes associated with the natural frequencies switch their orders. A way to overcome the latter problem is to track each mode by observing the correlation between the modes during the variation of crack length or crack location. In this chapter, the modal assurance criterion [89] (MAC) is employed as the measure of

correlation.

Denoting the crack length as $p\ (= l_c)$, it is noted that $\mathbf{N}$ and $\boldsymbol{\lambda}$ are dependent on p. That is, $\mathbf{N} = \mathbf{N}(p)$ and $\boldsymbol{\lambda} = \boldsymbol{\lambda}(p)$. The eigenvector is also dependent on p, or $\boldsymbol{\phi} = \boldsymbol{\phi}(p)$, and the correlation between the ith mode shape of the system with $p = p_0$ and the jth mode shape with the perturbed crack length $p = p_0 + \Delta p$ can be characterized by

$$MAC_{ij}^{k} = \frac{|\boldsymbol{\phi}_i^k(p_0)^{\mathrm{T}}\boldsymbol{\phi}_j^k(p_0+\Delta p)|^2}{||\boldsymbol{\phi}_i^k(p_0)||^2||\boldsymbol{\phi}_j^k(p_0+\Delta p)||^2}, \quad k = 1, 2 \tag{4.15}$$

where $\boldsymbol{\phi}$ is the eigenvector of the system defined by Eq. (4.13), the subscripts i and j denote the indices for modes, the superscript k indicates the state, and MAC_{ij}^{k} takes the value between 0 and 1, which respectively correspond to no correlation, and consistent correlation between $\boldsymbol{\phi}_i(p_0)$ and $\boldsymbol{\phi}_j(p_0 + \Delta p)$. Namely, the ith eigenvector is tracked based on the value of MAC throughout the variation of the crack length (p), such that the correct natural frequencies for the ith eigenvector in Eq. (4.14) can be calculated.

In order to better clarify the behavior of the natural frequencies of the system with open and sliding boundary conditions, as well as the bilinear frequencies, the above mentioned analysis framework was applied to the reduced-order model of the cracked plate with $h_c/h = 0.50$. As an example, the veering region between the fifth and sixth modes are shown in Fig. 4.8. As was shown in 4.3.2, the modes of interest are the in-plane and out-of-plane bending modes. In Fig. 4.8, two significant insights into the behavior of the frequencies are shown. The first is that the existence and location vary between the cases with open and sliding boundary conditions, and bilinear frequency. For the case with sliding boundary condition, the veering between fifth and sixth modes does *not* exist. On the other hand for the open boundary condition case, the loci of fifth and sixth modes approach and veer away where $10 \leqslant l_c/l \leqslant 15\%$. Therefore the bilinear frequency also has the veering region due to that for the open boundary condition, but slightly shifted toward

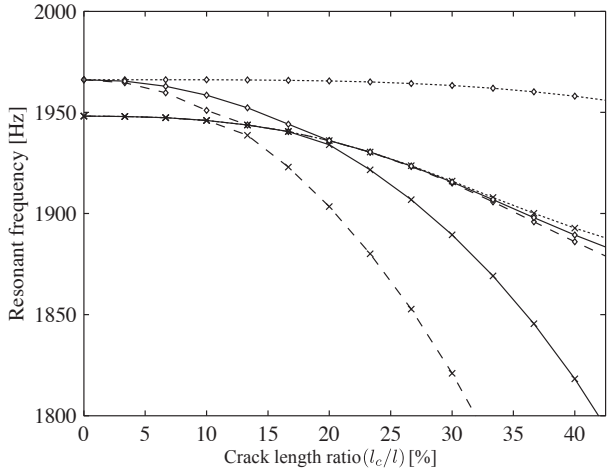

(a)

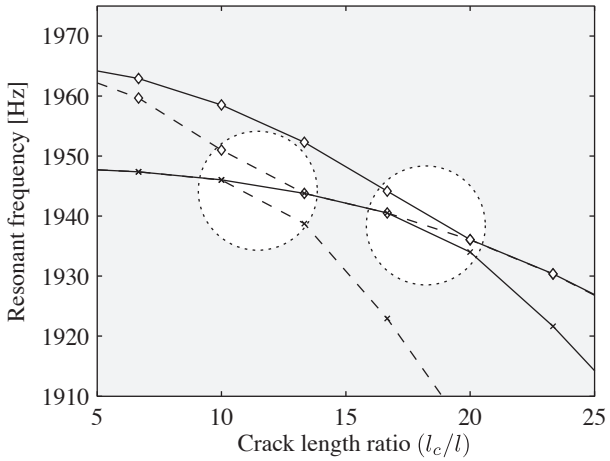

(b)

Figure 4.8: Comparison between natural frequencies with open and sliding B.C.'s., and bilinear frequencies for the system with $h_c/h = 0.50$: (a) The fifth and sixth natural frequencies of the system with sliding and open B.C.s, and bilinear frequencies: ---◇---, sixth mode with sliding B.C.; ---×---, fifth mode with sliding B.C.; – – ◇ – –, sixth natural frequency with open B.C.; – – × – –, fifth natural frequency with open B.C.; —◇—, sixth bilinear frequency; —×—, fifth bilinear frequency.; (b) Close-up view of the veering region for natural frequencies with open B.C. and bilinear frequencies: – – ◇ – –, sixth natural frequency with open B.C.; – – × – –, fifth natural frequency with open B.C.; —◇—, sixth bilinear frequency; —×—, fifth bilinear frequency.

larger crack length ratio because of the absence of the veering for the sliding boundary condition case (Fig. 4.8(b)). The second is that the bilinear frequency is *always* bounded by the frequencies corresponding to the cases with sliding and open boundary conditions, which are respectively the upper and lower bounds (Fig. 4.8(a)). This can also be easily verified from Eq. (4.14), i.e., if $\omega_{1i} \leqslant \omega_{2i}$, then $\omega_{1i} \leqslant \omega_{bi}$ and $\omega_{bi} \leqslant \omega_{2i}$. Furthermore, it is noted that the width between the upper and lower bounds indicates the strength of the effect of contact nonlinearity on the resonant frequency. For instance, for the fifth bilinear frequency that corresponds to the in-plane bending mode, the width between the bounds is much larger than that for the sixth bilinear frequency, which corresponds to the out-of-plane bending mode. This is due to the fact that the motion of the in-plane bending mode is greatly influenced by the existence of the contact force at the crack surfaces, whereas the out-of-plane bending modes is not so much affected by the contact force considering that the motion of the crack surfaces is almost perpendicular to the crack surfaces.

4.5.2 Comparison with the results of forced response analysis

Using the bilinear frequency approximation described above, the nonlinear vibration frequencies of the cracked plate are calculated, and they are compared with those obtained by the HFT method. It is noted that the comparison between the resonant frequencies obtained by forced response analysis, and the bilinear frequencies, namely the vibration frequencies of *unforced* system, has been made based on the assumption that the resonant frequencies reside in the vicinity of the frequencies associated with the nonlinear normal modes [90]. Furthermore, the resonant frequencies are assumed to be independent of the amplitude of forcing, based on the fact that the resonant frequencies of piecewise linear systems with the vanishing gap at the equilibrium are not dependent on vibration amplitude [31, 56].

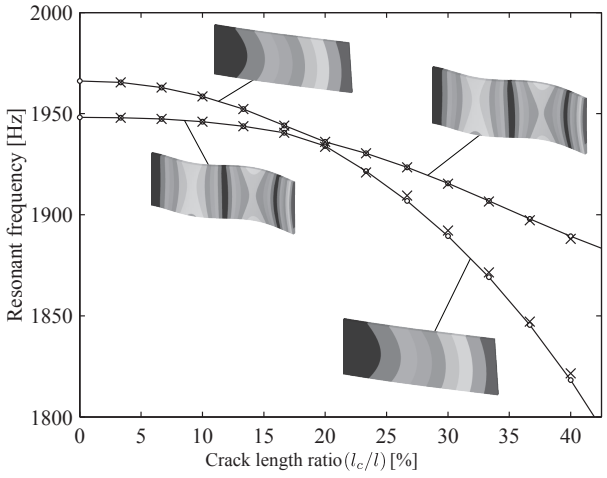

(a)

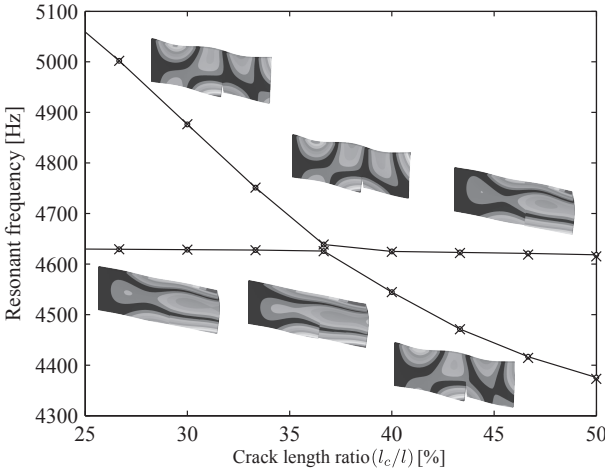

(b)

Figure 4.9: Comparison between bilinear frequency assumption and HFT method, and corresponding mode shapes with open B.C. : (a) $h_c/h = 0.50$, $-\circ-$, bilinear frequency, '$\times$', HFT method; (b) $h_c/h = 0.60$, $-\circ-$, bilinear frequency, '$\times$', HFT method.

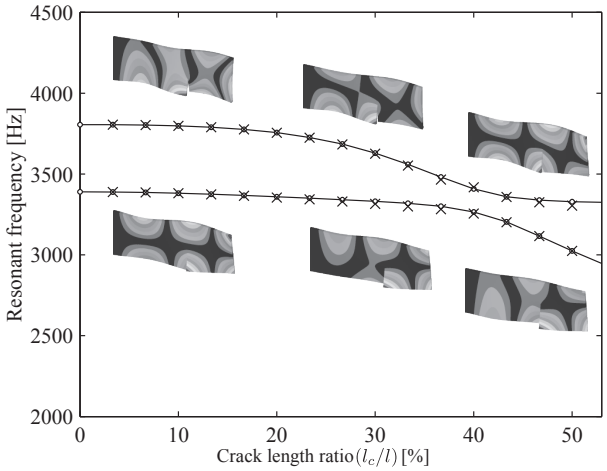

Figure 4.10: Comparison between bilinear frequency assumption and HFT method, and corresponding mode shapes with open B.C. : $h_c/h = 0.63$, $-\circ-$, bilinear frequency, '$\times$', HFT method.

Three representative veering regions are considered, which are the cases where (a) the interaction between the loci is weak and the corresponding modes are: (1) in-plane and out-of-plane bending modes, and (2) both out-of-plane bending modes, and (b) the interaction between the loci is strong and veering occurs in a continuous way and the associated modes are both out-of-plane bending modes.

First, the veering between an in-plane bending mode and an out-of-plane bending mode is considered, using the modes five and six, for $h_c/h = 0.50$, as shown in Fig. 4.3(b). The results of forced response analysis as well as the calculation based on bilinear frequency assumption are shown in Fig. 4.9(a). As can be seen, the order-switching of modes can be observed even for this nonlinear system. The most notable distinction from the linear assumption, i.e., Fig. 4.3(b), is that the veering occurs with longer crack length, i.e., around 20% whereas it occurs around 10% in Fig. 4.3(b). This is due to the *stiffening* effect because of the contact/impact of crack surfaces during the vibration cycle, which represents the dynamics of the cracked plates appropriately. Regarding the bilinear frequency

approximation, a notable result has been observed: the bilinear frequency assumption predicts the resonant frequency calculated by HFT method quite well even for relatively large crack length ratio ($l_c/l \leqslant 40\%$).

Second, the veering between two out-of-plane bending modes is considered, using the modes nine and ten for $h_c/h = 0.60$, and the calculation results are shown in Fig. 4.9(b). This result also shows that bilinear frequency approximates the resonant frequencies quite well for the case of veering between out-of-plane bending modes, with relatively large crack length. Even though the effect of nonlinearity on the vibration frequency is smaller than that on the in-plane bending modes, as it does not involve much contact/impact between crack surfaces, this clearly indicates that the bilinear frequency approximation can also be used for the prediction of nonlinear vibration frequencies of out-of-plane bending modes.

Third, the veering between the torsion and out-of-plane bending modes are examined, using the modes seven and eight for $h_c/h = 0.63$ and results are shown in Fig. 4.10. This veering region features a switching of modes in a continuous way, or in other words, the mode shapes gradually change as the crack length is varied. This result shows that the bilinear frequency approximation predicts the nonlinear vibration frequency quite well even for the modes that exhibit complicated geometry due to coupling between modes. Moreover, the results show that the approximation is accurate even for large cracks.

4.6 Conclusions

In this chapter, the linear and nonlinear vibration response of a cracked cantilevered rectangular plate have been investigated. In particular, the veering phenomena for the natural frequencies of the cracked plate were investigated. It was observed that veerings appear in plots of natural frequencies versus crack length or crack location ratio. It was shown

that a wider veering region entails continuous interchanging between the modes, whereas a smaller veering (or crossing) region shows fast mode switching. Then, the nonlinear vibration response of the cracked plate due to contact of the crack surfaces was considered. A hybrid frequency/time-domain (HFT) method was applied to the calculation of nonlinear resonant frequencies in representative veering/crossing regions. It was shown that the characteristics of veerings/crossings are affected to some extent by the nonlinearity induced by the crack closing effect, although in general they are similar to those of the linear counterparts. Furthermore, an alternative method for estimating the nonlinear resonant frequencies was proposed by generalizing the bilinear frequency approximation. The results of the proposed method were validated with the resonant frequencies obtained by the nonlinear forced response analysis for three typical veering scenarios. Moreover, it was shown that the method works even for relatively large crack length ratio.

CHAPTER V

An Efficient Reduced Order Modeling Technique for Nonlinear Vibration Analysis of Structures with Intermittent Contact

5.1 Introduction

Vibration problems of structures with intermittent contact have been studied extensively for several decades. These problems have practical importance and feature theoretical complexity due to their nonlinear nature. A numerical modeling procedure of such problems based on the finite element (FE) method is presented in this chapter. This work is motivated by a need for developing a model-based crack detection algorithm of elastic structures based on their spectral properties, such as resonant frequencies and response shapes. In order to properly predict the resonant frequencies of such structures, one has to consider the nonlinearity caused by intermittent contact at the cracks, the so-called closing crack or breathing crack effect. This has hindered analysts from accurately calculating the resonant frequencies of cracked structures, because they cannot be calculated from classical linear modal analysis. As some sophisticated contact algorithms have been developed, such as the penalty method [30] and the augmented Lagrangian method [45], the accuracy of the results of time transient simulation with FE models involving intermittent contact has been improved. Furthermore, studying vibration problems of such structures

with an FE model with a realistic complexity is becoming feasible with the aid of high-performance computers. However, in turn, due to the advancement of these technologies, analysts tend to create models with a large number of degrees of freedom (DOF). This is based on the expectation that, as the model becomes more realistic and the results become more accurate, the problem can still be solved in a reasonable amount of time. However, at some point the number of DOF will overwhelm even the most advanced hardware and software. In fact, as the model complexity increases, the cost of solving contact problems increases dramatically, even when the potential contact areas are known a priori. This occurs even if one uses reduced order modeling techniques, such as the Craig-Bampton method [26]. For forced response vibration problems of such structures, one can use accurate and efficient semi-analytical methods such as the ones based on the harmonic balance method (e.g., Ref. [17]), by representing the steady-state dynamic response of the model with a truncated Fourier series. However, such methods still suffer from the increase of computational cost as it requires a fair number of harmonics to be included for the Fourier transform, in order to obtain an accurate result. Therefore, the goal of this chapter is to propose an efficient reduced order modeling framework for vibration problems of elastic structures involving intermittent contact, with particular attention to modeling nonlinear vibration of cracked structures. The focus is placed upon reducing the number of DOF involved in the contact regions, in an automatic manner.

This chapter is organized as follows. In section 5.2, a literature survey over the related fields is provided. In section 5.3, the proposed modeling framework is presented, including the reduced order modeling approach and contact DOF selection method. As applications of the method, a case study is shown in section 5.4, using an FE model of a cantilevered cracked plate.Conclusions of the chapter are then given in section 5.5.

5.2 Background

The issues of reducing and selecting DOF of FE models have been extensively studied by various methods and perspectives, such as the reduction of the interface DOF between substructures, selection of master DOF for Guyan reduction [91], optimal sensor placement, and optimal constraint locations. However, many of the available methods share to some extent similar goals and related to each other as described later.

Firstly, the issue of *reducing the number of interface DOF* between the components has been studied by several researchers. Brahmi *et al.* [92] proposed a method for reducing the number of interface DOF before the assembly of substructures, where basis vectors are chosen based on the combination of secondary modal analysis of the interface DOF partitions of the matrices, and the truncation of modes based on the singular value decomposition. Balmés [93] introduced the framework for generalizing interface DOF such as constraint modes, by considering the new basis representing the actual interface displacements. Castanier *et al.* [94] also proposed a technique for reducing the number of interface DOF by applying the modal analysis and mode truncation to the constraint mode partition of the matrices produced by the Component Mode Synthesis (CMS) [26], the resulting modes of which are called the characteristic constraint modes after being transformed back into the finite element coordinates. All of these methods achieve the order reduction of the DOF at the interface. However, they do not provide any criteria as to *how* the interface DOF need be selected for accurately enforcing the boundary conditions.

Secondly, the *selection of master DOF* has been a crucial factor for determining the spectral property of the reduced order model for Guyan reduction-based reduction techniques, and many algorithms for the selection of the master DOF have been developed. As it shall be discussed later, this class of methods produces the results that tend to solve

the optimization problem for the problems studied in this study, thus it is very relevant to our objective. An automatic master DOF selection algorithm was first proposed by Henshell and Ong [95], in which the master DOF are chosen where the inertia is high and the stiffness is low, whereas the slave DOF are chosen where the inertia is low and the stiffness is high. This process can be automated by examining the radian frequency ω_s defined by fixing all DOF except the DOF i, i.e., $\omega_s = \sqrt{k_{ss}/m_{ss}}$, for $s = 1, \ldots, n$ where k_{ij} and m_{ij} are the entries at the ith row and jth column in FE stiffness and mass matrices of size n, and eliminating the largest ω_s at each iteration step, which means that a degree of freedom whose inertia is low and stiffness is high is selected, and eliminated. This process can be repeated until the number of master DOF reaches the desired number. An approach similar to this algorithm was proposed by Shah and Raymund [96] based on the discussion of Kidder and Flax [97–99], where the number of master DOF is controlled by iteratively eliminating the DOF whose ω_s is larger than the pre-defined cut-off frequency ω_c that is chosen to be approximately three times the highest significant frequency in the frequency range of interest. Independently from the work by Henshell and Ong, Grinenko and Mokeev developed an order reduction technique named frequency-dynamic condensation [100], which also proposed a criterion to select master degrees of freedom. Although their criterion was legitimate, the implementation of the selection algorithm still suffers from tedious exhaustive-search calculation for selecting the DOF. The selection method proposed by Matta [101] also uses the ratio k_{ss}/m_{ss} with the similar criterion to that proposed by Henshell and Ong [95]. It was addressed that the method can be applied not only to the Guyan reduction but also to the CMS, where both static and vibration modes are used as basis vectors, onto which the system dynamics are projected. A method proposed by Bouhaddi and Fillod [102] used a different concept where if a DOF a is a *node* of an eigenmode, then fixing the DOF a results in $\hat{\lambda}_i = \lambda_i$ where λ_i is the ith eigenvalue of the

non-fixed system, and $\hat{\lambda}_i$ is the eigenvalue of the system with DOF a being fixed. This concept may be understood using a vibration problem of a string with both ends fixed. That is, the lowest natural frequency of the string with a single support becomes the highest, if the support is placed at the node of the second mode of vibration [103]. This is because the first mode with the constraint then becomes identical to the second mode of the unconstrained string, which has the eigenvalue as the feasible upper bound of the first eigenvalue with a single constraint. It is noteworthy that Bouhaddi and Fillod explicitly aimed for *maximizing the minimum eigenvalue of the system where all the master DOF fixed*. This concept will be revisited in 5.3.3. The methods for the node selection reviewed so far are based on Henshell and Ong method to some extent. Another class of methods is that based on the concept of modal energy. The method proposed by Kim and Choi [104] uses the energy distribution among the DOF for each mode, and by taking the partial sum over the rows of what they call energy distribution matrix, primary DOF set can be chosen. On the other hand the method proposed by Cho and Kim [105] utilizes the energy estimation in element-level by the Rayleigh quotient value of each element. Kim and Cho then proposed a selection method consisting of two steps [106]; model order reduction by Improved Reduced System (IRS) [107] using the master DOF selected via a method based on energy estimation of each element [105], and subsequent sequential elimination method [95] with an iterative IRS. Another automatic DOF selection method named modal energy selection method proposed by Li [108] uses metric called index of classification, based on the approximate modal energy associated with each DOF. The method was successfully applied to an FE model of a cantilever beam problem. Oh and Park [109] also proposed a criterion for selecting the master DOF based on singular values of the modal matrix, however, it suffers from the computational cost due to exhaustive search over the possible master DOF sets, and depends on engineer's knowledge and intuition.

Thirdly, a similar but slightly different issue is the *selection of measurement locations* for vibration testing. For example, one may need to measure vibration displacements of a structure to determine vibration modes, typically with a limited number of sensors or the locations where the sensors can be placed. Thus, one may like to maximize the information one can obtain as much as possible, with the limited number of sensors or locations. However the question arises as to *how* the sensors need to be located, since the optimal configuration of sensors for such objective cannot be easily determined. There have been many methods developed to date for achieving this goal with various approaches. In particular, one of the successful approaches are based on information theory, which determine the sensor locations by optimizing a norm of the Fisher information matrix [110]. Among them, one of the most widely used techniques is the effective independence vector method, or the EIDV [111] method developed by Kammer [112]. The method determines the placement of sensors within the candidate locations while maintaining as much independent information as possible, i.e., maintaining the measured mode shapes as independent as possible. Therefore, it is natural to hypothesize that the application of the nonlinear boundary conditions to the optimum sensor locations would also well represent the real boundary conditions where the boundary conditions are applied to all locations in the region. This method is hereby considered in this study and the formulation is discussed in detail in 5.3.3.

Lastly, the issue of finding the optimal *constraint locations* to *maximize the fundamental natural frequency* of a structure is considered. This issue has an important relationship with the optimal master DOF selection. For instance, suppose there is a structure that can vibrate, and one may want to increase the lowest natural frequency as much as possible, by allocating a finite number of supports or kinematical constraints to the structure. However, the problem of finding the optimal number and the locations of such supports is not as

easy as it appears. Therefore, it may be necessary to apply mathematically expensive optimization algorithms to obtain such support locations, such as done in the work by Zhu and Zhang [113]. On the other hand, Åkesson and Olhoff [114] studied the problem by applying the Courant's maximum-minimum principle. Namely if there is a discrete dynamical system of size n and there are r $(< n)$ kinematical constraints applied to the system, all the eigenvalues of the structure increase, and the increased eigenvalues are bounded by the following formula:

$$\lambda_i^0 \leqslant \lambda_i \leqslant \lambda_{i+r}^0, \quad i \in \{1, 2, \ldots, n\} \tag{5.1}$$

where λ_i^0 and λ_{i+r}^0 denote the ith and $(i + r)$th eigenvalues of the structure without the constraints, and λ_i is the ith eigenvalue of the constrained structure. Also based on the same principle and the findings of Ref. [115], Won and Park [116] applied minimization method to obtain the optimal support location to achieve the maximum fundamental natural frequency of a cantilevered plate. They showed that the optimal support locations should be on the nodal lines of the $(r + 1)$th mode of the unconstrained structure. It is noted that this result conforms to the vibration problem of a fixed string mentioned above. This method was successfully applied to their specific examples, but the method can be applied only to special cases if the potentially-constrained region is the entire region of the structure, where the points on the nodal lines can be selected. Namely, if the regions to which the constraints are applied are limited to some specific regions of the structure, then the nodal lines may not exist in such regions, and the minimization problem becomes more complicated.

It is interesting to note that the idea of constraining the nodal lines was used to optimally select the master DOF for Guyan reduction by Bouhaddi and Fillod [102], but they were not aware of the applicability of their method to optimally select the support positions, while Won and Park were not aware of the applicability of their method to optimally

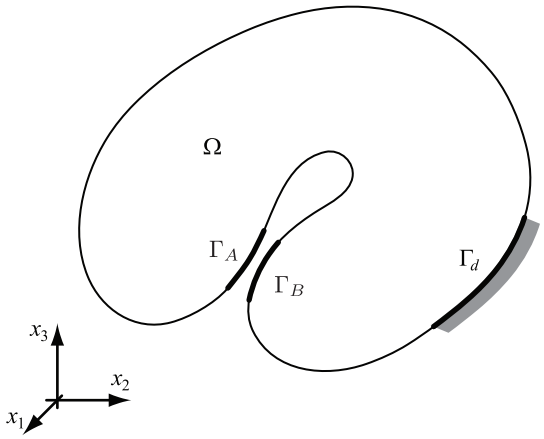

Figure 5.1: An elastic structure with potentially contacting boundaries

select the master DOF locations for Guyan reduction. In this chapter, we take advantage of this similarity between the optimal master DOF selections and the constraint locations, in order to achieve the optimal selection of the DOF where the nonlinear boundary conditions are applied.

5.3 Mathematical Formulation

Consider small vibration problems of an elastic structure represented as Ω with a fixed boundary Γ_d, where the structure may or may not involve intermittent contact at Γ_A and Γ_B during the vibration cycles, such as shown in Fig. 5.1. Namely the boundaries open and close, thus the vibration problem is nonlinear because the condition for the the boundaries to be in contact is dependent on the displacement field itself. That is, the boundary conditions at Γ_A and Γ_B are nonlinear. Here a crack is assumed to consist of such boundaries as Γ_A and Γ_B. It is well known that the system eigenvectors and eigen-frequencies are different from the actual response shapes and resonant frequencies of this nonlinear problem. In this chapter, they are respectively referred to as the nonlinear normal modes (NNMs) and NNM frequencies.

Now, if the structure is discretized with a method such as finite element method, the nonlinearity associated with the contact is *localized*, in the sense that the nonlinearity is caused only by a small portion of the entire structure. In the following formulations, a set of indices of DOF in such region is denoted as $\mathcal{B}$ (boundary), whereas a set of indices of the DOF in the rest of the regions is denoted as $\mathcal{I}$ (internal), and partitions of vectors and matrices associated with these sets are designated with subscripts of the associated lower-case italic letters, i.e., b and i. The sizes of the sets are denoted as $|\mathcal{B}| = n_{\mathcal{B}}$ and $|\mathcal{I}| = n_{\mathcal{I}}$. All the other DOF sets defined hereinafter follow the same notation.

If the finite element mass and stiffness matrices are denoted as $\mathbf{M} \in \mathbb{R}^{n\times n}$ and $\mathbf{K} \in \mathbb{R}^{n\times n}$ and the nodal displacement vector is given as $\mathbf{x} \in \mathbb{R}^n$, the governing equations of the vibration problem with the absence of external forcing and damping may be written in a partitioned matrix-vector form as follows:

$$\begin{pmatrix} \mathbf{M}_{bb} & \mathbf{M}_{bi} \\ \mathbf{M}_{ib} & \mathbf{M}_{ii} \end{pmatrix} \begin{bmatrix} \ddot{\mathbf{x}}_b \\ \ddot{\mathbf{x}}_i \end{bmatrix} + \begin{pmatrix} \mathbf{K}_{bb} & \mathbf{K}_{bi} \\ \mathbf{K}_{ib} & \mathbf{K}_{ii} \end{pmatrix} \begin{bmatrix} \mathbf{x}_b \\ \mathbf{x}_i \end{bmatrix} = \begin{bmatrix} \mathbf{f}_b(\mathbf{x}_b) \\ \mathbf{0} \end{bmatrix} \tag{5.2}$$

where a dot $(\dot{})$ denotes a time derivative, and $\mathbf{f}_b \in \mathbb{R}^{n_{\mathcal{B}}}$ denotes the nonlinear force associated with the intermittent contact. When dealing with this type of nonlinear vibration problems, one can apply linear reduced order modeling techniques, such as Guyan reduction [91], system equivalent reduction expansion process (SEREP) [117], iterated improved reduced system (IIRS) [118, 119], or Component mode synthesis (CMS) [26]. With such methods, one can obtain smaller system matrices by reducing the size of $\mathbf{x}_i$ by means of Rayleigh-Ritz coordinate transformation comprising of various basis vectors such as static deformations and vibration modes, yet keeping the accessibility to the physical coordinates of $\mathbf{x}_b$. For instance, with the help of CMS, one can obtain a system with desired spectral properties *and* accessibility to $\mathbf{x}_b$, the size of which is as small as $n_{\mathcal{B}}$ DOF plus the number of linear normal modes whose frequencies lie in the frequency ranges

of interest. The use of such linear reduced order modeling methods greatly helps ones to analyze the dynamic response of systems with localized nonlinearities, such as transient dynamic analysis [120], and nonlinear harmonic response analysis [56]. However, even with these reduced order modeling methods, if the number of DOF involved in the b partition becomes large, especially the cases with very fine mesh in the contacting regions, one cannot take advantage of the linear reduced order modeling techniques, as the computational cost associated with the nonlinear dynamic analysis typically grows as the number of DOF in the b partition increases. Furthermore, if one simply attempts to eliminate some of the DOF in the b partition, it results in inaccurate, or even wrong results, in comparison to the results obtained with a full set of DOF in the b partition. Therefore, in order to obtain accurate computational results, such as those of nonlinear forced response, one needs to keep as many boundary DOF as possible, which could easily result in prohibitively costly calculations. Typically as a "workaround" to avoid the inaccurate results due to the lack of sufficient DOF considered and at the same time to obtain efficient computational model, one has to select the DOF in a heuristic way, which greatly depends on the system characteristics and analyst's experience and intuition. Moreover, if the model is developed in such ways, the error contained in the following analysis results cannot be estimated a priori. Our aim here is to develop an automatic way to select the DOF in $\mathcal{B}$ for a desired number of DOF to be selected.

5.3.1 Primary Model Reduction

In order to reduce the number of DOF included in $\mathcal{I}$ to make the subsequent development more efficient, first a model reduction is applied to Eq. (5.2). Namely, $\mathcal{I}$ is further divided into two sets, i.e., $\mathcal{I} = \mathcal{O} \cup \mathcal{D}$ where $\mathcal{O}$ is a set of DOF indices associated with the nodes to be used in the following analysis, such as observing the behavior of the system or

applying external loading, and $\mathcal{D}$ is the rest of DOF indices in $\mathcal{I}$, which is to be apparently deleted from the system by the reduction methods. In addition, a set of DOF indices to be used as the *master* DOF is defined as active DOF, designated as $\mathcal{A}$, and $\mathcal{A} = \mathcal{B} \cup \mathcal{O}$. Now consider an eigenvalue problem of the system Eq. (5.2), where the eigenvalue λ and the corresponding eigenvector $\boldsymbol{\phi}$ must satisfy the following:

$$\begin{pmatrix} \mathbf{K}_{aa} & \mathbf{K}_{ad} \\ \mathbf{K}_{oa} & \mathbf{K}_{dd} \end{pmatrix} \begin{bmatrix} \boldsymbol{\phi}_a \\ \boldsymbol{\phi}_d \end{bmatrix} = \lambda \begin{pmatrix} \mathbf{M}_{aa} & \mathbf{M}_{ad} \\ \mathbf{M}_{da} & \mathbf{M}_{dd} \end{pmatrix} \begin{bmatrix} \boldsymbol{\phi}_a \\ \boldsymbol{\phi}_d \end{bmatrix} \tag{5.3}$$

where $\boldsymbol{\phi} = [\boldsymbol{\phi}_a^{\mathrm{T}}, \boldsymbol{\phi}_d^{\mathrm{T}}]^{\mathrm{T}}$. In this study, a mixed-boundary CMS of Hintz-Herting [57, 83] is chosen for the primary model reduction. Namely, without the presence of rigid body modes, the coordinate transformation is defined as

$$\begin{bmatrix} \mathbf{x}_a \\ \mathbf{x}_d \end{bmatrix} = \mathbf{H}\mathbf{y} = \begin{pmatrix} \boldsymbol{\Psi} & \hat{\boldsymbol{\Phi}} \end{pmatrix} \begin{bmatrix} \mathbf{y}_a \\ \mathbf{y}_m \end{bmatrix} \tag{5.4}$$

where $\mathbf{x}_a = \mathbf{y}_a$, $\mathbf{y}_m$ is a vector of modal coordinates, $\boldsymbol{\Psi}$ and $\hat{\boldsymbol{\Phi}}$ are so-called constraint modes and truncated free-interface normal modes in a modified form, which are respectively defined as

$$\boldsymbol{\Psi} = \begin{pmatrix} \mathbf{I} \\ -\mathbf{K}_{dd}^{-1}\mathbf{K}_{da} \end{pmatrix} \tag{5.5}$$

$$\hat{\boldsymbol{\Phi}} = \begin{pmatrix} \mathbf{0} \\ \boldsymbol{\Phi}_d + \mathbf{K}_{dd}^{-1}\mathbf{K}_{da}\boldsymbol{\Phi}_a \end{pmatrix} \tag{5.6}$$

and $\boldsymbol{\Phi} = [\boldsymbol{\phi}_{(1)}, \boldsymbol{\phi}_{(2)}, \ldots, \boldsymbol{\phi}_{(k)}]$, $k < n$, each subscript in parentheses denoting the corresponding mode number. Using the transformation defined as Eq. (5.4), the projected eigenvalue problem is obtained as

$$\mathbf{K}_H\mathbf{y} = \mu\mathbf{M}_H\mathbf{y} \tag{5.7}$$

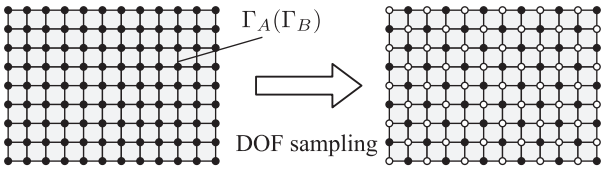

Figure 5.2: Schematic of the node sampling: •, selected node ($\mathcal{N}$)

where $\mathbf{M}_H = \mathbf{H}^{\mathrm{T}}\mathbf{M}\mathbf{H}$ and $\mathbf{K}_H = \mathbf{H}^{\mathrm{T}}\mathbf{K}\mathbf{H}$. It should be noted that the projected eigenvalue problem Eq. (5.7) possesses at least the same eigenvalues of the original systems, i.e., $\lambda_{(1)}, \lambda_{(2)}, \ldots \lambda_{(k)}$ (the indices may be different from the ones for the projected system.) This is because the subspace spanned by the columns of $(\boldsymbol{\Psi}, \hat{\boldsymbol{\Phi}})$ contains the eigenvectors of Eq. (5.3), i.e., $\boldsymbol{\phi}_{(j)} \in \mathrm{span}(\boldsymbol{\Psi}, \hat{\boldsymbol{\Phi}})$ for $j = 1, \ldots k$, as $\mathrm{span}(\boldsymbol{\Psi}, \hat{\boldsymbol{\Phi}}) = \mathrm{span}(\boldsymbol{\Psi}, \boldsymbol{\Phi})$, and hence the projected eigenvalue problem has the same eigenvalues as the original ones. It means that, the eigenvalues of the projected system Eq. (5.7) does *not* contain any error in the eigenvalues and eigenvectors, with respect to those of the original eigenvalue problem of the finite element. Although this advantage comes with the expense of calculating the eigenvalues and eigenvectors of the finite element model, it is not a major drawback considering that the computational cost involved in the nonlinear computations with the original finite element would be more prohibitively expensive, than calculating a few normal modes of the finite element model.

5.3.2 Nonlinear DOF sampling

With the reduced order model obtained in 5.3.1, the next step is to select the DOF in $\mathcal{B}$ such that the nonlinear characteristics of the system can be well approximated by applying the nonlinear boundary conditions *only* on the selected DOF.

As mentioned, accurately calculating the NNM frequencies is of primary interest of this study. The NNM frequencies of the system can be obtained in several ways, such

as time integration of Eq. (5.2) for harmonic loading, or harmonic-balance-based frequency/time domain analysis [20, 56]. It was shown by the authors that the NNM frequencies for cracked plates obtained by the nonlinear harmonic response analysis can be well approximated by the application of bilinear frequency approximation even when the crack surfaces involve multiple DOF [121]. Therefore, as a measure to evaluate the results obtained with the selected DOF, bilinear frequency is used in the following development. Namely, the ith NNM frequency ω_{ni} can be approximated by a bilinear frequency ω_{bi} defined as

$$\omega_{bi} = \frac{2\omega_o\omega_s}{\omega_o + \omega_s} \tag{5.8}$$

where ω_o and ω_s are the natural frequencies of the corresponding linear systems, which can be respectively obtained by solving the following eigenvalue problems:

$$\mathbf{K}_H\mathbf{y} = (\omega_o^2)\mathbf{M}_H\mathbf{y}, \quad \text{subject to } \textit{open} \text{ B.C.'s} \tag{5.9}$$

$$\mathbf{K}_H\mathbf{y} = (\omega_s^2)\mathbf{M}_H\mathbf{y}, \quad \text{subject to } \textit{sliding} \text{ B.C.'s} \tag{5.10}$$

The open B.C. is a boundary condition where no constraint is imposed on the nodes on Γ_A and Γ_B, or the DOF in $\mathcal{B}$. Thus in fact Eq. (5.9) is identical to Eq. (5.7). On the other hand for the sliding B.C., it is assumed that Γ_A can freely slide with respect to Γ_B but cannot separate along the normal directions, as described as follows.

Here a contact pair is defined as a pair of nodes on Γ_A and Γ_B, which may or may not be in contact during the vibration, and a set of numbers denoting all the contact pairs is defined as $\mathcal{C}_{cp}$. For the jth contact pair in $\mathcal{C}_{cp}$, three mutually perpendicular normal vectors at a node on Γ_A are defined as $\mathbf{n}_1^j$, $\mathbf{n}_2^j$, and $\mathbf{n}_3^j$ where $\mathbf{n}_1^j$ is the normal vector pointing outward from the surface, $\mathbf{n}_2^j$ and $\mathbf{n}_3^j$ are unit vectors that are tangent to the surface and perpendicular to each other. Using these vectors, a coordinate transformation matrix $\mathbf{P}_A^j = (\mathbf{n}_1^j, \mathbf{n}_2^j, \mathbf{n}_3^j)$ is defined for each contact pair, with the assumption that a nodal displacement

vector contains only translational DOF, such that the x_1 component of the displacement vector of the node is aligned with $\mathbf{n}_1^i$, and pointing outward from the surface. For the other node of the jth contact pair on Γ_B, the corresponding coordinate transformation matrix that aligns the x_1 component of the nodal displacement vector with the normal vector is defined as $\mathbf{P}_B^j = -\mathbf{P}_A^j$. Now assembling $\mathbf{P}_A^j$ and $\mathbf{P}_B^j$ for all $j \in \mathcal{C}_{cp}$, a coordinate transformation is defined as

$$\mathbf{P} = \begin{pmatrix} \mathbf{P}_b & \mathbf{0} & \mathbf{0} \\ \mathbf{0} & \mathbf{I}_o & \mathbf{0} \\ \mathbf{0} & \mathbf{0} & \mathbf{I}_m \end{pmatrix}, \quad \text{where} \quad \mathbf{P}_b = \underset{j=1}{\overset{n_{\mathcal{C}_{cp}}}{\mathrm{A}}} (\mathbf{P}_A^j, \mathbf{P}_B^j) \tag{5.11}$$

and A is an assembly operator, $\mathbf{P}_b \in \mathbb{R}^{n_\mathcal{B} \times n_\mathcal{B}}$, $\mathbf{I}_o \in \mathbb{R}^{n_\mathcal{O} \times n_\mathcal{O}}$, and $\mathbf{I}_m \in \mathbb{R}^{n_\mathcal{M} \times n_\mathcal{M}}$. Next, for the jth contact pair, the x_1 components of the nodal displacement vectors, which are denoted as u_A^j and u_B^j, are transformed to a relative displacement $u^j \triangleq (u_A^j + u_B^j)/\sqrt{2}$ and a displacement $v^j \triangleq (u_A^j - u_B^j)/\sqrt{2}$. Namely, denoting the set of DOF corresponding to u_A^j and u_B^j for all jth contact pair,

$$\begin{bmatrix} u^j \\ v^j \end{bmatrix} = \frac{1}{\sqrt{2}} \begin{pmatrix} 1 & 1 \\ 1 & -1 \end{pmatrix} \begin{bmatrix} u_A^j \\ u_B^j \end{bmatrix} \tag{5.12}$$

Now defining sets $\mathcal{X}$, $\mathcal{Y}$, and $\mathcal{Z}$ ($\mathcal{X} \cup \mathcal{Y} \cup \mathcal{Z} = \mathcal{B}$ and $n_\mathcal{X} = n_\mathcal{Y} = n_\mathcal{Z} = n_{\mathcal{C}_{cp}}$) that respectively contain sets of indices of the DOF corresponding to x_1, x_2, and x_3 for all $j \in \mathcal{C}_{cp}$, and denoting the coefficient matrix in the Eq. (5.12) as $\mathbf{R}^j$, one can define a transformation matrix $\mathbf{R}$ by assembling $\mathbf{R}^j$ for $j \in \mathcal{C}_{cp}$ as follows

$$\mathbf{R} = \begin{pmatrix} \mathbf{R}_x & \mathbf{0} \\ \mathbf{0} & \mathbf{I} \end{pmatrix}, \quad \text{where} \quad \mathbf{R}_x = \underset{j=1}{\overset{n_{\mathcal{C}_{cp}}}{\mathrm{A}}} (\mathbf{R}^j) \tag{5.13}$$

and $\mathbf{R}_x \in \mathbb{R}^{n_\mathcal{X} \times n_\mathcal{X}}$. Considering that $\mathbf{P}^{-1} = \mathbf{P}^{\mathrm{T}}$ and $\mathbf{R}^{-1} = \mathbf{R}^{\mathrm{T}}$, the eigenvalue problem Eq. (5.7) can be transformed to

$$\mathbb{K}\mathbf{z} = (\omega_o^2)\mathbb{M}\mathbf{z} \tag{5.14}$$

where $\mathbf{y} = \mathbf{PRz}$, $\mathbb{M} = (\mathbf{PR})^{\mathrm{T}}\mathbf{M}_H\mathbf{PR}$, and $\mathbb{K} = (\mathbf{PR})^{\mathrm{T}}\mathbf{K}_H\mathbf{PR}$. Now noting that $\mathbf{z}$ can be partitioned into $\mathbf{z} = [\mathbf{z}_r, \mathbf{z}_g]$ where $\mathbf{z}_r$ is the vector of relative DOF, or $u^j, \forall j \in \mathcal{C}_{cp}$, and $\mathbf{z}_g$ is the generalized internal DOF containing $v^j, \forall j \in \mathcal{C}_{cp}$, x_2 and x_3 components of the nodal displacement vectors of the nodes of the contact pairs, displacement vectors of the observer nodes, and modal coordinates. That is, Eq. (5.14) can be written as

$$\begin{pmatrix} \mathbb{K}_{rr} & \mathbb{K}_{rg} \\ \mathbb{K}_{gr} & \mathbb{K}_{gg} \end{pmatrix} \begin{bmatrix} \mathbf{z}_r \\ \mathbf{z}_g \end{bmatrix} = (\omega_o^2) \begin{pmatrix} \mathbb{M}_{rr} & \mathbb{M}_{rg} \\ \mathbb{M}_{gr} & \mathbb{M}_{gg} \end{pmatrix} \begin{bmatrix} \mathbf{z}_r \\ \mathbf{z}_g \end{bmatrix} \tag{5.15}$$

where $\mathcal{R} \subset \mathcal{X}$ and $\mathcal{G} = (\mathcal{A} \backslash \mathcal{R}) \cup \mathcal{M}$.

The best approximation to the NNM frequency can be obtained when the sliding boundary conditions are imposed on all of the nodes on the surface Γ_A and Γ_B. Namely the associated eigenvalue problem with the sliding boundary conditions can be obtained by constraining *all* the relative DOF, or $\mathbf{z}_r = \mathbf{0}$, i.e.,

$$\mathbb{K}_{gg}\mathbf{z}_g = (\omega_s^2)\mathbb{M}_{gg}\mathbf{z}_g \tag{5.16}$$

Now, we assume that we do *not* like to consider all nodes in $\mathcal{R}$ for the subsequent forced response analysis due to the large number of DOF involved in $\mathcal{R}$. In other words, the nodes where the nonlinear boundary conditions are applied should be sampled such as illustrated in Fig. 5.2. The selected DOF is designated as nonlinear DOF, and a set of indices of the nonlinear DOF is denoted as $\mathcal{N}$, where $\mathcal{N} \subset \mathcal{R}$. The rest of DOF in $\mathcal{R}$ is designated as linear DOF, and associated set is denoted as $\mathcal{L}$ where $\mathcal{N} \cup \mathcal{L} = \mathcal{R}$. Therefore, the bilinear frequency should be calculated with ω_s such that the sliding B.C. is applied only on the DOF in $\mathcal{N}$, or $\mathbf{z}_n = \mathbf{0}$, i.e.,

$$\begin{pmatrix} \mathbb{K}_{ll} & \mathbb{K}_{lg} \\ \mathbb{K}_{gl} & \mathbb{K}_{gg} \end{pmatrix} \begin{bmatrix} \mathbf{z}_l \\ \mathbf{z}_g \end{bmatrix} = (\omega_s^2) \begin{pmatrix} \mathbb{M}_{ll} & \mathbb{M}_{lg} \\ \mathbb{M}_{gl} & \mathbb{M}_{gg} \end{pmatrix} \begin{bmatrix} \mathbf{z}_l \\ \mathbf{z}_g \end{bmatrix} \tag{5.17}$$

Considering that the value of the natural frequency of the system with the open boundary conditions, ω_o, is independent on neither the number nor the pattern of the selected DOF

(recalling that span$(\boldsymbol{\Psi}_c, \hat{\Phi})$ contains the chosen eigenvectors), one can see from Eq. (5.8) that ω_{bi} is dependent only on ω_s for a fixed ω_o. Now considering the Rayleigh's theorem of constraints defined by Eq. (5.1), it is known that all the system's eigenvalues increase if a single constraint is imposed on a system. Therefore, as the number of constraints on Eq. (5.7) to calculate ω_s increases, ω_s increases. Furthermore, considering that ω_{bi} is a monotonically increasing function of ω_s for a fixed ω_o, or $\partial\omega_{bi}/\partial\omega_s = 2\omega_o^2/(\omega_o + \omega_s)^2 \geqslant 0$, one can state that the best approximation of ω_{bi} for a given number of $n_{\mathcal{N}}$ can be obtained when the maximum ω_s is achieved. Thus a corresponding maximization problem is stated as follows:

$$\begin{aligned} &\max_{\mathcal{N}\subset\mathcal{R}} \omega_s(\mathcal{N}) \\ &\text{subject to} \quad |\mathcal{N}| = n_{\mathcal{N}} \end{aligned} \tag{5.18}$$

This maximization problem may be solved by mathematical programming methods, such as integer programming or topology optimization methods as was done in Ref. [113]. As it shall be discussed next, this maximization problem can in fact be treated in a more efficient way by the use of Guyan reduction and some methods to choose the *master DOF* for reduced order modeling techniques.

5.3.3 Automatic master DOF selection

The methods for automatically selecting the master DOF for the Guyan reduction have been previously developed, such as in Refs. [95, 96, 102]. In particular, the method proposed by Henshell and Ong [95] appears to be the most successful approach. Although it has been known to be computationally expensive due to the nature of eliminating a single DOF per iteration and successive application of Guyan reduction, this can be alleviated by the application of the primary model reduction by the CMS as developed in 5.3.1. As was mentioned by Bouhaddi and Fillod [102], and Shah and Raymund [96], the master DOF of Guyan reduction should be chosen such that the valid eigenvalue range of the reduced

order model is maximized. In general, it has been known that the eigenvalue range of validity is "bounded" by the lowest eigenvalue of the system with all the master DOF fixed. Here this concept is applied to the problem of finding the optimal $\mathcal{N}$ that solves Eq. (5.18). Namely, the corresponding eigenvalue problem is Eq. (5.17) by regarding $\mathbf{z}_n$ as the master DOF. As was discussed in the Ref. [122], the error bounds in the ith eigenvalue of the reduced model produced by the Guyan reduction can be obtained a priori by the following relationship

$$0 \leqslant \varepsilon_i \leqslant \frac{\lambda_i}{\lambda_{s,min} - \lambda_i} \tag{5.19}$$

where $\varepsilon_i \triangleq (\overline{\lambda}_i - \lambda_i)/\lambda_i$ is the relative error in the ith eigenvalue, $\overline{\lambda}_i$ is the ith eigenvalue of the reduced order model, λ_i is the ith eigenvalue of the original finite element model, and $\lambda_{s,min}$ is the smallest eigenvalue of the system with *all the master DOF fixed*. For $\lambda_i/\lambda_{s,min} \ll 1$, the upper bound asymptotically converges to the following value [123],

$$0 \leqslant \varepsilon_i \leqslant \lambda_i/\lambda_{s,min} \tag{5.20}$$

Therefore, it is apparent that maximizing $\lambda_{s,min}$ results in minimizing the upper bound of the error for all the eigenvalues of the reduced order model. Hence this gives us a guideline for selecting the master DOF for Guyan reduction such that the errors in the eigenvalues of the resulting reduced order model are minimized.

By observing this fact from another point of view, one may see that if a certain set of master DOF can achieve the maximum $\lambda_{s,min}$, we can obtain not only an accurate reduced order model that can well approximate the first few lowest eigenvalues of the original system, but also as a "byproduct", a good estimate on the *optimal constraint locations that maximize the fundamental frequency*. Recasting this to our original problem of selecting the optimal set $\mathcal{N}$, the error bounds Eq. (5.20) associated with the eigenvalue problem

Eq. (5.17) are written as

$$0 \leqslant \varepsilon_i \leqslant \frac{(\omega_o^2)_i}{(\omega_s^2)_1 - (\omega_o^2)_i} \tag{5.21}$$

where $\varepsilon_i \triangleq [(\bar{\omega}_o^2)_i - (\omega_o^2)_i]/(\omega_o^2)_i$, $(\bar{\omega}_o^2)_i$ is the ith eigenvalue of a reduced order model, $(\omega_s)_1$ is the lowest natural frequency of Eq. (5.17). The corresponding maximization problem is Eq. (5.18), and by solving this problem for the lowest eigenvalue, $(\omega_s)_1$, one can expect that the chosen nodes pattern is at least sub-optimal.

According to Refs. [123, 124], the sequential elimination method by Henshell and Ong [95] tends to keep $\lambda_{s,min}$ high, as it eliminates the DOF associated with the highest constrained frequency at each iteration as the slave DOF. Namely after the elimination procedure, if the chosen master DOF are all fixed, the system is left with the DOF that were chosen as the slave DOF that were identified to have the highest constrained frequency at each elimination process. Thus the resulting system with all the master DOF fixed tends to have a larger $\lambda_{s,min}$ than that calculated with systems with other possible combinations of master DOF fixed. The Henshell and Ong's method that is adapted specifically for this problem is shown in Fig. 5.3. First, at each iteration, the ratios of the diagonal terms of the stiffness matrix k_{jj} to the diagonal terms of the mass matrix m_{jj} are calculated for $\forall j \in \mathcal{R}$, and the index q_1 that gives the maximum ratio among $j \in \mathcal{R}$ is obtained. Next, the set $\mathcal{L}$ is updated such that it contains q_1, and all the other DOF that are associated with the contact pair $k \in \mathcal{C}_{cp}$ to which the q_1th DOF belongs, e.g., the DOF that are perpendicular to the normal direction. The set $\mathcal{N}$ is then updated such that it excludes the selected DOF of $\mathcal{L}$ from $\mathcal{R}$, and the set $\mathcal{R}$ is re-defined as $\mathcal{N}$. A constraint mode is calculated by solving a problem where a unit displacement is applied to a DOF in $\mathcal{N}$ whereas all the other DOF in $\mathcal{N}$ being fixed. This is repeated for all DOF in $\mathcal{N}$, resulting in the following matrix:

$$\mathbf{\Psi} = \begin{pmatrix} \mathbf{I} \\ -\left(\mathbb{K}_{ll}\right)^{-1} \mathbb{K}_{ln} \end{pmatrix} \tag{5.22}$$

for $i = 1$ to $i = n_{\mathcal{R}} - n_{\mathcal{N}}$ **do**
  Calculate $\sqrt{k_{jj}/m_{jj}}$ for $j \in \mathcal{R}$
  Find q_1 such that $\sqrt{k_{q_1q_1}/m_{q_1q_1}} = \max_{j \in \mathcal{R}} \sqrt{k_{jj}/m_{jj}}$
  $\mathcal{L} \leftarrow \{q_1, \ldots, q_{n_k}\}$ where q's are the DOF associated with the kth contact pair ($k \in \mathcal{C}_{cp}$) and n_k is the number of DOF in kth contact pair
  $\mathcal{N} \leftarrow \mathcal{R} \backslash \mathcal{L}$
  $\mathcal{R} \leftarrow \mathcal{N}$
  Calculate constraint modes Eq. (5.22)
  Apply Guyan reduction to the system matrices: $\mathbb{M} \leftarrow \mathbf{\Psi}^{\mathrm{T}} \mathbb{M} \mathbf{\Psi}$, $\mathbb{K} \leftarrow \mathbf{\Psi}^{\mathrm{T}} \mathbb{K} \mathbf{\Psi}$
end for

Figure 5.3: DOF selection based on Henshell and Ong method

Calculate $\mathbf{\Phi}_k$
for $i = 1$ to $i = n_{\mathcal{R}} - n_{\mathcal{N}}$ **do**
  $\mathbf{A} \leftarrow \mathbf{\Phi}_k^{\mathrm{T}} \mathbf{\Phi}_k$
  $\mathbf{E} \leftarrow \mathbf{\Phi}_k \mathbf{A}^{-1} \mathbf{\Phi}_k^{\mathrm{T}}$
  Find q_1 such that $e_{q_1q_1} = \min_{j \in \mathcal{R}} e_{jj}$
  $\mathcal{L} \leftarrow \{q_1, \ldots, q_{n_k}\}$ where q's are the DOF associated with the kth contact pair ($k \in \mathcal{C}_{cp}$) and n_k is the number of DOF in kth contact pair
  $\mathcal{N} \leftarrow \mathcal{R} \backslash \mathcal{L}$
  $\mathcal{R} \leftarrow \mathcal{N}$
  Delete rows of $\mathbf{\Phi}_k$ corresponding to the DOF in $\mathcal{L}$
end for

Figure 5.4: DOF selection based on EIDV method

where $\mathbf{\Psi}$ is the matrix of constraint modes for all DOF in $\mathcal{N}$. The Guyan reduction is then applied to the mass and stiffness matrices. The iteration continues until the number of DOF in $\mathcal{N}$ reaches the specified value of $n_{\mathcal{N}}$ using $\mathbf{\Psi}$.

In order to clarify the appropriateness of the algorithm in Fig. 5.3 to this problem, another algorithm for selecting DOF is shown here for comparison. The method of effective independence vector, or the EIDV method developed by Kammer [112], is a method to choose the sensor placement locations for the vibration measurement of large scale structures. The method aims to make the measured eigenvectors as linearly independent as possible. According to Penny *et al.* [111], many of the criteria for choosing the master DOF for model order reduction have similar criteria for choosing measurement locations

in a way such that the *lower frequency modes can be captured accurately*. In fact, as examined by Penny *et al.*, both the Henshell and Ong method and the EIDV method produce acceptable selections in most cases, in a sub-optimal manner. The DOF selection algorithm based on the EIDV method is shown as Algorithm 5.4. First, the eigenvalue problem Eq. (5.16) is solved for the first k modes, and the associated modal matrix is designated as $\mathbf{\Phi}_k = (\boldsymbol{\phi}_1, \boldsymbol{\phi}_2, \ldots, \boldsymbol{\phi}_k)$, or $\mathbb{K}\mathbf{\Phi}_k = \mathbb{M}\mathbf{\Phi}_k\mathbf{\Lambda}_k$ where $\mathbf{\Lambda}_k = \mathrm{diag}_{j=1,\ldots,k}\left((\omega_o^2)_j\right)$. The Fisher information matrix $\mathbf{A}$ is then calculated as $\mathbf{A} = \mathbf{\Phi}_k^{\mathrm{T}}\mathbf{\Phi}_k$, and an idempotent matrix $\mathbf{E}$ is computed as $\mathbf{E} = \mathbf{\Phi}_k\mathbf{A}^{-1}\mathbf{\Phi}_k^{\mathrm{T}}$, the diagonal of which is called the independence distribution vector (see Ref. [112] for detailed formulations.) The least contributing DOF to the independence of the modes among the ones in $\mathcal{R}$ is identified as the one with the smallest diagonal element in $\mathbf{E}$. The associated DOF are also identified and stored in $\mathcal{L}$, and both $\mathcal{N}$ and $\mathcal{R}$ are updated as in the Henshell and Ong method. Finally the rows of $\mathbf{\Psi}_k$ corresponding to the DOF in $\mathcal{L}$ are deleted. The iteration continues until the size of $\mathcal{N}$ reaches the desired number $n_{\mathcal{N}}$.

Although the EIDV method shares similar objective for choosing DOF with the Henshell and Ong method, the objective of the EIDV method is not exactly the maximization problem of Eq. (5.18). Therefore it is expected that the Henshell and Ong method returns better solutions to the given maximization problem than the EIDV method, as it is shown in the next section.

5.4 Case study

In section 5.3, the method to select the nonlinear DOF has been introduced. In this section, the validity and applicability of the method are discussed by applying the algorithm to an example problem. With the case study, the validity of the proposed method is discussed in terms of the bilinear frequencies and forced response. Furthermore a metric

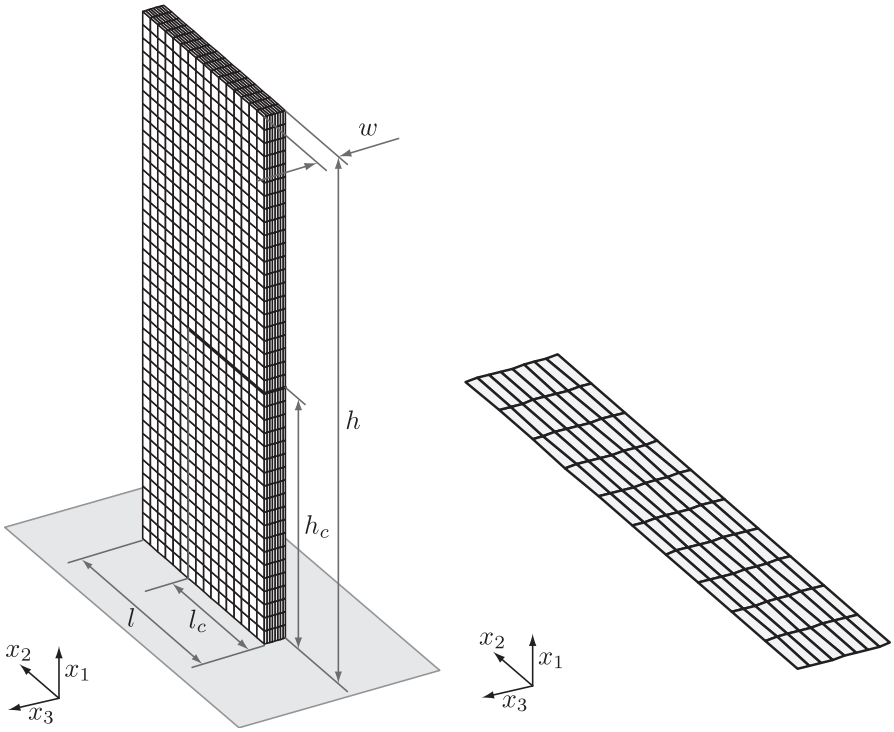

(a) (b)

Figure 5.5: Cantilevered cracked plate model: (a) FE model, (b) Magnified crack surface

to assess their accuracy is introduced and examined.

5.4.1 Simple cracked plate model

Problem description

A cantilevered cracked plate model was constructed with Young's modulus $E = 2.0 \times 10^{11}$ Pa, Poisson's ratio $\nu = 0.3$, and density $\rho = 7800$ kg/m^3, and its geometry is shown as Fig. 5.5(a) where $w = 6.0 \times 10^{-3}$m, $l = 6.0 \times 10^{-2}$m, $h = 1.5 \times 10^{-1}$m, $l_c/l = 0.625$, and $h_c/h = 0.475$. The model was discretized with 5,120 linear solid elements and resulted in mass and stiffness matrices with 18,630 DOF. On the crack surfaces as shown in Fig. 5.5(b), there are 180 nodes, or 90 contact pairs on the surfaces hence the number of the associated DOF is 540. The CMS method shown in the section 5.3.1 was then applied to the FE model, and it resulted in the 681 DOF (3.6% of the original size)

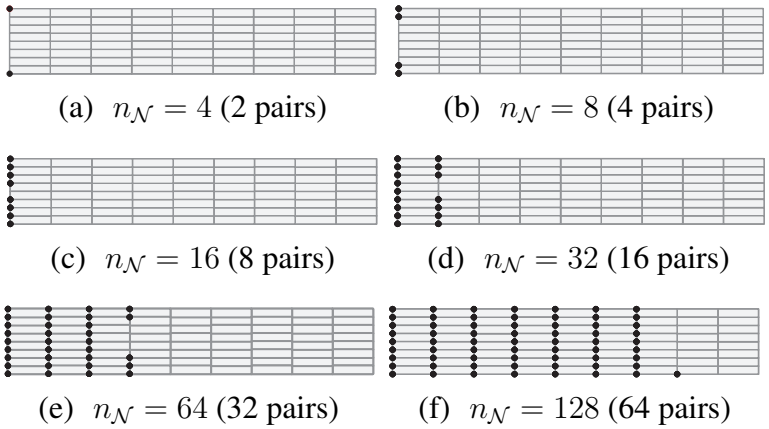

Figure 5.6: Selected nodes by an intuitive approach (left edge open)

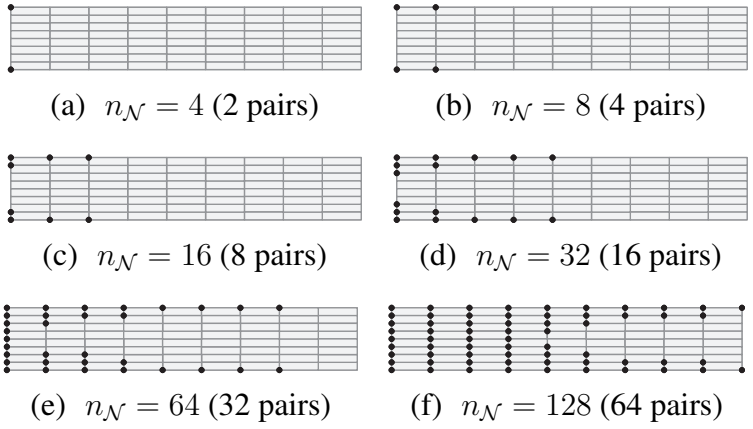

Figure 5.7: Selected nodes by EIDV method (left edge open)

system consisting of 621 physical DOF and 60 modal coordinates corresponding to the free-interface normal modes. With this reduced order model, both algorithms in Figs. 5.3 and 5.4 were applied for $n_{\mathcal{N}}$ =4, 8, 16, 32, 64, and 128. For the EIDV method, the first four modes were considered.

In order to compare these results with an "intuitive" selection method, a selection criteria was also employed, where the nonlinear DOF were chosen based on the amount of *penetration* between the nodes in a contact pair for the modes of interest, which in this case is the fourth mode. Namely, it was hoped that penalizing the inter-penetration of the

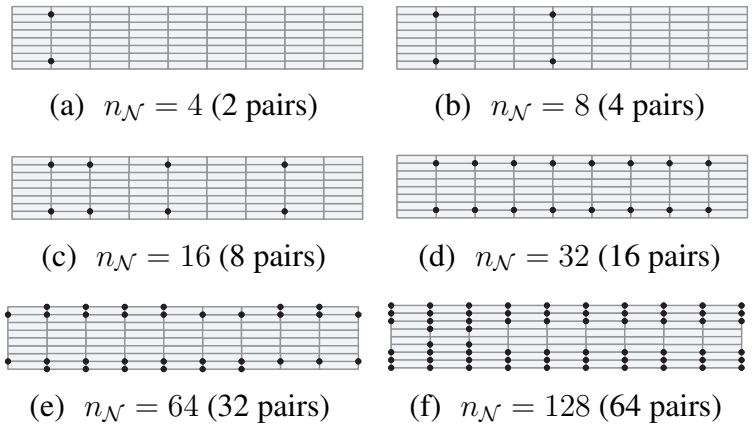

Figure 5.8: Selected nodes by the modified Henshell and Ong method (left edge open)

most penetrating contact pairs would produce the "stiffest" system response. The selected node pattern with such criterion is shown as Fig. 5.6, and the results of the EIDV method and the Henshell and Ong method are shown as Figs. 5.7 and 5.8. As can be seen in Fig. 5.6, if the nodes are chosen based on the amount of penetration, the selection starts from the nodes near the crack edge (open side) for $n_{\mathcal{N}} = 4$, and it then proceeds toward the tip of the crack (closed side) as $n_{\mathcal{N}}$ increases. It makes sense because the motion of the crack surfaces is significant near the open edge than that near the closed edge. On the other hand with the EIDV method, the method also starts to select the nodes near the crack edge, but it tends to choose more nodes on the crack rims than the nodes near the crack edge as shown in Fig. 5.7. Finally with the Henshell and Ong method, it also select the nodes near the crack edge first, for $n_{\mathcal{N}} = 4$, but it then tends to select the nodes over the crack surface in a more distributed manner as can be seen in Fig. 5.8.

Forced Response Analysis

Next, in order to see the influence of the application of the nonlinear B.C. onto the selected nodes on an NNM frequency, forced response analysis was carried out by applying an external harmonic loading to the cracked plate. As one might notice, when the

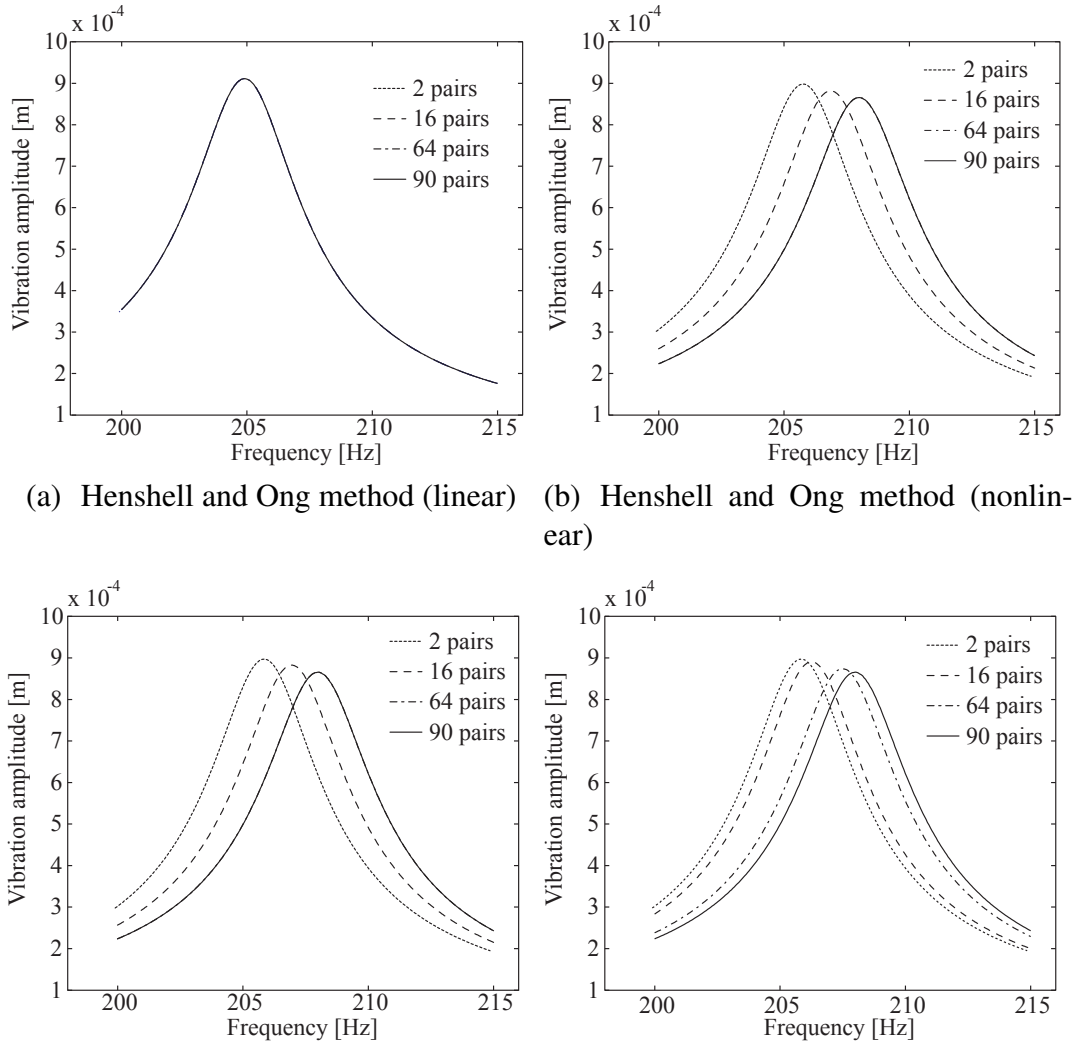

(a) Henshell and Ong method (linear) (b) Henshell and Ong method (nonlinear)

(c) EIDV method (nonlinear) (d) Intuitive approach (nonlinear)

Figure 5.9: Results of forced response analysis of the cracked plate

forced response of this structure with a crack is considered, the repetitive opening and closing of the crack faces must be treated appropriately with contact algorithms. As a result, the vibration is nonlinear and the steady-state response of the displacement may not be expressed as a harmonic function even if the external force is a harmonic function. Therefore in this study, the steady-state response was obtained by assuming that the displacement can be expressed as a truncated Fourier series, and the nonlinear boundary condition can be enforced by the penalty method [30]. The method is called the hybrid

frequency-time domain method [20, 56], which is based on the concept of harmonic balance method [17]. Detailed formulation of the method is described in previous chapters. It is noted that the system matrices were further reduced by the application of Eq. (5.4) to the reduced-order model before the forced response calculation, by keeping the selected node pairs as the active DOF and condensing out the other DOF including physical and modal coordinates. For example, with $n_{\mathcal{N}} = 64$ (32 pairs), the system size was reduced down to 155 DOF, which is 0.83% of the original system size.

A harmonic forcing of magnitude 3 N was then applied at the tip of the plate, in order to excite the first vibration mode, which corresponds to the first out-of-plance bending mode. The forced response was calculated for both linear case, i.e., with the open B.C., and nonlinear case with the nonlinear boundary conditions imposed on $\mathcal{N}$ with the selections by the Henshell and Ong method. The results are shown in Figs. 5.9(a) and 5.9(b). As can be seen in Fig 5.9(a), the selection pattern does not alter the linear forced response. This is because the selection of the active DOF does not alter the eigenvalues of the reduced order model, and it was assumed that the system was completely linear when the forced response was calculated. On the other hand, the number of contact pairs greatly affects the results of nonlinear forced response as shown in Fig. 5.9(b). One may observe that the response with 64 contact pairs is almost identical to that with the full set of 90 contact pairs, which implies that for accurately calculating the nonlinear resonant frequencies, it may not be necessary to enforce nonlinear boundary conditions for all the contact pairs on the crack faces. The same forced response calculations were carried out with the node patterns selected by the EIDV method and the method based on the amount of penetration, and they are respectively shown in Figs. 5.9(c) and 5.9(d). As can be seen in Fig. 5.9(c), the results with the patterns chosen by the EIDV method are comparable with the ones produced by the Henshell and Ong method. On the other hand as can be seen in Fig. 5.9(d),

the forced response with the node patterns chosen by the "intuitive" approach produced worse results than the other two methods, i.e., for a given number of $n_{\mathcal{N}}$, the predicted resonant frequency by the approach is lower than that calculated by the other methods. This is the most visible in the results for $n_{\mathcal{N}} = 64$, for which both the Henshell and Ong method and the EIDV methods produced results that are almost identical to the results for $n_{\mathcal{N}} = 90$.

Bilinear Frequency Approximation

Finally, the influence of the selected node pattern on the bilinear frequencies is discussed. The first four bilinear frequencies were calculated for the model with the selected node patterns with the three methods, and the results are shown in Fig. 5.10. The first four modes correspond to the first out-of-plane bending, the first torsion, the second out-of-plane bending, and the first in-plane bending modes respectively. The plots in Fig. 5.10 show the percentage errors in the bilinear frequency versus the number of contact pairs, where the error is defined as the ratio of the difference between the bilinear frequency with the sampled contact pairs and that with the full set of contact pairs, to that with the full set of contact pairs. As can be seen, the Henshell and Ong method consistently provides the best results among all the methods for the first four modes. Moreover, it shows the best convergence rate in terms of the number of contact pairs.

A posteriori accuracy assessment

As seen above, even though the intuitive approach chooses the contact pairs that show the most penetration, application of the nonlinear boundary conditions to these nodes does not result in the "stiffest" vibration response. To be specific, the Henshell and Ong method and the EIDV method produced the node patterns that yield the closer results to the reference results in terms of forced response and bilinear frequencies, than the patterns chosen

by the intuitive approach. In particular, the Henshell and Ong method iteratively aims to solve the maximization problem Eq. (5.18) in a sub-optimal manner. Therefore the bi-linear frequencies as well as the resonant frequencies were well approximated with the nodes chosen by the Henshell and Ong method. In order to better understand the governing factor for the accuracy of the results, a more physical interpretation of the results is provided here. Namely, the key effect for achieving the good approximation of the NNM frequency is to ensure, as much as possible, the non-penetrability condition on the contact pairs where the nonlinear B.C.s' are *not* applied. The penetration should be evaluated during a vibration cycle, thus both the depth and the duration of the penetration should be taken into account. These quantities vary in space, and depend on the frequency of vibration. Hence as a metric to characterize not only the amount but also the duration of penetration over the entire crack surfaces for a given vibration frequency, the following quantity is introduced:

$$\hat{F} = \int_0^T \left(\int_{\Gamma_A(\Gamma_B)} k_e u_p(\mathbf{r}, t) \mathrm{d}\Gamma \right) \mathrm{d}t \tag{5.23}$$

where $\hat{F}$ is a quantity with the dimension of impulse named "virtual impulse", k_e is an equivalent spring constant per unit length determined by the ratio between the Young's modulus multiplied by the characteristic area and the characteristic length, u_p is the amount of penetration along the surface normals, and T is the period of vibration associated with the NNM frequency. The quantity $\hat{F}$ is calculated based on the calculated time trajectory of displacements of the nodes on the crack surfaces, and can be thought of as an impulse that does *not* contribute to the system response, as this impulse is not applied to the system when the response is calculated. In other words, the smaller the value of $\hat{F}$ is, the stricter the boundary conditions are imposed on the nodes over the entire crack surfaces.

First, the forced response analysis was carried out, and the corresponding time history of u_p over the entire crack surface was recovered from the vibration response. The integrals

in the Eq. (5.23) were then evaluated by a simple quadrature rule both in space and time. The metric was calculated for the first and the fourth modes for 8 and 32 pairs chosen by the methods, and the results are shown in Figs. 5.11 and 5.12. As can be seen in Figs. 5.11 and 5.12, the virtual impulse varies over the frequency range. In particular, when the frequency of excitation is close to the resonant frequency, or the NNM frequency, then the amount of penetration increases as well. However for all cases, the Henshell and Ong method consistently results in the smallest impulse over the frequency range among the three methods considered. It means that the nonlinear B.C. on the crack faces is the most strictly enforced by the node patterns chosen by the Henshell and Ong method.

5.5 Conclusion

In this chapter, a novel reduced order modeling framework for the nonlinear vibration analysis of elastic structures with intermittent contact was proposed. In section 5.3, the modeling framework was developed based on a method of component mode synthesis. The master DOF selection scheme for Guyan reduction was formulated by considering the close relationship between the optimal master DOF selection and the optimal constraint locations for maximizing the fundamental frequency. The method is a combination of the sequential elimination method proposed by Henshell and Ong, and appropriate coordinate transformations to the reduced order model. Another method for choosing the nodes was also introduced for the sake of comparative study, which is based on a method to optimally choose the measurement locations such that the measured mode becomes as linearly independent as possible. The method was then applied to a representative finite element model in section 5.4. In 5.4.1, the methods were applied to a cracked plate model. Using the selected node patterns, forced response analysis was carried out to see the effects of the selection patterns on the frequency response. Furthermore the resonant frequencies

were calculated by the application of bilinear frequency approximation. It was confirmed that the selected DOF resulted in accurate prediction of nonlinear resonant frequencies in comparison to the benchmark case of using all DOF on the crack surfaces. Moreover, a posteriori accuracy assessment procedure was introduced by examining the amount of penetration on the crack surfaces during a vibration cycle. The results showed that the selected node patterns by the proposed method consistently shows the best results among the methods compared in the other methods.

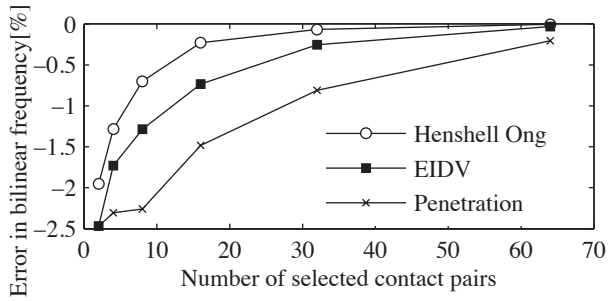

(a)

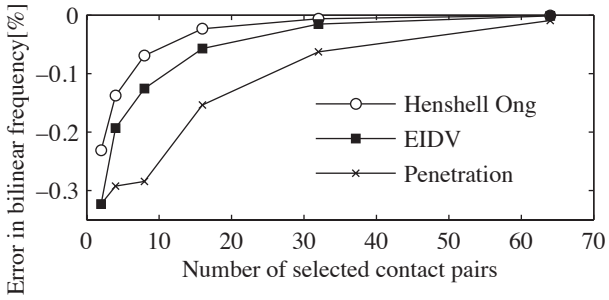

(b)

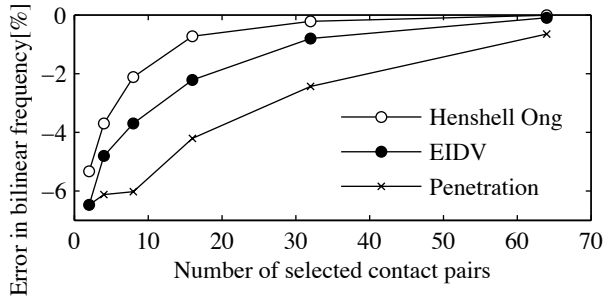

(c)

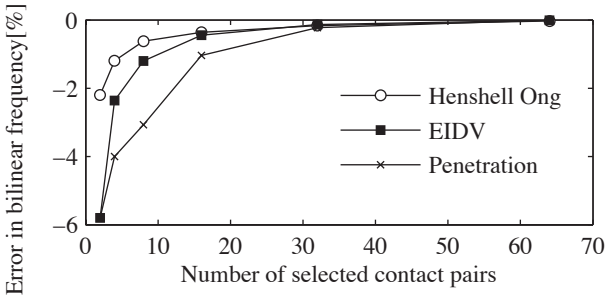

(d)

Figure 5.10: Errors in the first four bilinear frequencies:(a) NNM 1, (b) NNM 2, (c) NNM 3, (d) NNM 4

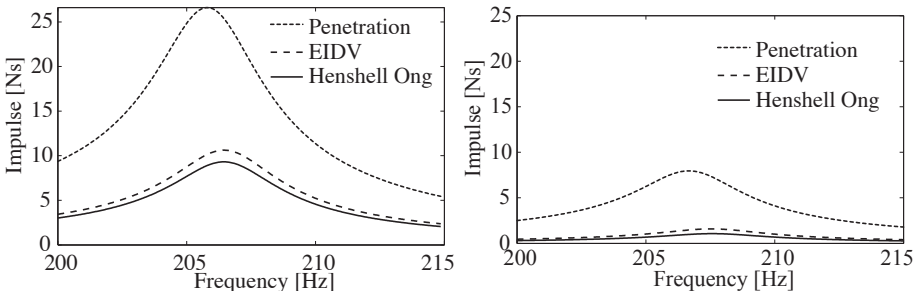

(a) $n_{\mathcal{N}} = 16$ (8 pair) (b) $n_{\mathcal{N}} = 64$ (32 pair)

Figure 5.11: Virtual impulse for a period of vibration for NNM 1

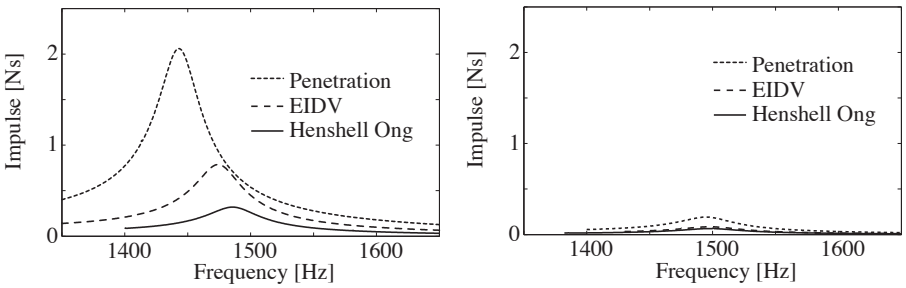

(a) $n_{\mathcal{N}} = 16$ (8 pair) (b) $n_{\mathcal{N}} = 64$ (32 pair)

Figure 5.12: Virtual impulse for a period of vibration for NNM 4

CHAPTER VI

Conclusion

The fundamental difficulty of the vibration problems of cracked structures is that the problems are nonlinear, which is caused by the repetitive opening and closing of the crack faces. Due to this difficulty, traditional analysis tools can no longer be applied for the prediction of the vibration characteristics of the cracked systems, such as resonant frequencies and mode shapes. Therefore, one may have to use very time consuming computational methods to obtain these quantities, or to use approximation methods that are not accurate. As a consequence, even fundamental characteristics of the dynamics of such structures have not been fully investigated to date. The results obtained in this dissertation demonstrate that the proposed analysis framework can be used to examine various aspects of cracked structures accurately and efficiently.

6.1 Contributions

The original contributions of this dissertation are described as follows:

- In Chapter II, an efficient method was presented for reduced-order modeling and nonlinear vibration analysis of rotating cracked structures. This method accounts for the change in the equilibrium configuration of the crack surfaces due to rotation and the attendant influence on the forced vibration response due to the intermittent

contact of the crack surfaces. The individual and combined effects of rotation and intermittent contact on the forced response were examined in detail for an example of a cracked blade.

- In Chapter III, a modeling and analysis framework for the nonlinear forced response of a rotor with a cracked blade was presented. The basic approach is to employ a combination of a hybrid-interface CMS modeling method, a contact detection algorithm, and the HFT nonlinear vibration analysis method. It was observed that both mistuning and cracks can lead to strong localization of the forced response, and the mistuning can lead to localization about different blades for different mode families. Furtheremore, a crack tends to lead to localization about the same (cracked) blade for all mode families. For certain mode families, the effect of the crack will be relatively strong compared to that of mistuning, such that the cracked-blade-dominated response may appear at a significantly lower frequency and may also include unique characteristics such as a double resonance peak. The relative strength of the effects of a crack on the system response for different mode families, and thus the observability of the cracked-blade-dominated resonance, can be estimated to some extent with a nonlinear vibration analysis of a single blade

- In Chapter IV, the linear and nonlinear vibration response of a cracked cantilevered rectangular plate near eigenvalue loci veerings have been investigated. It was observed that veerings appear in plots of natural frequencies versus crack length or crack location ratio. It was shown that a wider veering region entails continuous interchanging between the modes, whereas a smaller veering (or crossing) region shows fast mode switching. It was shown that the characteristics of veerings/crossings are affected to some extent by the nonlinearity induced by the crack

closing effect, although in general they are similar to those of the linear counterparts. Furthermore, an alternative method for estimating the nonlinear resonant frequencies was proposed by generalizing the bilinear frequency approximation. The results of the proposed method were validated with the resonant frequencies obtained by the nonlinear forced response analysis for three typical veering scenarios. Moreover, it was shown that the method works even for relatively large crack length ratio.

- In Chapter V, a reduced order modeling framework for the nonlinear vibration analysis of elastic structures with intermittent contact was proposed, with special emphasis on an optimal node selection method on the crack faces. The method was developed based on a master DOF selection scheme for Guyan reduction that maximize the fundamental natural frequency. The method was then applied to representative finite element models, and nonlinear forced response analysis as well as the bilinear frequency approximation have been employed. It was confirmed that the selected DOF resulted in accurate prediction of nonlinear resonant frequencies compared with the benchmark case of using all DOF on the crack surfaces.

6.2 Future research

Below are some ideas for future research that may further expand the research topics presented in this dissertation.

- **Development of efficient nonlinear vibration analysis framework for mistuned rotors, and applications to structural health monitoring**

  The implementation of blade mistuning in a model of a bladed disk with a cracked blade was done at the finite element level in the approach provided in chapter III. However, this approach is not suitable for parametric studies of randomly mistuned

bladed disks with a cracked blade, due to the high computational cost associated with repeatedly changing the FEM for each mistuning pattern and then performing the finite element analysis needed to generate the corresponding ROM. A much more efficient approach is to model the blade mistuning directly in the ROM.

There have been a substantial number of studies on efficient mistuning modeling approaches, such as the Subset of Nominal Modes (SNM) method [125], the Frequency Response Function (FRF) matrix method [126], and the Component Mode Mistuning (CMM) method [127]. In particular, the CMM method utilizes the mistuning projection method of Bladh *et al.* [128], which accomplishes the practical implementation of mistuning in the reduced-order subspace. However, the method was developed for linear vibration analysis of a rotor for which all blades are identical in the tuned case, and thus it is not readily applicable to cracked structures.

The major computational challenge of this problem is that cyclic symmetry is broken by both mistuning and the crack in one blade. Therefore, the highly efficient cyclic symmetry analysis routines that are applied to obtain normal modes of tuned bladed disks cannot be used if there is a crack in one blade. Moreover, the accessibility to physical degrees of freedom from the reduced order subspace must be ensured, so that the nonlinear contact force due to crack surface interaction can properly be evaluated within the alternating frequency/time-domain framework.

Thus, a new mistuning modeling approach needs to be considered for handling bladed disks with cracked blades.

- **Enhancement of the Hybrid Frequency/Time domain method**

  When the HFT method is applied to solving the nonlinear ordinary differential equations for vibration problems of rotating cracked structures, there are two major chal-

lenges: (1) numerical instability as well as high computational cost caused from the large penalty parameter, and (2) the existence of multiple solutions due to initial gaps at the crack interfaces.

The first issue is intrinsic to the penalty method, because the penalty parameter must be chosen *as large as possible* to ensure the satisfaction of the nonlinear boundary condition at the crack surfaces, yet *small enough* to avoid numerical ill-conditioning [129]. In particular, the penalty parameter, or the inter-penetration of the crack nodes, has been shown to influence the resonant frequency of a cracked beam [29]. One of the possible solutions to this may be the application of the dynamic Lagrangian mixed frequency-time domain method (DLFT) [84], which is essentially the extension of the the augmented Lagrangian method [45] from the time-domain analysis to frequency-domain analysis. It could achieve accurate solutions with relatively small penalty coefficient, and hence the stabilization and faster convergence of the algorithm.

The latter problem may happen for the cases with initial gaps, which result from the rotation of the structures. It typically results in a jump phenomenon in the frequency response. The problem is that in the neighborhood of the point at which the jump occurs, or the bifurcation point, the algorithm of solving the nonlinear equations could fail due to the lack of good initial guess. In order to circumvent this type of difficulty, the numerical continuation methods [130] are typically employed for solving algebraic equations of various types of nonlinear systems. The continuation methods have been applied to many algorithms for solving nonlinear algebraic equations that arise from Harmonic Balance type methods, such as the Multi-term Harmonic Balance Method for rotor/stator contact problems [44], structures with three-dimensional frictional constraints [131], or a polynomial-based method [132].

Application of continuation methods could improve the algorithm in terms of the stability near the bifurcation point, and the feasibility to investigate the unstable branch of the multiple solutions.

BIBLIOGRAPHY

BIBLIOGRAPHY

[1] M. -H. H. Shen and C. Pierre. Natural modes of Bernoulli-Euler beams with symmetric cracks. *Journal of Sound and Vibration*, 138(1):115–134, 1990.

[2] M. -H. H. Shen and C. Pierre. Free vibrations of beams with a single-edge crack. *Journal of Sound and Vibration*, 170(2):237–259, 1994.

[3] P. Gudmundson. The dynamic behavior of slender structures with cross-sectional cracks. *Journal of the Mechanics and Physics of Solids*, 31(4):329–345, 1983.

[4] M. -H. H. Shen and Y. C. Chu. Vibrations of beams with a fatigue crack. *Computers and Structures*, 45(1):79–93, 1992.

[5] T. G. Chondros, A. D. Dimarogonas, and J. Yao. Vibration of a beam with a breathing crack. *Journal of Sound and Vibration*, 239(1):57–67, Jan 2001.

[6] N. Pugno, C. Surace, and R. Ruotolo. Evaluation of the non-linear dynamic response to harmonic excitation of a beam with several breathing cracks. *Journal of Sound and Vibration*, 235(5):749–762, 2000.

[7] A. P. Bovsunovsky and C. Surace. Consideration regarding superharmonic vibrations of a cracked beam and the variation in damping caused by the presence of the crack. *Journal of Sound and Vibration*, 288(4-5):865–886, 2005.

[8] A. Bazoune. Survey on modal frequencies of centrifugally stiffened beams. *The Shock and Vibration Digest*, 37(6):449–469, 2005.

[9] A. V. Srinivasan. Flutter and resonant vibration characteristics of engine blades. *Journal of Engineering for Gas Turbines and Power*, 119(4):742–775, 1997.

[10] J. C. Slater, G. R. Minkiewicz, and A. J. Blair. Forced response of bladed disk assemblies — a survey. *Shock and Vibration Digest*, 31(1):17–24, 1999.

[11] M. P. Castanier and C. Pierre. Modeling and analysis of mistuned bladed disk vibration: Status and emerging directions. *Journal of Propulsion and Power*, 22:384–396, March 2006.

[12] J. H. Kuang and B. W. Huang. The effect of blade crack on mode localization in rotating bladed disks. *Journal of Sound and Vibration*, 227:85–103, Oct 1999.

[13] J. H. Kuang and B. W. Huang. Mode localization of a cracked blade disk. *Journal of Engineering for Gas Turbines and Power*, 121(2):335–341, Apr 1999.

[14] B. W. Huang and J. H. Kuang. Variation in the stability of a rotating blade disk with a local crack defect. *Journal of Sound and Vibration*, 294:486–502, Jul 2006.

[15] X. Fang, J. Tang, E. Jordan, and K.D. Murphy. Crack induced vibration localization in simplified bladed-disk structures. *Journal of Sound and Vibration*, 291:395–418, Mar 2006.

[16] J. F. Hou. Cracking-induced mistuning in bladed disks. *AIAA Journal*, 44:2542–2546, Nov 2006.

[17] A. Nayfeh and D. Mook. *Nonlinear Oscillations*. John Wiley & Sons, 1979.

[18] C. Pierre, A. A. Ferri, and E. H. Dowell. Multi-harmonic analysis of dry friction damped systems using an incremental harmonic balance method. *Journal of Applied Mechanics*, 52(4):958–964, 1985.

[19] J. J. Chen and C. H. Menq. Periodic response of blades having three-dimensional nonlinear shroud constraints. *Journal of Engineering for Gas Turbines and Power*, 123:901–909, Oct 2001.

[20] O. Poudou and C. Pierre. Hybrid frequency-time domain methods for the analysis of complex structural systems with dry friction damping. In *Proceedings of of the 44th AIAA/ASME/ASCE/AHS/ASC Structures, Structural Dynamics, and Materials Conference*, volume 1, pages 111–124, Apr 2003.

[21] E. P. Petrov and D. J. Ewins. Method for analysis of nonlinear multiharmonic vibrations of mistuned bladed disks with scatter of contact interface characteristics. *Journal of Turbomachinery-Transactions of the ASME*, 127:128–136, Jan 2005.

[22] E. P. Petrov and D. J. Ewins. Effects of damping and varying contact area at blade-disk joints in forced response analysis of bladed disk assemblies. *Journal of Turbomachinery-Transactions of the ASME*, 128:403–410, Apr 2006.

[23] T. Cameron and J. Griffin. An alternating frequency/time domain method for calculating the steady-state response of nonlinear dynamic systems. *Journal of Applied Mechanics*, 56:149–154, 1989.

[24] F. H. Ling and X. X. Wu. Fast galerkin method and its application to determine periodic-solutions of nonlinear oscillators. *International Journal of Non-Linear Mechanics*, 22:89–98, 1987.

[25] J. Guillen and C. Pierre. An efficient, hybrid, frequency-time domain method for the dynamics of large-scale dry-friction damped structural systems. In F. Pfeiffer and Ch. Glocker, editors, *IUTAM Symposium on Unilateral Multibody Contacts*. Kluwer Academic Publishers, Dordrecht, Netherlands, 1999.

[26] R. R. Craig and M. C. C. Bampton. Coupling of substructures for dynamic analyses. *AIAA Journal*, 6(7):1313–1319, 1968.

[27] M. J. D. Powell. A hybrid method for nonlinear equations. In P. Rabinowitz, editor, *Numerical Methods for Nonlinear Algebraic Equations*. Gordon and Breach Science Publishers, London, 1970.

[28] O. Poudou, C. Pierre, and B. Reisser. A new hybrid frequency-time domain method for the forced vibration of elastic structures with friction and intermittent contact. In *Proceedings of the 10th International Symposium on Transport Phenomena and Dynamics of Rotating Machinery, paper ISROMAC10-2004-068*, Honolulu, Hawaii, March 2004.

[29] O. Poudou and C. Pierre. A new method for the analysis of the nonlinear dynamics of structures with cracks. In *Proceedings of NOVEM 2005*, Saint-Raphaël, France, April 2005.

[30] J. T. Oden and E. B. Pires. Algorithms and numerical results for finite-element approximations of contact problems with non-classical friction laws. *Computers & Structures*, 19:137–147, 1984.

[31] S. W. Shaw and P. J. Holmes. A periodically forced piecewise linear oscillator. *Journal of Sound and Vibration*, 90(1):129–155, 1983.

[32] E. A Butcher. Clearance effects on bilinear normal mode frequencies. *Journal of Sound and Vibration*, 224(2):305–328, 1999.

[33] M. Chati, R. Rand, and S. Mukherjee. Modal analysis of a cracked beam. *Journal of Sound and Vibration*, 207(2):249–270, Oct 1997.

[34] U. Andreaus, P. Casini, and F. Vestroni. Non-linear dynamics of a cracked cantilever beam under harmonic excitation. *International Journal of Non-Linear Mechanics*, 42(3):566–575, 2007.

[35] A. D. Dimarogonas. Vibration of cracked structures: A state of the art review. *Engineering Fracture Mechanics*, 55(5):831–857, 1996.

[36] M. Mercadal, A. von Flotow, and P. Tappert. Damage identification by nsms blade resonance tracking in mistuned rotors. In *Aerospace Conference, 2001, IEEE Proceedings*, volume 7, pages 3263–3277, 2001.

[37] W. W. Van Arsdell and S. B. Brown. Subcritical crack growth in silicon mems. *Journal of Microelectromechanical Systems*, 8(3):319–327, 1999.

[38] J. Guillen and C. Pierre. Analysis of the forced response of dry-friction damped structural systems using an efficient hybrid frequency-time method. In Anil K. Bajaj, N. Sri Namachchivaya, and Matthew A. Franchek, editors, *Nonlinear Dynamics and Controls*, volume DE-91, pages 41–49. American Society of Mechanical Engineers, New York, NY, 1996.

[39] K. B. Subrahmanyam and K. R. V. Kaza. Vibration and buckling of rotating, pretwisted, preconed beams including coriolis effects. *Journal of Vibration, Acoustics, Stress, and Reliability in Design*, 108(2):140–149, 1986.

[40] ANSYS, Inc., Pittsburgh, PA. *ANSYS Release 10.0 Documentation*, 2005.

[41] E. Pesheck and C. Pierre. An analysis of a friction damped system using two component mode methods. In *Proceedings of the 1997 ASME Design Engineering Technical Conferences*, volume Paper DETC97/VIB-3844, New York, NY, 1997. American Society of Mechanical Engineers.

[42] O. Poudou. *Modeling and Analysis of the Dynamics of Dry-Friction-Damped Structural Systems*. PhD thesis, The University of Michigan, 2007.

[43] Ali H. Nayfeh and Balakumar Balachandran. *Applied Nonlinear Dynamics: Analytical, Computational, and Experimental Methods*. Wiley-Interscience, 1995.

[44] G. von Groll and D. J. Ewins. The harmonic balance method with arc-length continuation in rotor/stator contact problems. *Journal of Sound and Vibration*, 241:223–233, Mar 2001.

[45] J. C. Simo and T. A. Laursen. An augmented lagrangian treatment of contact problems involving friction. *Computers & Structures*, 42:97–116, Jan 1992.

[46] D. Jiang, C. Pierre, and S. W. Shaw. Large-amplitude non-linear normal modes of piecewise linear systems. *Journal of Sound and Vibration*, 272(3-5):869–891, 2004.

[47] L. Zuo and A. Curnier. Nonlinear real and complex-modes of conewise linear-systems. *Journal of Sound and Vibration*, 174(3):289–313, Jul 1994.

[48] S. L. Chen and S. W. Shaw. Normal modes for piecewise linear vibratory systems. *Nonlinear Dynamics*, 10(2):135–164, Jun 1996.

[49] W. Weaver, S. P. Timoshenko, and D. H. Young. *Vibration Problems in Engineering*, chapter 2. Wiley-IEEE, fifth edition, Jan 1990.

[50] S. Deshpande, S. Mehta, and G. N. Jazar. Optimization of secondary suspension of piecewise linear vibration isolation systems. *International Journal of Mechanical Sciences*, 48:341–377, Apr 2006.

[51] A. Narimani, M. E. Golnaraghi, and G. N. Jazar. Frequency response of a piecewise linear vibration isolator. *Journal of Vibration and Control*, 10:1775–1794, Dec 2004.

[52] D. A. McAdams, D. Comella, and I. Y. Tumer. Exploring effective methods for simulating damaged structures with geometric variation: Toward intelligent failure detection. *Journal of Applied Mechanics-Transactions of The ASME*, 74:191–202, Mar 2007.

[53] J. -J. Sinou and A. W. Lees. The influence of cracks in rotating shafts. *Journal of Sound and Vibration*, 285:1015–1037, Aug 2005.

[54] T. C. Kim, T. E. Rook, and R. Singh. Super- and sub-harmonic response calculations for a torsional system with clearance nonlinearity using the harmonic balance method. *Journal of Sound and Vibration*, 281(3-5):965–993, 2005.

[55] E. P. Petrov and D. J. Ewins. Advanced modeling of underplatform friction dampers for analysis of bladed disk vibration. *Journal of Turbomachinery*, 129(1):143–150, 2007.

[56] A. Saito, M. P. Castanier, C. Pierre, and O. Poudou. Efficient nonlinear vibration analysis of the forced response of rotating cracked blades. *Journal of Computational and Nonlinear Dynamics-Transactions of the ASME*, 4(1):011005, 2009.

[57] D. N. Herting. A general purpose, multi-stage, component modal synthesis method. *Finite Elements in Analysis and Design*, 1(2):153–164, 1985.

[58] Alberto Carpinteri and Nicola Pugno. Towards chaos in vibrating damaged structures—part i: Theory and period doubling cascade. *Journal of Applied Mechanics*, 72(4):511–518, 2005.

[59] Alberto Carpinteri and Nicola Pugno. Towards chaos in vibrating damaged structures—part ii: Parametrical investigation. *Journal of Applied Mechanics*, 72(4):519–526, 2005.

[60] I. B. Carrington, J. R. Wright, J. E. Cooper, and G. Dimitriadis. A comparison of blade tip timing data analysis methods. *Proceedings of the I MECH E Part G Journal of Aerospace Engineering*, 215(5):301–312, 2001.

[61] A. Saito, M. P. Castanier, and C. Pierre. Effects of a cracked blade on mistuned turbine engine rotor vibration. In *Proceedings of IDETC 2007, paper DETC2007-35663*, Las Vegas, Nevada, USA, September 2007.

[62] J. R. Kuttler and V. G. Sigillito. On curve veering. *Journal of Sound and Vibration*, 75(4):585–588, 1981.

[63] Arthur W. Leissa. On a curve veering aberration. *Zeitschrift für Angewandte Mathematik und Physik (ZAMP)*, 25(1):99–111, 1974.

[64] N. C. Perkins and C. D. Mote. Comments on curve veering in eigenvalue problems. *Journal of Sound and Vibration*, 106(3):451–463, 1986.

[65] C. Pierre and E. H. Dowell. Localization of vibrations by structural irregularity. *Journal of Sound and Vibration*, 114(3):549–564, 1987.

[66] C. Pierre. Mode localization and eigenvalue loci veering phenomena in disordered structures. *Journal of Sound and Vibration*, 126(3):485–502, 1988.

[67] M. S. Triantafyllou and G. S. Triantafyllou. Frequency coalescence and mode localization phenomena: A geometric theory. *Journal of Sound and Vibration*, 150(3):485–500, 1991.

[68] Stefano Vidoli and Fabrizio Vestroni. Veering phenomena in systems with gyroscopic coupling. *Journal of Applied Mechanics*, 72(5):641–647, 2005.

[69] Noel Challamel, Christophe Lanos, and Charles Casandjian. Localization in the buckling or in the vibration of a two-span weakened column. *Engineering Structures*, 28(5):776–782, 2006.

[70] Marco Lepidi, Vincenzo Gattulli, and Fabrizio Vestroni. Static and dynamic response of elastic suspended cables with damage. *International Journal of Solids and Structures*, 44(25-26):8194–8212, 2007.

[71] P. P. Lynn and N. Kumbasar. Free vibrations of thin rectangular plates having narrow cracks with simply supported edges. *Development in Mechanics*, 4:911–928, 1967.

[72] M. Petyt. The vibration characteristics of a tensioned plate containing a fatigue crack. *Journal of Sound and Vibration*, 8(3):377–389, 1968.

[73] B. Stahl and L. M. Keer. Vibration and stability of cracked rectangular plates. *International Journal of Solids and Structures*, 8(1):69–91, 1972.

[74] Y. Hirano and K. Okazaki. Vibration of cracked rectangular-plates. *Bulletin of the JSME-Japan Society of Mechanical Engineers*, 23:732–740, 1980.

[75] Roman Solecki. Bending vibration of a simply supported rectangular plate with a crack parallel to one edge. *Engineering Fracture Mechanics*, 18(6):1111–1118, 1983.

[76] J. Yuan and S. M. Dickinson. The flexural vibration of rectangular plate systems approached by using artificial springs in the rayleigh-ritz method. *Journal of Sound and Vibration*, 159(1):39–55, 1992.

[77] K. M. Liew, K. C. Hung, and M. K. Lim. A solution method for analysis of cracked plates under vibration. *Engineering Fracture Mechanics*, 48(3):393–404, 1994.

[78] C. C. Ma and C. H. Huang. Experimental and numerical analysis of vibrating cracked plates at resonant frequencies. *Experimental Mechanics*, 41(1):8–18, 2001.

[79] S. Christides and A. D. S. Barr. One-dimensional theory of cracked Bernoulli-Euler beams. *International Journal of Mechanical Sciences*, 26(11-12):639–648, 1984.

[80] T. G. Chondros, A. D. Dimarogonas, and J. Yao. A continuous cracked beam vibration theory. *Journal of Sound and Vibration*, 215(1):17–34, 1998.

[81] M. Kisa and J. Brandon. The effects of closure of cracks on the dynamics of a cracked cantilever beam. *Journal of Sound and Vibration*, 238(1):1–18, Nov 2000.

[82] Walter Lacarbonara, Haider N. Arafat, and Ali H. Nayfeh. Non-linear interactions in imperfect beams at veering. *International Journal of Non-Linear Mechanics*, 40(7):987–1003, 2005.

[83] R. M. Hintz. Analytical methods in component modal synthesis. *AIAA Journal*, 13(8):1007–1016, 1975.

[84] S. Nacivet, C. Pierre, F. Thouverez, and L. Jezequel. A dynamic lagrangian frequency-time method for the vibration of dry-friction-damped systems. *Journal of Sound and Vibration*, 265(1):201–219, Jul 2003.

[85] L. Ji, B. R. Mace, and R. J. Pinnington. A mode-based approach for the mid-frequency vibration analysis of coupled long- and short-wavelength structures. *Journal of Sound and Vibration*, 289(1-2):148–170, 2006.

[86] R. R. Craig. *Structural Dynamics: An Introduction to Computer Methods*. John Wiley & Sons, New York, 1981.

[87] D. Laxalde, F. Thouverez, J. J. Sinou, and J. P. Lombard. Qualitative analysis of forced response of blisks with friction ring dampers. *European Journal of Mechanics - A/Solids*, 26(4):676–687, 2007.

[88] J. -J. Sinou and A. W. Lees. A non-linear study of a cracked rotor. *European Journal of Mechanics A/Solids*, 26(1):152–170, Jan 2007.

[89] R. J. Allemang. The modal assurance criterion - twenty years of use and abuse. *Journal of Sound and Vibration*, 37(8):14–23, 2003.

[90] A. F. Vakakis, L. I. Manevitch, Y. V. Mikhlin, V. N. Pilipchuk, and A. A. Zevin. *Normal Modes and Localization in Nonlinear Systems*. John Wiley & Sons, Inc., New York, 1996.

[91] R. J. Guyan. Reduction of stiffness and mass matrices. *AIAA Journal*, 3(2):380, 1965.

[92] K. Brahmi, N. Bouhaddi, and R. Fillod. Reduction of junction degrees of freedom before assembly in dynamic substructuring. In *Proceedings of the ASME Design Engineering Technical Conference*, volume 3, pages 699–708, 1995.

[93] E. Balmés. Use of generalized interface degrees of freedom in component mode synthesis. In *Proceedings of International Modal Analysis Conference*, pages 204–210, Bethel, CT, 1996. Society for Experimental Mechanics.

[94] M. P. Castanier, Y. C. Tan, and C. Pierre. Characteristic constraint modes for component mode synthesis. *AIAA Journal*, 39(6):1182–1187, 2001.

[95] R. D. Henshell and J. H. Ong. Automatic masters for eigenvalue economization. *Earthquake Engineering & Structural Dynamics*, 3(4):375–383, 1975.

[96] V. N. Shah and M. Raymund. Analytical selection of masters for the reduced eigenvalue problem. *International Journal for Numerical Methods in Engineering*, 18(1):89–98, 1982.

[97] R. L. Kidder. Reduction of structural frequency equations. *AIAA Journal*, 11:892–892, 1973.

[98] A. H. Flax. Comment on "reduction of structural frequency equations". *AIAA Journal*, 13:701–702, 1975.

[99] R. L. Kidder. Reply by author to A. H. Flax. *AIAA Journal*, 13:702–703, 1975.

[100] N. I. Grinenko and V. V. Mokeev. Problems of studying vibrations of structures by the finite-element method. *International Applied Mechanics*, 21(3):231–235, 1985.

[101] K. W. Matta. Selection of degrees of freedom for dynamic analysis. *Journal of Pressure Vessel Technology - Transactions of the ASME*, 109:65–69, 1987.

[102] N. Bouhaddi and R. Fillod. A method for selecting master dof in dynamic substructuring using the guyan condensation method. *Computers & Structures*, 45(5-6):941–946, 1992.

[103] T. Hitziger, W. Mackens, and H. Voss. A condensation-projection method for generalized eigenvalue problems. In H. Power and C. A. Brebbia, editors, *High Performance Computing 1*, pages 239–282. Elservier Applied Science, London, 1995.

[104] K. O. Kim and Y. J. Choi. Energy method for selection of degrees of freedom in condensation. *AIAA Journal*, 38:1253–1259, 2000.

[105] M. Cho and H. Kim. Element-based node selection method for reduction of eigenvalue problems. *AIAA Journal*, 42:1677–1684, 2004.

[106] H Kim and M Cho. Two-level scheme for selection of primary degrees of freedom and semi-analytic sensitivity based on the reduced system. *Computer Methods in Applied Mechanics and Engineering*, 195:4244–4268, 2006.

[107] J. O'Callahan. A procedure for an improved reduced system (IRS) model. In *Proceedings of the 7th International Modal Analysis Conference*, pages 17–21, Las Vegas, NV, January 1989.

[108] W. Li. A degree selection method of matrix condensations for eigenvalue problems. *Journal of Sound and Vibration*, 259(2):409–425, 2003.

[109] Dongho Oh and Youngjin Park. Order reduction based on singular values of a modal matrix. *Mechanical Systems and Signal Processing*, 8(1):63–79, 1994.

[110] Firdaus E. Udwadia. Methodology for optimum sensor locations for parameter identification in dynamic systems. *Journal of Engineering Mechanics*, 120(2):368–390, 1994.

[111] J. E. T. Penny, M. I. Friswell, and S. D. Garvey. Automatic choice of measurement locations for dynamic testing. *AIAA Journal*, 32:407–414, 1994.

[112] D. C. Kammer. Sensor placement for on-orbit modal identification and correlation of large space structures. *Journal of Guidance Control and Dynamics*, 14(2):251–259, 1991.

[113] J. Zhu and W. Zhang. Maximization of structural natural frequency with optimal support layout. *Structural and Multidisciplinary Optimization*, 31:462–469, 2006.

[114] B. ÅKesson and N. Olhoff. Minimum stiffness of optimally located supports for maximum value of beam eigenfrequencies. *Journal of Sound and Vibration*, 120(3):457–463, 1988.

[115] D. Szelag and Z. Mroz. Optimal design of vibrating beams with unspecified support reactions. *Computer Methods in Applied Mechanics and Engineering*, 19(3):333–349, 1979.

[116] K. M. Won and Y. S. Park. Optimal support positions for a structure to maximize its fundamental natural frequency. *Journal of Sound and Vibration*, 213(5):801–812, 1998.

[117] J. O'Callahan, P. Avitabile, and R. Riemer. System equivalent reduction expansion process (SEREP). In *Proceedings of the 7th International Modal Analysis Conference*, pages 29–37, Las Vegas, NV, January 1989.

[118] M. I. Friswell, S. D. Garvey, and J. E. T. Penny. Model-reduction using dynamic and iterated IRS techniques. *Journal of Sound and Vibration*, 186:311–323, 1995.

[119] M. I. Friswell, S. D. Garvey, and J. E. T. Penny. The convergence of the iterated IRS method. *Journal of Sound and Vibration*, 211:123–132, 1998.

[120] M. I. Friswell, J. E. T. Penny, and S. D. Garvey. Using linear model reduction to investigate the dynamics of structures with local non-linearities. *Mechanical Systems and Signal Processing*, 9(3):317–328, 1995.

[121] A. Saito, M. P. Castanier, and C. Pierre. Vibration analysis of cracked cantilevered plates near natural frequency veerings. In *Proceedings of the 49th AIAA/ASME/ASCE/AHS/ASC Structures, Structural Dynamics, and Materials Conference, paper AIAA 2008-1872*, Reston, VA, 2008. AIAA.

[122] H. Voss. An error bound for eigenvalue analysis by nodal condensation. In J. Albrecht, L. Collatz, and W. Velete, editors, *Numerical Treatment of Eigenvalue Problems*, volume 3, pages 205–214. Birkhäuser Verlag, Stuttgart, 1983.

[123] D. L. Thomas. Errors in natural frequency calculations using eigenvalue economization. *International Journal for Numerical Methods in Engineering*, 18:1521–1527, 1982.

[124] H. Voss W. Mackens. Nonnodal condensation of eigenvalue problems. *Zeitschrift für Angewandte Mathematik und Mechanik (ZAMM)*, 79(4):243–255, 1999.

[125] M. T. Yang and J. H. Griffin. A reduced-order model of mistuning using a subset of nominal system modes. *Journal of Engineering for Gas Turbines and Power-Transactions of the ASME*, 123:893–900, Oct. 2001.

[126] E. P. Petrov, K. Y. Sanliturk, and D. J. Ewins. A new method for dynamic analysis of mistuned bladed disks based on the exact relationship between tuned and mistuned systems. *Journal of Engineering for Gas Turbines and Power-Transactions of the ASME*, 124:586–597, Jul 2002.

[127] S.-H. Lim, R. Bladh, M. P. Castanier, and C. Pierre. Compact, generalized component mode mistuning representation for modeling bladed disk vibration. *AIAA Journal*, 45(9):2285–2298, 2007.

[128] R. Bladh, M. P. Castanier, and C. Pierre. Reduced order modeling and vibration analysis of mistuned bladed disk assemblies with shrouds. *Journal of Engineering for Gas Turbines and Power*, 121(3):515–522, 1999.

[129] T. A. Laursen and B. N. Maker. An augmented lagrangian quasi-newton solver for constrained nonlinear finite-element applications. *International Journal for Numerical Methods in Engineering*, 38:3571–3590, Nov 1995.

[130] Rüdiger Seydel. *Practical Bifurcation and Stability Analysis: From Equilibrium to Chaos*. Springer, 1994.

[131] J. J. Chen, B. D. Yang, and C. H. Menq. Periodic forced response of structures having three-dimensional frictional constraints. *Journal of Sound and Vibration*, 229(4):775–792, 2000.

[132] T. Rook. An alternate method to the alternating time-frequency method. *Nonlinear Dynamics*, 27:327–339, Mar 2002.